

Polimery w Medycynie

Polymers in Medicine

BIANNUAL ISSN: 0370-0747 e-ISSN: 2451-2699

polimery.umw.edu.pl

2022, Vol. 52, No. 2 (July–December)

Ministry of Science and Higher Education – 70 pts.
Index Copernicus (ICV) – 120.65 pts.



WROCLAW
MEDICAL UNIVERSITY

Polimery w Medycynie
Polymers in Medicine



Polimery w Medycynie

Polymers in Medicine

ISSN 0370-0747 (PRINT)

ISSN 2451-2699 (ONLINE)

polimery.umw.edu.pl

BIANNUAL
2022, Vol. 52, No. 2
(July–December)

“Polymers in Medicine” is an independent, multidisciplinary forum to exchange scientific and clinical information, which publishes original papers (technical, analytical, experimental, clinical), preliminary reports and reviews regarding the use of polymers (natural and synthetic) and biomaterials in different specialties of medicine (biochemistry, clinical medicine, pharmacology, dentistry, implantology), biotechnology and veterinary science.

Address of Editorial Office

Marcinkowskiego 2–6
50-368 Wrocław, Poland
Tel.: +48 71 784 11 33
E-mail: redakcja@umw.edu.pl

Publisher

Wrocław Medical University
Wybrzeże L. Pasteura 1
50-367 Wrocław, Poland

Online edition is the original version of the journal

Editor-in-Chief

Prof. Witold Musiał

Deputy Editor

Dr. Konrad Szustakiewicz, DSc., Eng.

Scientific Committee

Prof. Mirosława El-Fray
Prof. Franciszek Główka
Prof. Jörg Kreßler
Dr. Anna Krupa
Prof. Maciej Małecki
Prof. Bożena B. Michniak-Kohn

Statistical Editors

Wojciech Bombała, MSc
Anna Kopszak, MSc
Dr. Krzysztof Kujawa

Prof. Wojciech Miltyk
Prof. Masami Okamoto
Prof. Elżbieta Pamuła
Prof. Wiesław Sawicki
Prof. Szczepan Zapotoczny

Section Editors

Dr. Tomasz Urbaniak
(synthesis, evaluation, medical use of polymers, sensitive to environmental factors, applied in controlled and targeted drug delivery)

Dr. Monika Gasztych
(preparation, assessment and application of polymers in pharmaceutical technology and medical devices)

Dr. BEng., Agnieszka Gadomska-Gajadur
(synthesis and characterization of polymers having biomedical potential, composites for regenerative medicine)

Manuscript editing

Marek Misiak, Jolanta Krzyżak

Editorial Policy

During the review process, the Editorial Board conforms to the "Uniform Requirements for Manuscripts Submitted to Biomedical Journals: Writing and Editing for Biomedical Publication" approved by the International Committee of Medical Journal Editors (<http://www.icmje.org/>). Experimental studies must include a statement that the experimental protocol and informed consent procedure were in compliance with the Helsinki Convention and were approved by the ethics committee.

For more information visit the following page: <https://polimery.umw.edu.pl>

Indexed in: OCLC, WorldCat, PBL, EBSCO, MEDLINE, Index Copernicus

Typographic design: Monika Kołęda, Piotr Gil

Cover: Monika Kołęda

DTP: Wrocław Medical University Press

Printing and binding: Drukarnia I-BiS Bierońscy Sp.k.

Circulation: 11 copies

Contents

55 Preface

Original papers

- 57 Kornelia M. Batko, Izabella Ślęzak-Prochazka, Sławomir Marek Grzegorzczyn, Anna Pilis, Paweł Dolibog, Andrzej Ślęzak
Energy conversion in Textus Bioactiv Ag membrane dressings using Peusner's network thermodynamic descriptions
- 67 Bernard O. Patani, Olufunke Dorothy Akin-Ajani, Arul Kumaran, Oluwatoyin Adepeju Odeku
***Irvingia gabonensis* (O'Rorke) Bail polymer matrix system for controlled drug delivery**
- 77 Majid Neamah Ali, Ayaid Khadem Zgair
Extracellular product of *Pseudomonas aeruginosa* in growth medium is involved in the pro-inflammatory cytokine response of human oral epithelial cells in vitro
- 83 Olufunke Dorothy Akin-Ajani, Temiloluwa Mary Hassan, Oluwatoyin Adepeju Odeku
***Talinum triangulare* (Jacq.) Willd. mucilage and pectin in the formulation of ibuprofen microspheres**
- 93 Betina Chairelo Commar, Marcelle Danelon, Paulo Augusto Panitente, Emily Vivianne Freitas da Silva, Sandro Basso Bitencourt, Valentim Adelino Ricrdo Barão, Clóvis Lamartine de Moraes Melo Neto, Marcelo Coelho Goiato, Daniela Micheline dos Santos
Effect of glaze and chlorhexidine on physical and mechanical properties of bis-acryl resin: An in situ study

Reviews

- 101 Dominik Strojewski, Anna Krupa
Spray drying and nano spray drying as manufacturing methods of drug-loaded polymeric particles

PREFACE

Dear Readers, Authors, Reviewers,
Members of the Scientific Committee and Section Editors,



The scientific life enables investigation of numerous phenomena, including the transport processes, which take place on the interfacial borders: drug carrier–environment of drug activity. In the present issue, we provide our audience three articles which directly involve the polymeric entities as drug carriers. Two of these entities are of plantar origin, and may fall in the interest of pharmaceutical industry seeking new natural sources of polymeric drug carriers. On the other hand, there is the third article, which deals with highly processed polymeric artificial lenses that may act as sophisticated drug carriers. Some new techniques emerge and creatively change the landscape of pharmaceutical production. Nowadays, spray drying competes with 3D printing, and we present to our readers a updated review on the state-of-the-art technique employed in the field of spray drying as a method which allows for drug loading into polymeric particles.

We are just entering the Christmas Holidays season, and probably the entire free world is curious when and how the worldwide empathy and unity will finally resolve the ongoing situation on the territories being so close to the eastern border of the European Union, and being so devastated by incomprehensible and appalling actions. The most important wishes should thus include the peace and the social and industrial reactivation for the people who were injured and excluded from normal life by unfounded and disproportionate acts. Therefore, I would like also to offer best Christmas wishes to all friends and readers of our Journal. On behalf of the entire Editorial Team of Polymers in Medicine, we wish you good luck and Happy New Year 2023!

Editor-in-Chief
Witold Musiał, Prof., PhD, DSc

Energy conversion in Textus Bioactiv Ag membrane dressings using Peusner's network thermodynamic descriptions

Konwersja energii w opatrunku membranowym Textus Bioactive Ag w opisie termodynamiki sieciowej Peusnera

Kornelia M. Batko^{1,B,C}, Izabella Ślęzak-Prochazka^{2,B,C}, Sławomir Marek Grzegorzczyn^{3,A,D–F}, Anna Pilis^{4,B}, Paweł Dolibog^{3,B}, Andrzej Ślęzak^{4,A,D–F}

¹ Faculty of Social Sciences, University of Silesia, Katowice, Poland

² Biotechnology Centre, Silesian University of Technology, Gliwice, Poland

³ Department of Biophysics, Faculty of Medical Sciences in Zabrze, Medical University of Silesia, Poland

⁴ Department of Health Science and Physiotherapy, Jan Długosz University, Częstochowa, Poland

A – research concept and design; B – collection and/or assembly of data; C – data analysis and interpretation;

D – writing the article; E – critical revision of the article; F – final approval of the article

Polymers in Medicine, ISSN 0370-0747 (print), ISSN 2451-2699 (online)

Polim Med. 2022;52(2):57–66

Address for correspondence

Sławomir Marek Grzegorzczyn
E-mail: grzegorzczyn@sum.edu.pl

Funding sources

This work was supported by the project of Medical University of Silesia No. PCN-1-172/N/0/1.

Conflict of interest

None declared

Received on May 18, 2022

Reviewed on June 13, 2022

Accepted on September 5, 2022

Published online on November 10, 2022

Cite as

Batko KM, Ślęzak-Prochazka I, Grzegorzczyn SM, Pilis A, Dolibog P, Ślęzak A. Energy conversion in Textus Bioactiv Ag membrane dressings using Peusner's network thermodynamic descriptions. *Polim Med.* 2022;52(2):57–66. doi:10.17219/pim/153522

DOI

10.17219/pim/153522

Copyright

Copyright by Author(s)

This is an article distributed under the terms of the Creative Commons Attribution 3.0 Unported (CC BY 3.0) (<https://creativecommons.org/licenses/by/3.0/>)

Abstract

Background. The Textus Bioactiv Ag membrane is an active dressing for the treatment of chronic wounds such as venous stasis ulcers and burns.

Objectives. Determination of the transport and internal energy conversion properties of the Textus Bioactiv Ag membrane using the Kedem–Katchalsky–Peusner model. This model introduces the coefficients L_{ij} necessary to calculate the degree of coupling (I_{ij} , Q_L), energy conversion efficiency (e_{ij}), dissipated energy (S-energy), free energy (F-energy), and internal energy (U-energy).

Materials and methods. The research material was the Textus Bioactiv Ag membrane that is used as an active dressing in the treatment of difficult-to-heal wounds, and KCl aqueous solutions. The research methods employed Peusner's formalism of network thermodynamics and Kedem and Katchalsky's thermodynamics of membrane processes. To calculate the L_{ij} coefficients, we used hydraulic conductivity (L_p), diffusion conductivity (ω) and reflection (σ) coefficients to perform experimental measurements in different conditions.

Results. The L_p coefficient for the Textus Bioactiv Ag membrane is nonlinearly dependent on the average concentrations of the solutions. In turn, the ω and σ coefficients are nonlinearly dependent on the differences in osmotic pressures ($\Delta\pi$). An increase in the $\Delta\pi$ causes the Textus Bioactiv Ag membrane to become more permeable and less selective for KCl solutions. The coefficients of Peusner (L_{ij}), couplings (I_{ij} , Q_L), energy conversion efficiency (e_{ij}), S-energy, F-energy, and U-energy also depend nonlinearly on $\Delta\pi$. Our results showed that for higher concentrations of KCl solutions transported through the Textus Bioactiv Ag membrane, the coupling and energy conversion coefficients were greater for larger $\Delta\pi$ up to their maximum values for large $\Delta\pi$. Coupling of the membrane structure with the electrolyte flux through the membrane is observed for $\Delta\pi$ greater than 10 kPa.

Conclusions. Textus Bioactiv Ag membrane dressings possess the properties of a solution component separator as well as an internal energy converter.

Key words: membrane transport, polymeric membrane, energy conversion, Kedem–Katchalsky–Peusner equations, Textus Bioactiv Ag

Streszczenie

Wprowadzenie. Membrana Textus Bioactive Ag to aktywny opatrunek do leczenia ran przewlekłych, takich jak owrzodzenia żyłne podudzi i oparzenia.

Cel pracy. Wyznaczenie właściwości transportowych i wewnętrznej konwersji energii w membranie Textus Bioactiv Ag, w oparciu o model Kedem–Katchalskiego–Peusnera (KKP). Model ten wprowadza współczynniki L_{ij} niezbędne do obliczenia stopnia sprzężenia (I_{ij} , Q_i), sprawności konwersji energii (e_{ij}), energii rozproszonej (S-energia), energii swobodnej (F-energia) i energii wewnętrznej (U-energia).

Materiały i metody. Badanym materiałem była membrana Textus Bioactive Ag, stosowana jako aktywny opatrunek w terapii trudno gojących się ran, oraz wodne roztwory KCl. Metody badawcze to formalizm sieciowej termodynamiki Peusnera oraz termodynamika procesów membranowych Kedem–Katchalsky'ego. Do obliczenia współczynników L_{ij} wykorzystaliśmy współczynniki przenikalności hydraulicznej (L_p), przenikalności dyfuzyjnej (ω) i odbicia (σ), zmierzone eksperymentalnie w różnych warunkach.

Wyniki. Współczynnik L_p dla membrany Textus Bioactiv jest nieliniowo zależny od średniego stężenia roztworów w membranie. Z kolei współczynniki ω i σ są nieliniowo zależne od różnicy ciśnień osmotycznych ($\Delta\pi$). Wzrost $\Delta\pi$ powoduje, że membrana Textus Bioactiv staje się bardziej przepuszczalna i mniej selektywna dla roztworów KCl. Współczynniki: Peusnera (L_{ij}), sprzężeń (I_{ij} , Q_i), sprawności konwersji energii (e_{ij}) oraz S-energii, F-energii i U-energii również zależą nieliniowo od $\Delta\pi$. Jak wynika z uzyskanych wyników, dla większych stężeń roztworów KCl transportowanych przez membranę Textus Bioactive współczynniki sprzężenia i konwersji energii są większe dla większych $\Delta\pi$, osiągając wartości maksymalne dla dużych wartości $\Delta\pi$. Sprzężenie struktury membrany ze strumieniem elektrolitu transportowanym przez membranę obserwuje się dla $\Delta\pi$ powyżej 10 kPa.

Wnioski. Opatrunek membranowy Textus Bioactive Ag posiada właściwości separatora składników roztworu, jak również wewnętrznego konwertera energii.

Słowa kluczowe: transport membranowy, membrana polimerowa, Textus Bioactiv Ag, równania Kedem–Katchalskiego–Peusnera, konwersja energii

Background

In recent years, due to the development of synthetic polymer technology, many types of synthetic membranes have found applications in modern medical therapy and diagnostics. These membranes act as selectively permeable barriers between biological tissues and the environment (e.g., hemodialyzers and active membrane dressings) or between an encapsulated drug and the internal environment of a living organism (controlled release), etc.^{1–5} When treating difficult-to-heal wounds, such as venous stasis ulcers or severe burns, selecting a dressing that is designed to maintain a moist environment, suitable temperature and pH of the wound is important. Various types of active dressings have been used in the treatment of chronic wounds.⁶ Their purpose is to protect nerve fibers from excessive stimulation during application and dressing changes, as well as protect delicate tissues from mechanical stimuli and external environmental influences to limit infections and bacterial contamination.⁷ One type of these active dressings is the Textus Bioactiv Ag membrane dressing.^{8,9} It is a composite/mixed polymer dressing containing thermoplastic polyethylene fibers and Ag zeolites.

According to the Kedem–Katchalsky (KK) model, the Textus Bioactiv Ag membrane has certain transport properties measured with the coefficients of hydraulic conductivity (of the solvent), reflection and diffusive conductivity (of the solution).⁹ This means that the Textus Bioactiv Ag membrane can separate appropriate solutions of different concentrations and has the property of free energy conversion, similarly to Nephrophan or Bioprocess membranes.^{10,11} The total energy of a thermodynamic

system is the sum of its internal energy (nuclear, chemical and thermal) and external energy (connected with gravitational, electromagnetic, electrical field, etc.).¹²

In both biological and physicochemical membrane systems, internal energy (U-energy) is mainly chemical energy. The internal energy consists of free energy (F-energy) and degraded energy (S-energy). The F-energy, also called exergy, defines the “quality of energy” and the part of the energy that can be practically used to do work. The S-energy, also called anergy, is the passive part of the energy that cannot be used practically.¹³ The conversion of chemical energy occurs in 2 stages. In the 1st stage, the F-energy is separated from the S-energy. In the 2nd stage, the F-energy is converted into useful work.

The biological cell, which functions like a chemodynamic machine, is the most efficient converter of chemical energy (U-energy) into useful energy (F-energy). The most important activity of this process is converting the F-energy contained within the chemical bonds of nutrients into high-energy compounds such as adenosine triphosphate (ATP).¹⁴ At the expense of ATP, mechanical work, osmotic work, electrical work, and biosynthesis work are performed. The production of S-energy depends on the rate of the biochemical process: the slower the process, the greater the efficiency of the cell.¹⁵

Transport processes, including membrane transport, constitute a group of fundamental phenomena occurring at all levels of physicochemical systems.¹⁶ The driving forces of these transporters are the physical quantities of scalar, vector and/or tensor nature, which participate in the creation of various types of physical fields that shape the field properties of nature. An example of a scalar field

is the field of concentrations, a vector field is the gravitational field, and a tensor field is the field of internal stresses. For a scalar field to formally participate in the creation of a thermodynamic force that generates thermodynamic flows, the appropriate gradients of scalar quantities such as concentration or temperature must be created. The generation of force results in the performance of work from the energy stored in the system.

Mathematical models developed using the framework of Onsager's linear nonequilibrium thermodynamics (LNET) and Peusner's network thermodynamics (NT)^{13,17–20} are convenient tools to study membrane transport properties. One of the more important ones is the Kedem–Katchalsky–Peusner (KKP) model,^{21–24} which is an extension of the KK model.²⁵ The classical KK equations contained transport coefficients that characterized the permeation of solvents and solutes through a membrane.^{18,25} These coefficients included hydraulic permeability (L_p), reflection (σ) and solute permeability (ω). Peusner introduced L, R, H, and P versions of the KKP equations containing Peusner coefficients L_{ij} , R_{ij} , H_{ij} , and P_{ij} ($i, j \in \{1, 2, \dots, n\}$) into the science of membranes and membrane techniques.²⁰ The Peusner coefficients are a combination of L_p , σ and ω coefficients and the average concentration of solutions in the membrane (\bar{C}). The coefficients of coupling (l_{ij} , r_{ij} , h_{ij} , p_{ij} ($i \neq j$)) and energy conversion efficiency ($(e_{ij})_l$, $(e_{ij})_r$, $(e_{ij})_h$, $(e_{ij})_p$ ($i \neq j$)) can be calculated using the L_{ij} , R_{ij} , H_{ij} , or P_{ij} coefficients, respectively. In addition, the so-called coupling coefficient "Super Q", which is also a coupling measurement, can also be calculated.

In this study, the L model of the KKP form was used to evaluate the transport properties of the Textus Bioactiv Ag membrane dressing. The relationships $L_p = f(\bar{C})$, $\sigma = f(\Delta\pi)$ and $\omega = f(\Delta\pi)$ for KCl aqueous solutions were determined experimentally according to the procedures described in previous papers.^{9,18} The dependencies of Peusner

(L_{11} , L_{12} , L_{21} , L_{22}), coupling (l_{12} , l_{21} , Q_L) and energy conversion efficiency ($(e_{12})_l$, $(e_{21})_l$) coefficients on osmotic pressure differences ($\Delta\pi$) were calculated experimentally from the measured characteristics of L_p , σ and ω as functions of osmotic pressure. Besides, dependencies $(\Phi_S)_L = f(\Delta\pi)$, $(\Phi_F)_L = f(\Delta\pi)$ and $(\Phi_U)_L = f(\Delta\pi)$ were calculated. The $(\Phi_S)_L$ is the dissipated energy flux (S-energy), $(\Phi_F)_L$ is the free energy flux (F-energy) and $(\Phi_U)_L$ is the internal energy flux (U-energy).

Materials and methods

Membrane system

Images of the membranous Textus Bioactiv Ag (Biocell Gesellschaft fur Biotechnologie GmbH, Engelskirchen, Germany) dressing, obtained using a scanning electron microscope (SEM; Zeiss Supra 35; Carl Zeiss AG, Jena, Germany) are shown in Fig. 1A,B. These images reveal 2 types of fibers and the mesh that prevents the membrane dressing from adhering to the wound.

Textus Bioactiv Ag is a double-layer membrane dressing used to treat wounds of various etiologies.⁹ It is made of 3 types of heterogeneous thermoplastic polymer fibers. The 1st layer contains polyethylene fibers, the core of which is hydrophobic and zeolites with silver ions are located on the hydrophilic surfaces. The task of the zeolites is to keep inactivated Ag^+ and/or micronized Ag inside a negatively charged polymer cage. This layer also contains hydrophilic polyethylene Super Absorbing Polymers (SAP) absorption fibers. The task of Ag^+ ions and Ag particles is to provide permanent and effective bactericidal protection of treated wounds against secondary infections. The 3rd type of polymer fibers is made of polyethylene and arranged parallelly to the skin surface, as in the 2nd layer

Textus Bioactive membrane

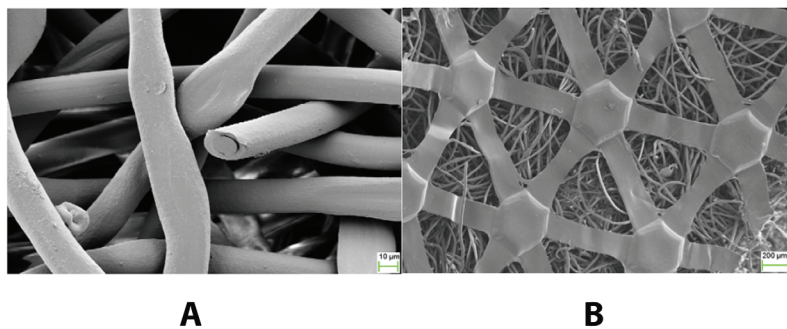


Fig. 1. Images of membrane surfaces obtained using a scanning electron microscope (SEM). A. The surface of the Textus Bioactiv Ag membrane from the side of the polymer fibers ($\times 1740$ magnification). The cross section of the fibers is visible, whose core is hydrophobic and on the hydrophilic surface of the fibers zeolites with silver ions next to the SAP fiber are visible; B. The surface of the Textus Bioactiv Ag membrane from the mesh side ($\times 94$ magnification) with polymer fibers visible in the meshes of the net; C. The single-membrane system

M – membrane; J_v – volume flux; J_s – solute flux; C_r and C_i – concentrations of solute separated by membrane; P_r and P_i – hydrostatic pressures.

of the membrane these create a special mesh that prevents the dressing from sticking to the wound. The polymer fibers used in this type of membrane are thermoplastic and able to attach to structures (zeolites, AgION™) containing silver ions. Depending on the manufacturer, membrane dressings are made of various types of fibers (polyethylene, polyamide, polypropylene, polyester, polystyrene, etc.). For example, in the case of the Textus Bioactiv Ag dressing, there are various types of polyethylene fibers, in Atrauman Ag dressing – polyamide fibers, and as in the Aquacel Ag dressing – sodium carboxymethyl cellulose fibers. The type of fibers used is important for determining the properties of the dressing. They absorb exudate and increase its volume, and prevent it from sticking to the wound (polyethylene). They ensure the correct pH (polyethylene, polyamide) or, as in the case of carboxymethyl cellulose, turn into a gel when absorbing exudate. The mesh showed in Fig. 1B has the characteristics of a non-selective membrane ($\sigma = 0$). The activation process of the dressing begins after wetting the dressing with Ringer's solution, which contains Na^+ , K^+ , Ca^{2+} , and Cl^- ions in various concentrations, and occurs abruptly from zeolites to SAP fibers. Due to the absorption properties of SAP fibers, the dressing has a very high absorption capability (4.2 kg/m²).

It should be mentioned that the surface area available to the solution on the grid side (Fig. 1B) is 60.7% smaller compared to the opposite side of the membrane (Fig. 1A). If we denote the actual membrane surface area by A_h and the membrane surface area on the grid side by A_l , then $A_l \approx 0.61 A_h$. Suppose that the A_h is in contact with a solution of concentration C_h , and the A_l is in contact with a solution of concentration C_l , then we will denote the volume flux induced by $\Delta\pi$ by J_{vh} . In this case, $\Delta\pi$ will increase solution volume (ΔV_h). If we reverse the location of the membrane, we will denote the flux for the same $\Delta\pi$, through the A_l by J_{vl} . In this case, $\Delta\pi$ will result in a solution volume increase of $\Delta V_l = 0.61 \Delta V_h$. Given this, $J_{vh} = (\Delta V_h)A_h^{-1}(\Delta t)^{-1}$ and $J_{vl} = (0.61\Delta V_h)(0.61A_h)^{-1}(\Delta t)^{-1}$. This means that $J_{vh} = J_{vl} = J_v$. This last relationship follows the flux continuity law. Similarly, it can be shown that for the solute flux, $J_{sh} = J_{sl} = J_s$.

Mathematical model

Figure 1C shows a model of the membrane system in which the membrane (M) separates 2 homogeneous electrolyte solutions with C_r and C_l concentrations ($C_r \geq C_l$) with hydrostatic pressures of P_r and P_l ($P_r > P_l$, $P_r = P_l$ or $P_r < P_l$). For binary electrolyte solutions, the KK equations are as follows^{18,26} (Equation 1–3):

$$J_v = L_p \left[\Delta P - \gamma \sigma RT(C_h - C_l) + \frac{P_E}{\kappa} I_m \right] \quad (1)$$

$$J_s = \gamma \omega RT(C_h - C_l) + \bar{C}(1 - \sigma)J_v + \frac{\tau_j}{z_j v_j F} I_m \quad (2)$$

$$I_m = -P_E J_v + \frac{\tau_j \kappa}{z_j v_j F} \Delta \mu_m + \kappa E \quad (3)$$

where J_v – volume flux; J_s – solute flux; I_m – electric ion current; L_p , σ , P_E and ω – coefficients of hydraulic permeability, reflection, electroosmotic permeability, and solute permeability, respectively; $\Delta P = P_r - P_l$ – difference of hydrostatic pressure; γ – Van 't Hoff coefficient; $\Delta\pi = RT(C_r - C_l)$ – differences in osmotic pressures (RT – the product of the gas constant and the absolute temperature; $\Delta\pi = RT(C_r - C_l)$ are solution concentrations, $C_h > C_l$); γ – Van 't Hoff coefficient ($1 \leq \gamma \leq 2$); κ – electrical conductivity; τ_j , z_j , v_j – transfer number, valence and ion number, respectively; and $\bar{C} = (C_h - C_l)(\ln C_h C_l^{-1})^{-1} \approx 0.5 (C_h + C_l)$ – average concentration of the solution.

If we assume that $I_m = 0$ in the system, we obtain equations analogous to those for non-electrolyte transport (Equation 4,5):

$$J_v = L_p \Delta P - L_p \gamma \sigma \Delta \pi \quad (4)$$

$$J_s = \gamma \omega \Delta \pi + \bar{C}(1 - \sigma)J_v \quad (5)$$

Therefore, the membrane transport properties are characterized by the hydraulic permeability (L_p), reflection (σ) and solute permeability (ω) coefficients, the definitions of which can be presented as $L_p = (J_v/\Delta P)_{\Delta\pi=0}$, $\sigma = (\Delta P/\gamma\Delta\pi)_{J_v=0}$ and $\omega = (J_s/\gamma\Delta\pi)_{J_v=0}$.

Relatively simple algebraic transformations allow for Equation 4,5 to be written in the form (Equation 6,7):

$$J_v = L_p(\Delta P - \gamma\Delta\pi) + \bar{C}(1 - \sigma)\gamma L_p \frac{\Delta\pi}{\bar{C}} \quad (6)$$

$$J_s = \bar{C}(1 - \sigma)L_p(\Delta P - \gamma\Delta\pi) + \bar{C} \left[\gamma\omega + \bar{C}(1 - \sigma)^2 \gamma L_p \right] \frac{\Delta\pi}{\bar{C}} \quad (7)$$

The above equations are called transformed KK equations or the L version of the KKP equations.^{20,22} Equation 6,7 written in matrix form containing Peusner coefficients L_{ij} ($i, j \in \{1, 2\}$) take the form of (Equation 8,9):

$$\begin{bmatrix} J_v \\ J_s \end{bmatrix} = [L] \begin{bmatrix} \Delta P - \gamma\Delta\pi \\ \gamma \frac{\Delta\pi}{\bar{C}} \end{bmatrix} \quad (8)$$

$$[L] = \begin{bmatrix} (L_{11})_T & (L_{12})_T \\ (L_{21})_T & (L_{22})_T \end{bmatrix} = \begin{bmatrix} L_p & L_p(1 - \sigma)\bar{C} \\ L_p(1 - \sigma)\bar{C} & \omega\bar{C} + L_p(1 - \sigma)^2\bar{C}^2 \end{bmatrix} \quad (9)$$

Using the definition proposed by Kedem and Caplan,^{20,27} the coefficients $(L_{ij})_T$ ($i, j \in \{1, 2\}$) can be used to calculate the coupling coefficients l_{12} and l_{21} defined by the expression (Equation 10):

$$l_{12} = l_{21} = \frac{L_{12}}{\sqrt{L_{11}L_{22}}} = \frac{L_{21}}{\sqrt{L_{11}L_{22}}} = \sqrt{\frac{L_p(1-\sigma)^2\bar{C}}{\omega + L_p(1-\sigma)^2\bar{C}}} \quad (10)$$

The value of the coefficients $l_{12} = l_{21} = 1$ is limited by the relation that $-1 \leq l \leq +1$. When $l = \pm 1$, the system is fully coupled and the processes become single processes. When $l = 0$, the 2 processes are completely unconjugated and no energy conversion occurs. The definition proposed by Kedem and Caplan²⁷ and Peusner²⁰ can be used to calculate the coefficient of maximum energy conversion efficiency (Equation 11):

$$\begin{aligned} (e_{12})_L &= \frac{(L_{12})^2}{L_{11}L_{22} \left(1 + \sqrt{1 - \frac{L_{12}L_{21}}{L_{11}L_{22}}}\right)^2} = \\ &= (e_{21})_L = \frac{(L_{21})^2}{L_{11}L_{22} \left(1 + \sqrt{1 - \frac{L_{12}L_{21}}{L_{11}L_{22}}}\right)^2} \end{aligned} \quad (11)$$

When Equation 10 is taken into account with Equation 11 we obtain (Equation 12):

$$\begin{aligned} (e_{21})_1 &= \frac{l_{21}^2}{\left(1 + \sqrt{1 - l_{12}l_{21}}\right)^2} = \\ &= (e_{12})_1 = \frac{l_{12}^2}{\left(1 + \sqrt{1 - l_{12}l_{21}}\right)^2} = \\ &= \frac{L_p(1-\sigma)^2\bar{C}}{\left[\omega + L_p(1-\sigma)^2\bar{C}\right] \left(1 + \sqrt{\frac{\omega_s}{\omega + L_p(1-\sigma)^2\bar{C}}}\right)^2} \end{aligned} \quad (12)$$

The values of the coefficients $(e_{12})_1 = (e_{21})_1 = (e_{\max})_1$ are limited by the relation that $0 \leq (e_{\max})_1 \leq +1$. Peusner proposed a Q_L coupling parameter called “super Q_L ”²⁰ (Equation 13):

$$\begin{aligned} Q_L &= \frac{2|L_{12}L_{21}|}{4L_{11}L_{22} - 2L_{12}L_{21}} = \\ &= \frac{l_{12}l_{21}}{2 - l_{12}l_{21}} = \frac{(1-\sigma)^2\bar{C}}{\frac{2\omega}{L_p} + (1-\sigma)^2\bar{C}} \end{aligned} \quad (13)$$

The coefficient Q_L is connected with $(e_{12})_1$ coefficient by using the Equation 14¹⁵:

$$\begin{aligned} (e_{12})_1 &= \frac{L_{21}Q_L}{L_{12}(1 + \sqrt{1 + Q_L^2})} = \\ &= (e_{21})_1 = \frac{L_{12}Q_L}{L_{21}(1 + \sqrt{1 + Q_L^2})} \end{aligned} \quad (14)$$

According to the first law of thermodynamics, in a membrane system, when the membrane separates 2 solutions

of different concentrations and the transport processes have an isothermal-isochoric character, the following equation is fulfilled (Equation 15):

$$(\Phi_U)_L = (\Phi_F)_L + (\Phi_S)_L \quad (15)$$

where $(\Phi_U)_L = A^{-1} dU/dt$ – flux of internal energy (U-energy); $(\Phi_F)_L = A^{-1} dF/dt$ – flux of free energy (F-energy); $(\Phi_S)_L = TA^{-1} d_iS/dt$ – flux of dissipation energy (S-energy); d_iS/dt is the rate at which entropy is created in the membrane system by irreversible processes (accumulated entropy flow); and T – absolute temperature. Equation 16 describes the conversions of U-energy to F-energy (exergy) and S-energy (anergy).

For one-membrane systems, $(\Phi_S)_L$ can be written in the following form (Equation 16):

$$\begin{aligned} (\Phi_S)_L &= (L_{11})_T(\Delta P - \gamma\Delta\pi)^2 + [(L_{12})_T + \\ &+ (L_{21})_T](\Delta P - \gamma\Delta\pi)\frac{\gamma\Delta\pi}{C} + (L_{22})_T\left(\frac{\gamma\Delta\pi}{C}\right)^2 \end{aligned} \quad (16)$$

Transforming the expression (Equation 17):

$$(e_{\max})_L = \frac{(\Phi_F)_L}{(\Phi_F)_L + (\Phi_S)_L} \quad (17)$$

and using Equation 16 we get (Equation 18,19):

$$(\Phi_F)_L = \frac{(e_{\max})_L}{1 - (e_{\max})_L} (\Phi_S)_L \quad (18)$$

$$(\Phi_U)_L = \frac{1}{1 - (e_{\max})_L} (\Phi_S)_L \quad (19)$$

Methodology for measuring the volume and solute fluxes and transport parameters

The studies on osmotic volume (J_v) and solute fluxes (J_s) were carried out using the measuring set described in a previous paper and presented in Fig. 2.²⁸ It consisted of 2 cylindrical vessels (l and h) with each containing a volume of 200 cm³ of aqueous KCl solution, one with a concentration in the range of 1–16 mol/m³ and the other with a constant concentration of 1 mol/m³. The solutions in the vessels were separated using a Textus Bioactiv Ag membrane dressing with an area of $A = 1.15$ cm², located in the horizontal plane.

A pipette graduated every 1 mm³ (KP) positioned in a plane parallel to the plane of the membrane was connected to the vessel (h) containing KCl at concentration C_h . The pipette was used to measure the change in volume (ΔV) of the solution in the measuring chamber (h). The vessel (l) was connected to a reservoir containing an aqueous solution of KCl with a concentration of $C_l = 1$ mol/m³, adjustable in height relative to the pipette. The measurement procedure for J_v and J_s was previously described.^{18,29} Briefly, increases in the ΔV were measured under conditions of intensive mechanical stirring of the solutions

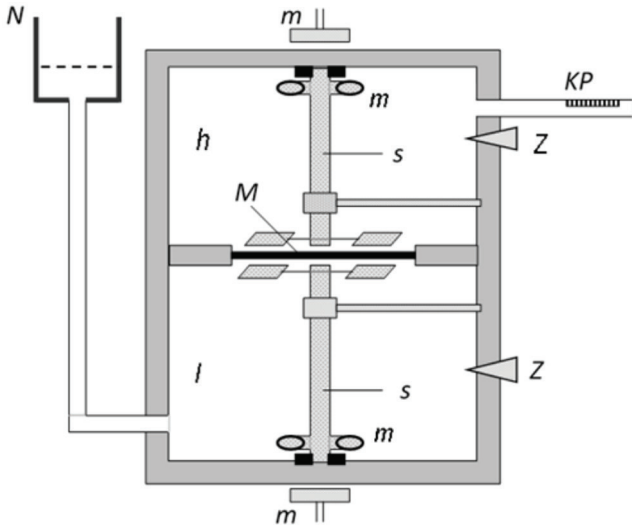


Fig. 2. Measuring system

h, l – measuring vessels; N – external solution tank; s – mechanical stirrers; M – membrane; K – calibrated pipette; m – magnets; z – plugs.²⁸

at 500 rpm. The volume flux was directed from the vessel with the lower concentration to the vessel with the higher concentration of solutions, and the flow of dissolved substances was in the opposite direction. The measurements were carried out at isothermal conditions ($T = 295$ K).

The volume flux through the surface (A) of the membrane was calculated based on the volume changes (ΔV) over time (Δt) measured in the pipette using the formula $J_v = (\Delta V)A^{-1}(\Delta t)^{-1}$. The fluxes of dissolved substances were calculated based on the formula $J_s = (V_u \cdot dC)A^{-1}(\Delta t)^{-1}$, where V_u was the volume of the measuring vessel and dC was the change in concentration of the solution measured with electrochemical methods.³⁰ The relative error in determining J_v and J_s was less than 10%. The values of coefficients L_{pT} , σ_T , and ω_T were calculated based on the formulas $L_{pT} = (J_v/\Delta P)_{C_h = C_l}$, $\sigma_T = (\Delta P/\Delta \pi)_{J_v = 0}$, and $\omega_T = (J_s/\Delta \pi)_{J_v = 0}$. Based on the characteristics $L_{pT} = f(\bar{C})$, $\sigma_T = f(\Delta \pi)$ and $\omega_T = f(\Delta \pi)$ presented in Fig. 3–5, the dependencies $L_{ij} = (\Phi_{S})_L$, $L_{det} = (\Phi_F)_L$, $I_{ij} = (\Phi_U)_L$, $Q_L = f(\Delta \pi)$, $(e_{ij})_l = f(\Delta \pi)$, $(\Phi_{S})_R = f(\Delta \pi)$, $(\Phi_F)_R = f(\Delta \pi)$, and $(\Phi_U)_R = f(\Delta \pi)$ were calculated.

Results

Determination of membrane transport parameters

Figures 3–5 show the dependencies $L_{pT} = f(\bar{C})$, $\omega_T = f(\Delta \pi)$ and $\sigma_T = f(\Delta \pi)$ were suitable. In the case of the $L_{pT} = f(\bar{C})$ characteristic, it was assumed that $\bar{C} \approx 0.5(C_r + C_l)$ ($C_r = C_l$). The characteristics shown in these figures are nonlinear. From the characteristics presented in Fig. 3, it follows that L_{pT} increases from $L_{pT} = 5 \times 10^{-8} \text{ m}^3/\text{Ns}$ (for $\bar{C} = 0$, pure water) to $L_{pT} = 68.5 \times 10^{-8} \text{ m}^3/\text{Ns}$ ($\bar{C} = 8 \text{ mol/m}^3$)

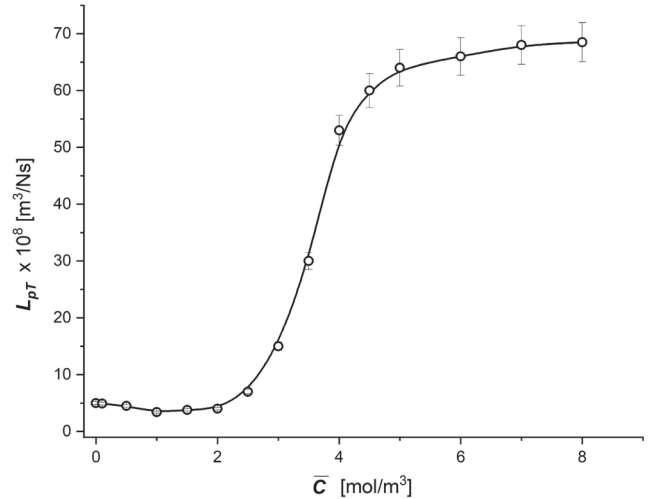


Fig. 3. Illustration of dependence $L_{pT} = f(\bar{C})$ for aqueous KCl solutions

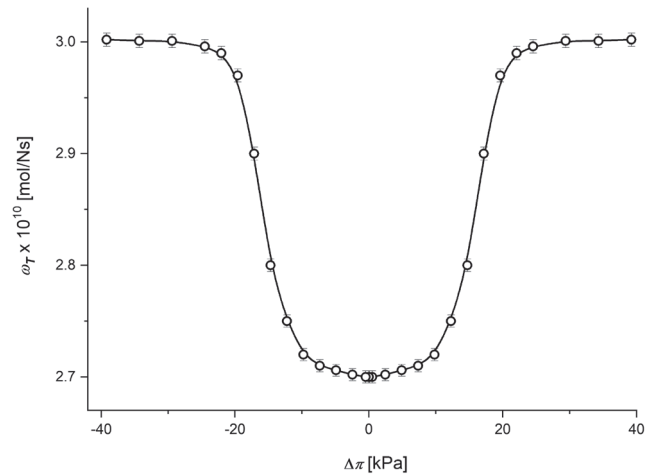


Fig. 4. Illustration of dependence $\omega_T = f(\Delta \pi)$ for aqueous KCl solutions

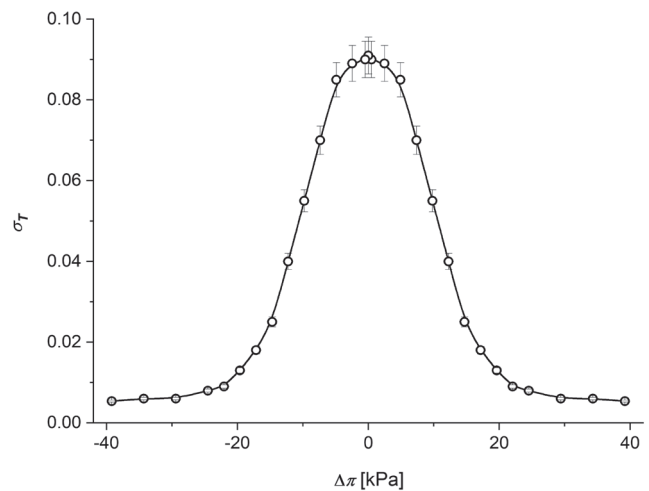


Fig. 5. Illustration of dependence $\sigma_T = f(\Delta \pi)$ for aqueous KCl solutions

– which is more than a 13-fold increase when concentrations of \bar{C} changes from 0 mol/m^3 to 8 mol/m^3).

The hydraulic permeability coefficient for most membranes is constant over a wide range of membrane concentrations. As can be seen in Fig. 3, this coefficient for the Textus Bioactiv

Ag membrane is not constant. The coefficient strongly depends on the KCl concentration in the membrane with increasing concentrations in the membrane, especially for concentrations above 3 mol/m^3 (in the range of $3\text{--}6 \text{ mol/m}^3$). Above 6 mol/m^3 , this coefficient does not change significantly. This causes a problem with the free use of the KK formalism over a wide range of electrolyte concentrations for this membrane. The relationship $L_{pT} = f(\bar{C})$ clearly shows 3 concentration ranges: an almost constant hydraulic permeability coefficient (ranges of low and high concentrations of KCl) and a transitional range of concentrations with a strong dependence of the L_{pT} coefficient on the concentration in the membrane. This indicates the complex nature of the interaction of the Textus Bioactiv Ag membrane with electrolyte solutions (aqueous KCl solutions). The strong dependence of the hydraulic permeability coefficient on the range of concentrations in the membrane may indicate possible dynamic structural changes in the membrane itself due to the interaction of its structure with electrolyte ions within the solution being transported through the membrane.

The value of coefficient ω_T increases from $2.7 \times 10^{-10} \text{ mol/Ns}$ (for $\Delta\pi = \pm 0.86 \text{ kPa}$) to $3.0 \times 10^{-10} \text{ mol/Ns}$ (for $\Delta\pi = \pm 39.22 \text{ kPa}$), which is an 11% increase when the concentration of $\Delta\pi$ changes from $\pm 0.86 \text{ kPa}$ to $\pm 39.22 \text{ kPa}$ (Fig. 4). Using the dependencies $\Delta\pi = \bar{C}RT \ln(C_r/C_l)$, it can be shown that $\Delta\pi = \pm 0.86 \text{ kPa}$ corresponds to $\bar{C} = 0.1 \text{ mol/m}^3$, while $\Delta\pi = \pm 39.22 \text{ kPa}$ corresponds to $\bar{C} = 8 \text{ mol/m}^3$. This indicates a significant change in the conditions of the solution transported through the membrane at this concentration range. This means that an increase in KCl concentrations in the Textus Bioactiv Ag membrane significantly improves the transport of KCl solutions through the membrane. Similarly to L_{pT} coefficient, the osmotic pressure ranges of almost constant value of the coefficient ω can be distinguished (low and high osmotic pressures) and the osmotic pressure range ($10\text{--}20 \text{ kPa}$) in which increase of osmotic pressure causes an increase in the coefficient ω .

The curve in Fig. 4A shows that σ_T decreases from 0.09 (for $\Delta\pi = \pm 0.86 \text{ kPa}$) to 0.005 (for $\Delta\pi = \pm 39.22 \text{ kPa}$) which is related to a 18-fold reduction in the reflection coefficient when the concentration in the membrane $\Delta\pi$ changes from 0.86 kPa to 39.22 kPa . This indicates a significant reduction in membrane selectivity for KCl solutions with increasing KCl concentrations in the membrane. This nonlinear relationship of the transport coefficients is caused by swelling of the hydrophilic fibers within the membrane and by the hydration of K^+ ions. These water coatings facilitate membrane transport by reducing the friction between the membrane and the substances penetrating it, and are dependent on the concentration of the solutions. For this reason, they increase the value of L_{pT} and ω_T and decrease the value of σ_T .

The Peusner coefficients $(L_{ij})_T$

The values L_{11} , $L_{12} = L_{21}$ and L_{22} were calculated using Equation 9,10. Figures 6A–C show the nonlinear

dependencies of $(L_{ij})_T = f(\Delta\pi)$ for the Textus Bioactiv Ag membrane when (a) $i = j = 1$, (b) $i = j = 2$, and (c) $i \neq j$.

The value of $(L_{12})_T = (L_{21})_T$ increases from $0.04 \times 10^{-7} \text{ m}^3/\text{Ns}$ (for $\Delta\pi = \pm 0.86 \text{ kPa}$) to $54.5 \times 10^{-7} \text{ m}^3/\text{Ns}$ (for $\Delta\pi = \pm 39.22 \text{ kPa}$). The dependence of $(L_{22})_T = f(\Delta\pi)$ for the Textus Bioactiv Ag membrane is nonlinear and the value of $(L_{22})_T$ increases from $0.04 \times 10^{-6} \text{ mol}^2/\text{m}^3\text{Ns}$

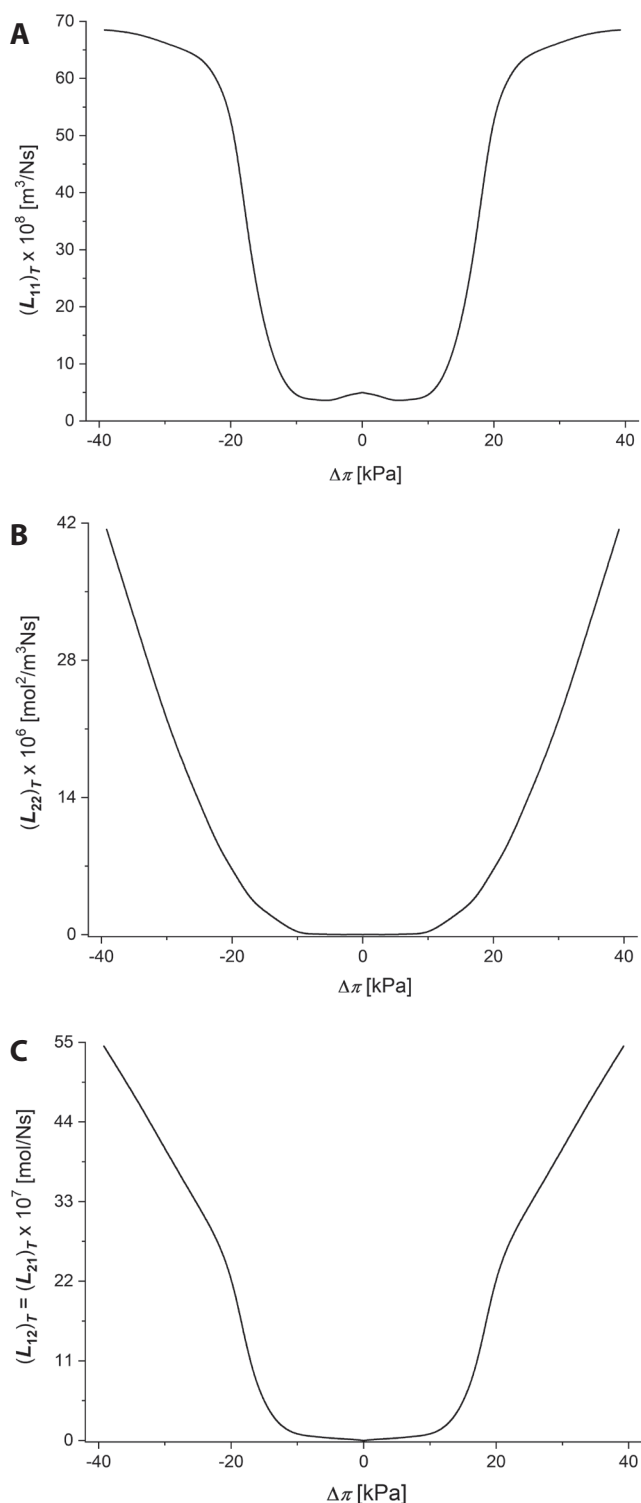


Fig. 6. Illustration of dependencies (A) $(L_{ij})_T = f(\Delta\pi)$ for $i = j = 1$, (B) $i = j = 2$, and (C) $i \neq j$ for Textus Bioactiv Ag membrane and aqueous KCl solutions

(for $\Delta\pi = \pm 0.86$ kPa) to 41.4×10^{-6} mol²/m³Ns (for $\Delta\pi = \pm 39.22$ kPa). For the $(L_{ij})_T$ coefficients for the Textus Bioactiv Ag membrane, 2 ranges of $\Delta\pi$ can be determined. For $\Delta\pi$ smaller than 10 kPa, the $(L_{ij})_T$ coefficients do not change much and are close to 0. Above $\Delta\pi = 10$ kPa, increasing the osmotic pressure causes a gradual increase in the $(L_{ij})_T$ coefficients.

The coefficients l_{ij} , $(e_{\max})_l$, and Q_L and fluxes $(\Phi_S)_L$ and $(\Phi_U)_L$

The dependencies $l_{12} = f(\Delta\pi)$, $(e_{\max})_l = f(\Delta\pi)$ and $Q_L = f(\Delta\pi)$ for Textus Bioactiv Ag membranes were calculated based on Equation 11–13 and are presented in Fig. 7. As seen in Fig. 7, as the value of $|\Delta\pi|$ increases, the l_{12} coefficient for Textus Bioactiv Ag membrane fulfills the condition $l_{12} \rightarrow 1$ when $|\Delta\pi| \rightarrow 40$ kPa. In turn, as the value of $|\Delta\pi|$ increases, the value of Q_L also increases and fulfills the conditions for Textus Bioactiv Ag membrane $Q_L \rightarrow 1$ when $|\Delta\pi| \rightarrow 40$ kPa. This means that the solvent and solute transport processes are coupled to different degrees. Therefore, they act as energy converters. The measurement of energy conversion efficiency is performed using the coefficients $(e_{\max})_l$ and Q_L . The curve (3) in Fig. 7 shows that the dependence $(e_{\max})_l = f(\Delta\pi)$ has an identical maximum and minimum. For $\Delta\pi = -7.9$ kPa or $+7.9$ kPa, the coefficient $[(e_{\max})_l]_{\max} = 0.83$ and for $\Delta\pi = -15.35$ kPa or $+15.35$ kPa the coefficient $[(e_{\max})_l]_{\min} = 0.53$, respectively. For $\Delta\pi > 15.35$ kPa and $\Delta\pi < -15.35$ kPa, the dependence $(e_{\max})_l = f(\Delta\pi)$ is of the saturation type. When $\Delta\pi \rightarrow -40$ kPa or $+40$ kPa, $(e_{\max})_l \rightarrow 0.7$. As can be seen from Fig. 7, for low KCl osmotic pressures, the coefficient values are small and close to 0, which indicates a lack of process coupling in the Textus Bioactiv Ag membrane. Increasing the osmotic pressure $\Delta\pi$ on the membrane causes a fast increase in coupling coefficients, which may

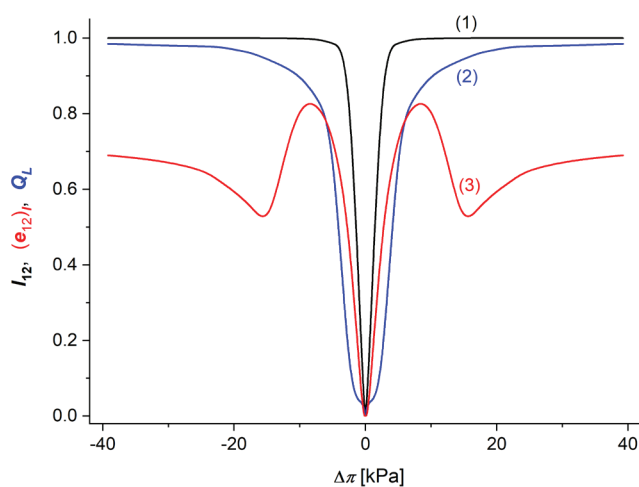


Fig. 7. Illustration of dependencies (1) $l_{12} = f(\Delta\pi)$, (2) $Q_L = f(\Delta\pi)$, and (3) $(e_{12})_l = (e_{\max})_l = f(\Delta\pi)$ for Textus Bioactiv Ag membranes and aqueous KCl solutions

indicate the increasing mutual influence of the membrane structure and the electrolyte flux through the membrane. This coupling, greater for the higher applied electrolyte osmotic pressure, causes the coefficients to establish at a high level for osmotic pressures $\Delta\pi$ greater than 10 kPa, which may indicate a strong coupling between membrane structure and electrolyte flux through the membrane for high KCl osmotic pressure values on the membrane.

The dependencies $(\Phi_S)_L = f(\Delta\pi)$, $(\Phi_F)_L = f(\Delta\pi)$ and $(\Phi_U)_L = f(\Delta\pi)$ calculated based on Equation 16,18,19 for the Textus Bioactiv Ag membrane are presented in Fig. 8. The calculations were performed for a fixed difference of hydrostatic pressures $\Delta P = 40$ kPa and different $\Delta\pi$.

As for the coupling coefficients, the energy fluxes, to a small extent, depend on $\Delta\pi$ in the range of small values of osmotic pressures on the membrane ($\Delta\pi < 12$ kPa). An increase in the osmotic pressure on the membrane above this range causes an increase in energy fluxes on the membrane. In contrast to the coupling coefficients, which remain nearly constant at the maximum level of osmotic pressures on the membrane, the energy fluxes initially increase strongly (in the range 12 kPa $\leq \Delta\pi \leq 25$ kPa), but then increase slower and slower with increases in osmotic pressures on the membrane. Moreover, in the same $\Delta\pi$ intervals, the largest values are reached by $(\Phi_U)_L$ and the smallest by $(\Phi_S)_L$.

It should be emphasized that the coupling coefficients and the energy fluxes through the Textus Bioactiv Ag membrane do not depend on the direction of applied $\Delta\pi$ on the membrane. This may indicate a different reason for the dependence of these coefficients and fluxes on the osmotic pressures of electrolytes than the 2-layer structure of the membrane. Rather, the reason for these effects may be the changes in the structure of the basic layer of the membrane itself than in the supporting layer.

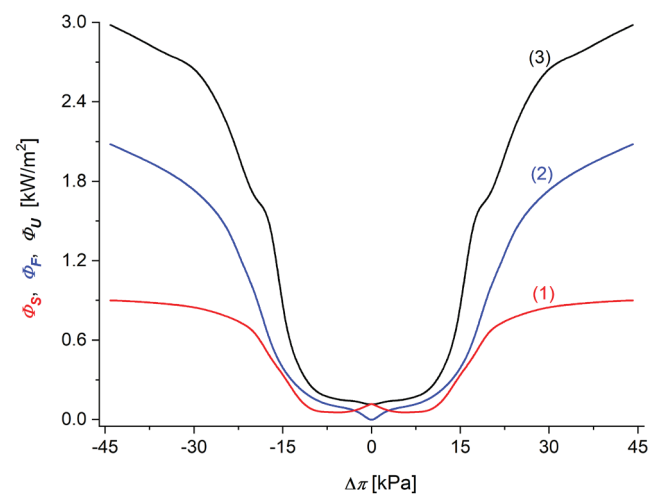


Fig. 8. Illustration of dependencies (1) $(\Phi_S)_L = f(\Delta\pi)$, (2) $(\Phi_F)_L = f(\Delta\pi)$, and (3) $(\Phi_U)_L = f(\Delta\pi)$ for Textus Bioactiv Ag membranes and aqueous KCl solutions

Discussion

The curves presented in Fig. 3–5 show that the dependencies $L_{pT} = f(\bar{C})$, $\omega_T = f(\Delta\pi)$ and $\sigma_T = f(\Delta\pi)$ are nonlinear. The L_{pT} value increases as \bar{C} values increase. In turn, the value of ω_T increases with increasing values of $\Delta\pi$. Contrary to L_{pT} and ω_T , the value of σ_T decreases as the value of $\Delta\pi$ increases. The courses of these curves indicate that the reason for the increase in the values of the L_{pT} and ω_T coefficients and the decrease in the value of the σ_T coefficient with increasing $\Delta\pi$ may be due to the swelling of the membrane fibers. The simultaneous increase in the volume of the membrane leads to an increase in the amount of free space for the electrolytes in the membrane. It is possible that the swelling of the fibers and the loosening of their structure in the membrane can lead to an increase in the porosity of the membrane and reduction in tortuosity of the membrane. This can be called the “relaxation” of the Textus Bioactiv Ag membrane structure under the influence of the electrolyte, and is greater for higher electrolyte concentrations in the membrane. The process of the membrane structure swelling depends on the concentration of KCl in the solutions separated by the membrane and in the membrane itself.

Contrary to the Textus Bioactiv Ag membrane, the values of the coefficients (L_p , ω , σ) of membranes made of regenerated cellulose (Nephrophan) and bacterial cellulose (Biofill) are constant (independent of the concentration of solutions separated by the membrane)^{26,31}. The nature of the dependence of $L_{pT} = f(\bar{C})$, $\omega_T = f(\Delta\pi)$ and $\sigma_T = f(\Delta\pi)$ is reflected in the dependencies of the coefficients $(L_{ij})_T$, as shown in Fig. 6, because these coefficients are a combination of the coefficients L_{pT} , ω_T and σ_T . In turn, the coefficients l_{12} , $(e_{\max})_l$ and Q_l presented in Fig. 7 are a combination of the coefficients L_{pT} , ω_T and σ_T . Equation 16 shows that $(\Phi_S)_L$, $(\Phi_F)_L$ and $(\Phi_U)_L$ are a combination of the coefficients $(L_{11})_T$, $(L_{12})_T = (L_{21})_T$ and $(L_{22})_T$ and thus a combination of L_{pT} , ω_T and σ_T coefficients.

Conclusions

The concentration dependencies of the hydraulic permeability (L_{pT}), reflection (σ_T) and solute permeability (ω_T) coefficients for Textus Bioactiv Ag membrane are nonlinear. Significant changes of these coefficients occur in the range of KCl concentrations from 2 mol/m³ to 4 mol/m³. The characteristics of the Peusner coefficients $(L_{ij})_T = f(\Delta\pi)$ for the Textus Bioactiv Ag membrane are nonlinear. This characteristic feature results in the very slow increase of these coefficients with increasing osmotic pressures on the membrane in ranges lower than 10 kPa and the significantly greater increase in values above these osmotic pressures. For the Textus Bioactiv Ag membrane, the coefficients of coupling $l_{12} = l_{21}$, energy conversion efficiency $(e_{12})_l = (e_{21})_l = (e_{\max})_l$, and Q_L

are functions of the KCl osmotic pressure differences. This means that the processes occurring in the system containing the Textus Bioactiv Ag membrane are almost completely coupled and strong energy conversion interactions occur. For the Textus Bioactiv Ag membrane, the calculated value of free energy production $(\Phi_F)_L$ is many times higher than the value of the energy dissipation function $(\Phi_S)_L$ (e.g., for $\Delta\pi = 44$ kPa, $(\Phi_F)_L$ is over 2 times higher than $(\Phi_S)_L$). This means that the Textus Bioactiv Ag membrane has the highest energy conversion efficiency. The KKP model, by introducing additional coefficients that allow one to take into account the energetic analysis of membrane processes, is a useful tool for exploring the transport properties of biomembranes, and extends the scope of analysis of processes occurring in the membrane.

ORCID iDs

Kornelia M. Batko  <https://orcid.org/0000-0001-6561-3826>
 Izabella Ślęzak-Prochazka  <https://orcid.org/0000-0002-0707-2213>
 Sławomir Marek Grzegorzczyn  <https://orcid.org/0000-0002-5248-3505>
 Anna Pilis  <https://orcid.org/0000-0002-5022-6820>
 Paweł Dolibog  <https://orcid.org/0000-0003-4781-5162>
 Andrzej Ślęzak  <https://orcid.org/0000-0001-6818-2099>

References

- Baker RW. *Membrane Technology and Applications*. 3rd ed. Chichester, UK-Hoboken, USA: John Wiley & Sons; 2012. ISBN:978-1-118-35971-6.
- Giuri D, Barbalinardo M, Sotgiu G, et al. Nano-hybrid electrospun non-woven mats made of wool keratin and hydroalcites as potential bio-active wound dressings. *Nanoscale*. 2019;11(13):6422–6430. doi:10.1039/C8NR10114K
- Dudek-Wicher R, Paleczny J, Brożyna M, Junka A, Bartoszewicz M. Modifications of bacterial cellulose in wound care. *Polim Med*. 2021; 51(2):77–84. doi:10.17219/pim/143330
- Shen S, Chen X, Shen Z, Chen H. Marine polysaccharides for wound dressings application: An overview. *Pharmaceutics*. 2021;13(10):1666. doi:10.3390/pharmaceutics13101666
- Lopez-Mendez TB, Santos-Vizcaino E, Pedraz JL, Orive G, Hernandez RM. Cell microencapsulation technologies for sustained drug delivery: Latest advances in efficacy and biosafety. *J Control Release*. 2021;335:619–636. doi:10.1016/j.jconrel.2021.06.006
- Savencu I, Iurian S, Porfire A, Bogdan C, Tomuța I. Review of advances in polymeric wound dressing films. *Reactive Functional Polym*. 2021;168:105059. doi:10.1016/j.reactfunctpolym.2021.105059
- Kushwaha A, Goswami L, Kim BS. Nanomaterial-based therapy for wound healing. *Nanomaterials*. 2022;12(4):618. doi:10.3390/nano12040618
- Kucharzewski M, Wilemska-Kucharzewska K, Kózka M, Spałkowska M. Leg venous ulcer healing process after application of membranous dressing with silver ions. *Phlebologie*. 2013;42(06):340–346. doi:10.12687/phleb2141-6-2013
- Ślęzak A, Grzegorzczyn S, Ślęzak IH, Bryll A. Study on the volume and solute flows through double-membranous polymeric dressing with silver ions. *J Membrane Sci*. 2006;285(1–2):68–74. doi:10.1016/j.memsci.2006.07.026
- Batko KM, Ślęzak A, Pilis W. Evaluation of transport properties of biomembranes by means of Peusner network thermodynamics. *Acta Bioeng Biomech*. 2021;23(2):63–72. PMID:34846049.
- Batko KM, Ślęzak-Prochazka I, Ślęzak A, Bajdur WM, Włodarczyk-Makuła M. Management of energy conversion processes in membrane systems. *Energies*. 2022;15(5):1661. doi:10.3390/en15051661
- Boeker E, van Grondelle R. *Environmental Physics: Sustainable Energy and Climate Change*. 3rd ed. Chichester, UK: Wiley; 2011. ISBN:978-0-470-66676-0.
- Demirel Y. *Nonequilibrium Thermodynamics: Transport and Rate Processes in Physical, Chemical and Biological Systems*. 3rd ed. Amsterdam, the Netherlands: Elsevier; 2014. ISBN:978-0-444-59581-2.

14. Glaser R. *Biophysics*. Berlin-Heidelberg, Germany: Springer Berlin Heidelberg; 2012. doi:10.1007/978-3-642-25212-9
15. Caplan SR. Nonequilibrium thermodynamics and its application to bioenergetics. In: *Current Topics in Bioenergetics*. Vol 4. Amsterdam, the Netherlands: Elsevier; 1971:1–79. doi:10.1016/B978-0-12-152504-0.50008-3
16. Batko KM, Ślęzak A. Evaluation of the global S-entropy production in membrane transport of aqueous solutions of hydrochloric acid and ammonia. *Entropy*. 2020;22(9):1021. doi:10.3390/e22091021
17. Onsager L. Reciprocal relations in irreversible processes. *Phys Rev*. 1931;37(4):405–426. doi:10.1103/PhysRev.37.405
18. Katchalsky A. *Nonequilibrium Thermodynamics in Biophysics*. Cambridge, USA: Harvard University Press; 2013. ISBN:978-0-674-49412-1.
19. Kedem O, Katchalsky A. Permeability of composite membranes. Part 1. Electric current, volume flow and flow of solute through membranes. *Trans Faraday Soc*. 1963;59(0):1918–1930. doi:10.1039/TF9635901918
20. Peusner L. *Studies in Network Thermodynamics*. Amsterdam, the Netherlands-New York, USA: Elsevier; 1986. ISBN:978-0-444-42580-5.
21. Ślęzak A, Grzegorzczyn S, Batko KM. Resistance coefficients of polymer membrane with concentration polarization. *Transp Porous Med*. 2012;95(1):151–170. doi:10.1007/s11242-012-0038-5
22. Batko KM, Slezak-Prochazka I, Grzegorzczyn S, Slezak A. Membrane transport in concentration polarization conditions: Network thermodynamics model equations. *J Por Media*. 2014;17(7):573–586. doi:10.1615/JPorMedia.v17.i7.20
23. Batko KM, Ślęzak-Prochazka I, Ślęzak A. Network hybrid form of the Kedem–Katchalsky equations for non-homogenous binary non-electrolyte solutions: Evaluation of P_{ij}^* Peusner's tensor coefficients. *Transp Porous Med*. 2015;106(1):1–20. doi:10.1007/s11242-014-0352-1
24. Ślęzak-Prochazka I, Batko KM, Wąsik S, Ślęzak A. H* Peusner's form of the Kedem–Katchalsky equations for non-homogenous non-electrolyte binary solutions. *Transp Porous Med*. 2016;111(2):457–477. doi:10.1007/s11242-015-0604-8
25. Kedem O, Katchalsky A. Thermodynamic analysis of the permeability of biological membranes to non-electrolytes. *Biochim Biophys Acta*. 1958;27:229–246. doi:10.1016/0006-3002(58)90330-5
26. Grzegorzczyn S, Ślęzak A. Kinetics of concentration boundary layers buildup in the system consisted of microbial cellulose biomembrane and electrolyte solutions. *J Membrane Sci*. 2007;304(1–2):148–155. doi:10.1016/j.memsci.2007.07.027
27. Kedem O, Caplan SR. Degree of coupling and its relation to efficiency of energy conversion. *Trans Faraday Soc*. 1965;61:1897. doi:10.1039/tf9656101897
28. Ślęzak A, Grzegorzczyn S, Jasik-Ślęzak J, Michalska-Matecka K. Natural convection as an asymmetrical factor of the transport through porous membrane. *Transp Porous Med*. 2010;84(3):685–698. doi:10.1007/s11242-010-9534-7
29. Ślęzak A. Irreversible thermodynamic model equations of the transport across a horizontally mounted membrane. *Biophys Chem*. 1989;34(2):91–102. doi:10.1016/0301-4622(89)80047-X
30. Grzegorzczyn S, Michalska-Matecka K, Slezak A. Time evolution of NaCl flux through the microbial cellulose membrane with concentration polarization. *Polim Med*. 2008;38(2):11–20. PMID:18810983.
31. Ślęzak A, Jasik-Ślęzak J, Grzegorzczyn S, Ślęzak-Prochazka I. Nonlinear effects in osmotic volume flows of electrolyte solutions through double-membrane system. *Transp Porous Med*. 2012;92(2):337–356. doi:10.1007/s11242-011-9906-7

Irvingia gabonensis (O'Rorke) Bail polymer matrix system for controlled drug delivery

Bernard O. Patani^{1,B,C,F}, Olufunke Dorothy Akin-Ajani^{1,C,D,F}, Arul Kumaran^{2,B,C,F}, Oluwatoyin Adepeju Odeku^{1,A,C-F}

¹ Department of Pharmaceutics and Industrial Pharmacy, University of Ibadan, Nigeria

² KTN College of Pharmacy, Kerala, India

A – research concept and design; B – collection and/or assembly of data; C – data analysis and interpretation; D – writing the article; E – critical revision of the article; F – final approval of the article

Polymers in Medicine, ISSN 0370-0747 (print), ISSN 2451-2699 (online)

Polim Med. 2022;52(2):67–76

Address for correspondence

Oluwatoyin Adepeju Odeku
E-mail: pejuodeku@yahoo.com

Funding sources

None declared

Conflict of interest

None declared

Received on May 20, 2022

Reviewed on July 11, 2022

Accepted on September 5, 2022

Published online on October 19, 2022

Cite as

Patani BO, Akin-Ajani OD, Kumaran A, Odeku OA. *Irvingia gabonensis* (O'Rorke) Bail polymer matrix system for controlled drug delivery. *Polim Med.* 2022;52(2):67–76. doi:10.17219/pim/153521

DOI

10.17219/pim/153521

Copyright

Copyright by Author(s)

This is an article distributed under the terms of the Creative Commons Attribution 3.0 Unported (CC BY 3.0) (<https://creativecommons.org/licenses/by/3.0/>)

Abstract

Background. *Irvingia gabonensis* kernel polymer has gained attention in drug delivery systems because of its compatibility and degradation under natural and physiological conditions.

Objectives. This study aimed to evaluate *Irvingia gabonensis* polymer as a matrix system for the controlled delivery of ibuprofen in comparison to xanthan gum and hydroxypropylmethylcellulose (HPMC).

Materials and methods. *Irvingia gabonensis* polymer was extracted using established methods and dried using the oven- and freeze-drying methods. Ibuprofen tablets were prepared by direct compression and the effects of polymer concentration (10–50%), excipients (lactose, microcrystalline cellulose and dicalcium phosphate dihydrate) and polymers (xanthan gum and HPMC) on the mechanical and drug release properties of the tablets were evaluated. Density measurements and the Heckel and Kawakita equations were used to determine the compression properties of the tablets. Friability, crushing strength and the crushing strength–friability ratio (CSFR) were used to evaluate the mechanical properties of the tablets, while dissolution times were used to evaluate drug release from the matrices. The drug release mechanisms were determined by fitting the dissolution data into classic kinetic equations.

Results. *Irvingia gabonensis* polymer deformed plastically with a fast onset and a high amount of plastic deformation compared with xanthan gum and HPMC. This polymer was directly compressible and formed intact non-disintegrating tablets; the mechanical and dissolution properties of *Irvingia gabonensis* polymer tablets generally decreased with increasing concentration of ibuprofen. The ranking of dissolution times was xanthan gum > freeze-dried *Irvingia gabonensis* > HPMC > oven-dried *Irvingia gabonensis*. The addition of the excipients improved the mechanical properties of the tablets, aided ibuprofen release, and altered the release kinetics, which was largely defined by the Korsmeyer–Peppas model. Increasing the proportion of xanthan gum and HPMC in the matrices resulted in a decreased amount of ibuprofen released after 9 h, with xanthan gum having a greater effect.

Conclusions. *Irvingia gabonensis* polymer matrices may be effective in the preparation of controlled release tablets, and their right combination with xanthan gum or HPMC could provide a time-independent release for longer durations.

Key words: polymer, tablet, compression properties, *Irvingia gabonensis*, controlled release

Introduction

Plant polymers have sparked a lot of interest as excipients in recent years due to their abundance, good biocompatibility, non-toxicity and, in some circumstances, superior drug release properties compared with synthetic polymers.¹ Because of their natural origins, they are appealing and suitable alternatives to the pharmaceutical excipients. There will always be a need to develop new excipients to meet drug formulation-specific requirements and to provide more effective and less expensive alternatives to conventional excipients. Hydrophilic polymers have been widely used as a directly compressible polymeric matrix for controlled and targeted drug delivery of pharmaceutical formulations. The direct compression method is an economical method for the preparation of matrix tablets due to its simple manufacturing process compared to other controlled release systems.^{2,3} Owing to their hydrophilic properties, a variety of natural and modified polymers, including xanthan gum, alginates, guar gum, carrageenan, karaya gum, and khaya gum,^{1,2,4–6} have been successfully used in the preparation of oral controlled release matrix tablets. A few of these polymer matrices are very effective in offering zero-order time-independent drug release kinetics and, in some cases, they have outperformed established polymers.

The seeds of *Irvingia gabonensis* (O'Rorke) Bail (Irvingiaceae family), also known as African bush mango or wild mango, has recently gained much interest. *Irvingia gabonensis* seed contains lipids and polymeric substances; the lipids from its seed are useful as a suppository base,⁷ tableting lubricant⁸ and sustained release agent⁹; additionally, the mucilage has been used as emulsifying and suspending agent,¹⁰ polymer for microbead formulations¹¹ and tablet binder.⁴ When *Irvingia gabonensis* was used as a binding agent in metronidazole tablets, they possessed lower mechanical strength and slower drug release properties than standard gelatin binder.⁴ Recent studies have reported the material and compression properties of *Irvingia gabonensis* kernel polymer.¹² The results showed that this polymer was directly compressible and formed intact non-disintegrating tablets with acceptable crushing strength and friability, comparable with standard polymers.¹² *Irvingia gabonensis* kernel polymer provided controlled release of model drugs when used as binding agent in metronidazole tablets and polymer for the formulation of microbeads, indicating its utility as a controlled release polymer.^{4,11} However, the suitability of *Irvingia gabonensis* polymer as a directly compressible excipient for the formulation of controlled release matrix tablets has not been investigated.

Thus, in the present study, *Irvingia gabonensis* polymer was evaluated as a directly compressible controlled release excipient in ibuprofen matrix tablets in comparison with xanthan gum and hydroxypropylmethylcellulose (HPMC).

The tablet properties and drug release from the matrices were studied, as well as the effects of drug concentration, excipient, polymer type, and polymer concentration on the release kinetics of the matrix formulations. Drug release mechanisms were also investigated to determine the effects of formulation excipients and other parameters on the drug release characteristics of matrix tablets.

Materials and methods

Materials

The materials used in the study included: ibuprofen (BASF AG, Ludwigshafen, Germany), microcrystalline cellulose (MCC; Person Pharmaceuticals Ltd., Bockinghenshire, UK), dibasic calcium phosphate anhydrous, dihydrate, dicalcium phosphate (DCP) dihydrate (BDH Chemicals Ltd., Poole, UK), directly compressible lactose (BDH Chemicals Ltd.), xanthan gum (Myprotein Co., Manchester, UK), hydroxypropylmethylcellulose (Ranbaxy Laboratories Ltd., Gurgaon, India), and *Irvingia gabonensis* mucilage (from *Irvingia gabonensis* kernel (dika nut), bought on the local market at Okolobiri, Nigeria). The procedure for the extraction of the polymer has been reported elsewhere.^{4,12}

Preparation of matrix tablets by direct compression

Ibuprofen–polymer matrix tablets were prepared to contain different concentrations (10% w/w, 20% w/w, 30% w/w, and 50% w/w) of ibuprofen. The drug–polymer blend was mixed in a mixer (VSF 3843C; Forster Equipment Co. Ltd., Leicester, UK) for 10 min. Tablets (500 ± 10 mg) were compressed for 30 s at different predetermined loads in a 10.5 mm die, in combination with flat-faced upper and lower punches, using a Carver hydraulic hand press (Model C; Carver Inc., Menomonee Falls, USA). Before compression, the die and flat-faced punches were lubricated with a 1% w/v dispersion of magnesium stearate in acetone. The tablets were then stored in an airtight container over silica gel for 24 h to allow elastic recovery and hardening to occur. Their weight and dimensions were determined, and the relative density of the tablets was calculated.¹³

The effects of excipient (microcrystalline cellulose, lactose and dicalcium phosphate) and polymers (xanthan gum and HPMC) and drug:*Irvingia gabonensis*:polymer ratio (1:3:1, 2:7:1, 2:6:2, 2:5:3, 2:4:4, and 2:0:8) were also evaluated.

Compression properties

The compression properties of the polymers were analyzed using Heckel and Kawakita equations.^{14–18}

The Heckel equation is used to compute the relationship between the relative density of the powder bed during compression (D) and the applied pressure (P), which is expressed as:

$$\ln [1/(1 - D)] = K P + A, \quad (1)$$

where K is the slope of the linear part, which is inversely proportional to the material's mean yield pressure (P_y); and \ln means natural logarithm. The intercept (A) was used to compute the relative density D_A using¹⁹:

$$D_A = 1 - e^{-A} \quad (2)$$

The relative density D_B , which characterizes the phase of rearrangement at low pressures, may be calculated using:

$$D_B = D_A - D_0 \quad (3)$$

The degree of volume reduction (C) in the Kawakita linear model¹⁷ is expressed as:

$$C = (V_o - V_p)/V_o = a b P/(1 + b P), \quad (4)$$

where V_o is the initial bulk volume and V_p is the bulk volume after compression. Equation 5 can be rewritten as:

$$P/C = P/a + 1/ab \quad (5)$$

The constant a defines the minimum porosity of the material before compression, whereas b represents its plasticity. The pressure term P_k is obtained by taking the reciprocal of b .²⁰

Tablet properties

Tablet crushing strength (CS) was determined with a DBK tablet hardness tester (model EHO1; DBK Instruments, Mumbai, India), while the tablet friability (F) was determined with a Thermonik Friability Apparatus (model C-FTA 20; Campbell Electronics, Mumbai, India) for 4 min at 25 rpm (100 revolutions). All tests were done in triplicate.

Disintegration test

The disintegration times of the matrices were determined with a disintegration tester model T-TD20 (Campbell Electronics) in distilled water at $37 \pm 0.5^\circ\text{C}$.

In vitro dissolution studies

The dissolution test was performed using the USP XXIII basket method (model T.DR-6; Kshitij Innovations, Amala, India), with 900 mL media maintained at $37 \pm 0.5^\circ\text{C}$ rotated at 50 rpm. To mimic the GI condition, the media contained 0.1 M hydrochloric acid (pH 1.2) for the first 2 h and Sorensen's phosphate buffer (pH 7.4) for the rest of the experiment. Samples (5 mL) were withdrawn at fixed intervals and replaced with fresh media to maintain a sink

condition. The sample was diluted and ibuprofen release was measured using a ultraviolet (UV) spectrophotometer at 222 nm (UV-Visible Spectrophotometer model U.V. Pharmaspec 1700E, 23 OCE; Shimadzu Corp., Kyoto, Japan). All tests were performed in triplicate.

Drug release kinetics

The in vitro drug release data were fitted to zero-order,^{21–23} first-order,^{22,23} Higuchi,²⁴ Hixson–Crowell,^{25,26} and Korsmeyer–Peppas²⁷ kinetic equations in order to study the mechanism(s) of drug release.

The zero-order equation is as follows^{21–23}:

$$Q = Q_0 + k_0 t, \quad (6)$$

where Q is the amount of drug release at time t ; k_0 is the apparent dissolution rate constant or zero-order release constant; and Q_0 is the initial concentration of the drug in the solution resulting from a burst effect.

The first-order equation is as follows^{22,23}:

$$\ln Q = \ln Q_0 + k_1 t, \quad (7)$$

where k_1 is the first order release constant.

The Higuchi equation is as follows²⁴:

$$Q = k_H t^{1/2}, \quad (8)$$

where k_H is the Higuchi release constant.

The Hixson–Crowell equation is as follows^{25,26}:

$$Q_o^{1/3} - Q^{1/3} = k_s t, \quad (9)$$

where k_s is the constant incorporating the surface/volume ratio.

The Korsmeyer–Peppas equation is as follows²⁷:

$$Qt/Q = k_k t^n, \quad (10)$$

where k_k is the release rate constant which considers the structural and geometric characteristics of the tablet; and n is the diffusional exponent or release exponent, indicative of the drug release mechanism. A value of $n = 0.5$ indicates Fickian Diffusion (Higuchi Matrix), $0.5 < n < 1.0$ indicates anomalous (non-Fickian) diffusion, $n = 1.0$ indicates case II transport (zero-order release), and $n > 1.0$ indicates super case II transport.²⁷

Comparing the correlation coefficient values enabled the identification of the best fit model(s).

Statistical analyses

To compare the effects of the drug concentration, excipients and polymers on the mechanical and drug release properties of the tablets, the analysis of variance (ANOVA) was performed using GraphPad Prism v. 4.0 software (GraphPad Software Inc., San Diego, USA). The Tukey–Kramer multiple comparison post-test was used and $p \leq 0.05$ was considered significant.

Results and discussion

Compression properties of ibuprofen matrix tablets

Representative Heckel plots for matrix tablets containing 20% w/w ibuprofen prepared through direct compression are shown in Fig. 1. The Heckel plots generally exhibited

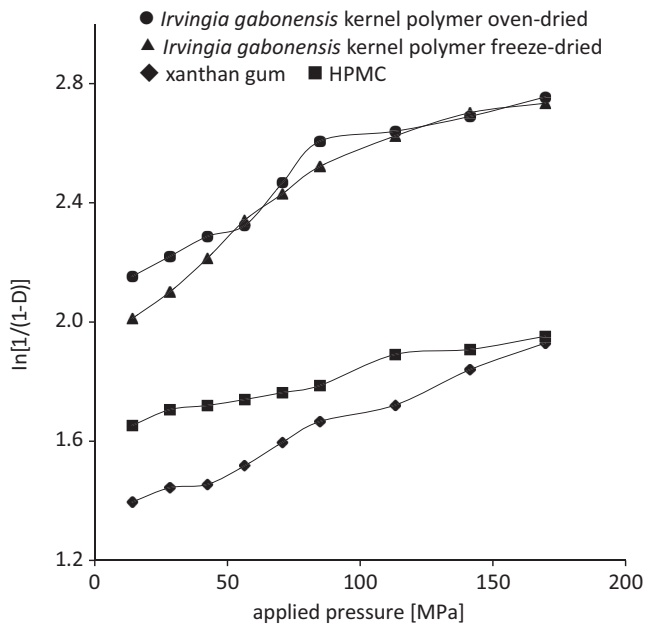


Fig. 1. Heckel plots matrix tablets containing 20% w/w ibuprofen prepared through direct compression

HPMC – hydroxypropylmethylcellulose; ln – natural logarithm; D – density.

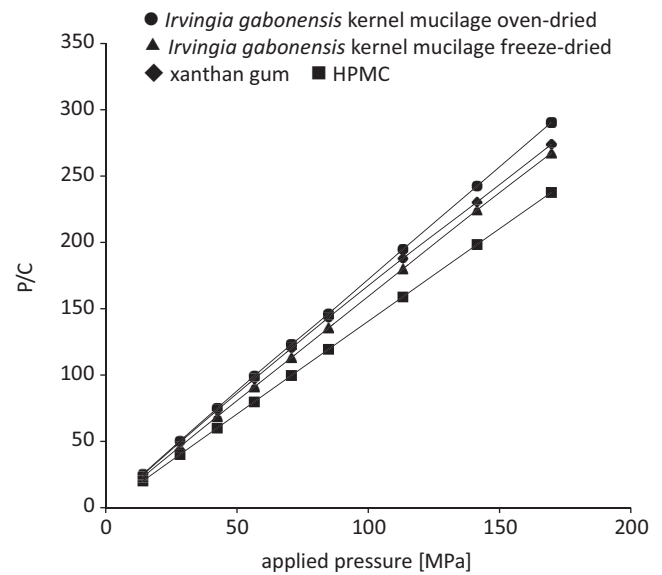


Fig. 2. Kawakita plots for matrix tablets containing 20% w/w ibuprofen prepared through direct compression

HPMC – hydroxypropylmethylcellulose; P/C – pressure/degree of volume reduction.

2 regions or 2 phases of compression for formulations containing *Irvingia gabonensis* polymer.²⁸ The mean yield pressure (P_y) was calculated from the regions of the plots showing the highest correlation coefficient for linearity, with $R \geq 0.990$, generally from 84.82 MPa to 169.69 MPa. Formulations containing HPMC and xanthan gum displayed $R \geq 0.990$ at all compression pressures, indicating that the formulations deformed mainly by plastic flow. Representative

Table 1. Parameters derived from Heckel and Kawakita plots of ibuprofen matrix tablets

Polymer	Concentration of ibuprofen	Heckel plot				Kawakita plot	
		D_0 [g/cm ³]	P_y [MPa]	D_A [g/cm ³]	D_B [g/cm ³]	P_K [MPa]	D_I [g/cm ³]
Oven-dried <i>Irvingia gabonensis</i>	10	0.229	333.33	0.820	0.591	1.638	0.427
	20	0.223	384.62	0.860	0.637	1.376	0.412
	30	0.214	454.55	0.883	0.669	0.799	0.372
	50	0.206	509.09	0.903	0.697	0.254	0.323
Freeze-dried <i>Irvingia gabonensis</i>	10	0.234	250.00	0.832	0.598	1.325	0.392
	20	0.218	263.16	0.872	0.654	1.152	0.363
	30	0.214	333.33	0.890	0.676	1.133	0.350
	50	0.210	500.00	0.905	0.695	1.047	0.337
Xanthan gum	10	0.254	454.55	0.774	0.520	3.266	0.432
	20	0.247	526.32	0.794	0.547	1.808	0.386
	30	0.243	526.32	0.898	0.655	1.299	0.373
	50	0.237	555.56	0.905	0.668	1.299	0.366
HPMC	10	0.202	370.37	0.801	0.599	0.334	0.293
	20	0.199	400.00	0.809	0.610	0.439	0.285
	30	0.197	625.00	0.838	0.641	0.399	0.279
	50	0.194	666.67	0.840	0.646	0.460	0.270

D_0 – relative density at loose packing; P_y – yield pressure; D_A – relative density at zero or low pressure; D_B – relative density at rearrangement phase at low pressures; P_K – pressure required to reduce the powder bed by 50%; D_I – packed initial relative density; HPMC – hydroxymethylpropylcellulose.

Kawakita plots for the matrix tablets containing 20% w/w ibuprofen are presented in Fig. 2 and demonstrate a linear correlation at all compression pressures with $R^2 > 0.999$. The parameters derived from density measurements and the Heckel and Kawakita plots are presented in Table 1.

It was found that the values of D_0 and D_1 decreased with increasing concentration of ibuprofen. The rankings for D_0 and D_1 were found to be xanthan gum > *Irvingia gabonensis* > HPMC. There was no significant difference between the density values for freeze-dried and oven-dried *Irvingia gabonensis* gum, indicating a comparable packing behavior.

In contrast, D_A and D_B increased as the ibuprofen concentration in the formulations increased. The rankings of D_A and D_B were found to be freeze-dried *Irvingia gabonensis* > oven-dried *Irvingia gabonensis* > HPMC > xanthan gum. There was no significant difference between the densification behaviors of the *Irvingia gabonensis* mucilage prepared employing both drying methods.

The P_k and P_y are pressure parameters that are inverse measures of plasticity.²⁹ The P_y relates mainly to the onset of plastic deformation, while P_k relates to the amount of plastic deformation occurring during the compression process.^{13,16} The P_y values of the formulations increased with an increase in the concentration of ibuprofen whereas P_k generally decreased. This suggested that ibuprofen delayed the onset of plastic deformation but increased the total amount of plastic deformation. Materials that are brittle or easily fragmenting are known to have high P_y values, while those that deform plastically or elastically typically exhibit low yield pressure.^{29–31} Thus, the addition of a non-polymeric material, such as ibuprofen, reduced the plasticity of the materials but increased the total amount

of plastic deformation.²⁹ The rankings for the P_y values for the formulations were found to be HPMC > xanthan gum > oven-dried *Irvingia gabonensis* > freeze-dried *Irvingia gabonensis*, while the ranking for P_k was found to be xanthan gum > oven-dried *Irvingia gabonensis* > freeze-dried *Irvingia gabonensis* > HPMC. Thus, formulations containing *Irvingia gabonensis* polymer exhibited a faster onset of plastic deformation than HPMC and xanthan gum, and higher amounts of plastic deformation than xanthan gum, but lower deformation than HPMC. Formulations containing HPMC exhibited the slowest onset of plastic deformation while xanthan exhibited the highest amount. High plastic deformation has been related to tablets with high crushing strength and a greater ability to withstand rigorous handling.²⁸

Effect of drug concentration

The mechanical and drug release properties of the ibuprofen matrices are shown in Table 2. It was found that the crushing strength of the matrix tablets decreased with increasing concentration of ibuprofen in the matrix tablets, while the friability increased. The ranking of the crushing strength was found to be HPMC > xanthan gum > freeze-dried > oven-dried *Irvingia gabonensis*; in contrast, the ranking was reversed for friability. Studies have shown that crushing strength assesses the strength of the tablet while friability tests assess the weakness of the tablet; the greater the crushing strength–friability ratio (CSFR), the stronger the tablet.^{1,13,29} It was determined that tablet crushing strength decreased with an increase in drug concentration, with the following ranks: HPMC > xanthan

Table 2. Effect of drug concentration on the mechanical and drug release properties of ibuprofen matrix tablets

Polymer	Ibuprofen concentration [% w/w]	Crushing strength [N]	Friability [%]	CSFR	t_{25} [h]
Oven-dried <i>Irvingia gabonensis</i>	10	15.33 ± 0.15	0.87 ± 0.00	17.62	3.25
	20	10.00 ± 0.26	0.94 ± 0.03	10.64	2.30
	30	8.67 ± 0.35	1.06 ± 0.07	8.18	1.90
	50	7.33 ± 0.25	2.79 ± 0.47	2.63	1.05
Freeze-dried <i>Irvingia gabonensis</i>	10	18.33 ± 0.46	0.74 ± 0.00	24.47	3.60
	20	12.00 ± 0.36	0.82 ± 0.07	14.63	3.40
	30	9.00 ± 0.10	0.89 ± 0.08	10.11	2.70
	50	8.67 ± 0.31	1.66 ± 0.20	5.22	1.95
Xanthan gum	10	73.67 ± 0.56	0.20 ± 0.00	368.35	5.75
	20	55.66 ± 0.97	0.34 ± 0.03	163.74	4.20
	30	52.33 ± 0.38	0.35 ± 0.33	149.51	3.90
	50	47.00 ± 0.89	0.42 ± 0.42	111.90	3.65
HPMC	10	91.33 ± 0.64	0.00 ± 0.00	–	3.70
	20	69.68 ± 0.25	0.24 ± 0.00	290.29	2.70
	30	60.00 ± 0.40	0.28 ± 0.15	214.29	2.25
	50	54.69 ± 0.42	0.34 ± 0.07	160.79	1.80

CSFR – crushing strength–friability ratio; HPMC – hydroxymethylpropylcellulose; t_{25} – time for 25% drug release.

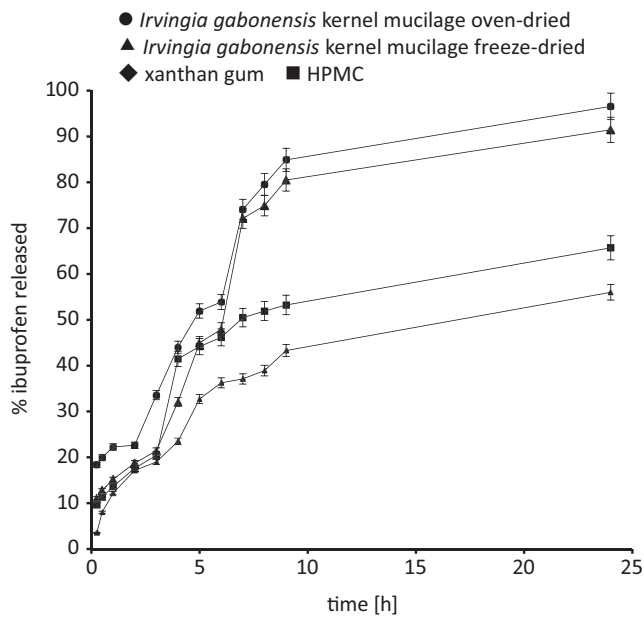


Fig. 3. Dissolution profiles of ibuprofen matrix tablets containing 20% w/w drug concentration

HPMC – hydroxymethylpropylcellulose.

gum > oven-dried *Irvingia gabonensis* > freeze-dried *Irvingia gabonensis*. Polymers are known to undergo plastic deformation, resulting in increased solid bond formation, which increases the strength of the tablet.^{32,33} However, the addition of drugs into the polymer reduces the number of solid bonds within the polymer, causing a decrease in tablet strength and an increase in friability. There were statistically significant differences ($p < 0.05$)

in the crushing strength, CSFR and friability values for all the polymers. Freeze-dried *Irvingia gabonensis* kernel produced tablets with significantly higher ($p < 0.05$) crushing strength and CSFR, and lower friability values than oven-dried *Irvingia gabonensis* kernel polymer.

The drug release profiles of ibuprofen tablets containing different drug concentrations are shown in Fig. 3, and the time for 25% drug release (t_{25}) is shown in Table 2. It was observed that the dissolution time decreased with an increase in drug concentration in the matrix. The decrease in tablet dissolution times could be attributed to the high concentration of the drug weakening the matrix lattice, which provides a diffusion pathway for matrix erosion/disintegration.³⁴ The ranking of t_{25} for the formulation was xanthan gum > HPMC > freeze-dried *Irvingia gabonensis* > oven-dried *Irvingia gabonensis*. Thus, the formulation containing *Irvingia gabonensis* polymer exhibited a faster dissolution rate, while xanthan gum showed the slowest dissolution rate.

Drug release kinetics from dosage forms are critical in improving the frequency of administration, bioavailability, patient acceptability, and, in many cases, the occurrence of harmful or toxic consequences.³⁵ The correlation coefficients obtained from the kinetic equations indicating the best fit for each of the models are presented in Table 3. The diffusional exponent or release exponent (n), obtained from the Korsmeyer–Peppas equation, is indicative of the drug release mechanism.²⁷ The drug release parameters derived from the Korsmeyer–Peppas equation for the matrices showed super case II drug release kinetics with $n > 1.0$. This indicates that drug release from these

Table 3. Drug release parameters for ibuprofen matrix tablets obtained from different release models

Polymer	Ibuprofen concentration (% w/w)	Zero-order		First-order		Higuchi		Hixson–Crowell		Korsmeyer		
		k_0 (h^{-1})	R^2	k	R^2	k_h	R^2	k	R^2	k	R^2	n
Oven-dried <i>Irvingia gabonensis</i>	10	3.74	0.685	0.05	0.855	22.17	0.842	1.33	0.850	0.53	0.882*	1.28
	20	3.69	0.722	0.06	0.947*	21.74	0.877	1.16	0.862	0.44	0.882	1.41
	30	3.75	0.719	0.08	0.972*	22.14	0.876	1.16	0.868	0.43	0.891	1.43
	50	2.94	0.680	0.03	0.764	17.66	0.858	1.03	0.913	0.40	0.939*	1.42
Freeze-dried <i>Irvingia gabonensis</i>	10	3.77	0.688	0.04	0.822	22.17	0.833	1.38	0.841	0.57	0.880*	1.21
	20	3.83	0.705	0.05	0.875	22.58	0.853	1.36	0.856	0.56	0.890*	1.25
	30	3.83	0.711	0.05	0.900	22.67	0.870	1.34	0.889	0.54	0.920*	1.30
	50	3.01	0.631	0.03	0.662	18.38	0.823	1.18	0.906	0.48	0.934*	1.32
Xanthan gum	10	2.06	0.843	0.03	0.898	11.81	0.957	1.22	0.968	0.67	0.980*	0.86
	20	1.93	0.712	0.01	0.778	11.78	0.910	1.16	0.972*	0.59	0.956	1.03
	30	1.96	0.679	0.01	0.740	12.09	0.889	1.12	0.968*	0.56	0.951	1.10
	50	1.69	0.690	0.01	0.751	10.38	0.900	0.99	0.968*	0.49	0.937	1.12
HPMC	10	1.91	0.670	0.01	0.713	11.73	0.867	1.01	0.939	0.47	0.952*	1.16
	20	1.90	0.466	0.01	0.512	12.79	0.729	1.10	0.891	0.49	0.891*	1.25
	30	1.92	0.461	0.01	0.508	13.02	0.725	1.10	0.895	0.48	0.895*	1.28
	50	1.55	0.439	0.01	0.477	10.70	0.717	0.10	0.916*	0.47	0.905	1.26

* drug release kinetics with the highest correlation coefficient; HPMC – hydroxymethylpropylcellulose; k_0 – the apparent dissolution rate constant or zero-order release constant; k_h – Higuchi constant.

formulations is controlled by more than one process, usually a combination of diffusion and erosion mechanisms. Drug release from hydrophilic matrices, such as HPMC, has been attributed to the formation of a strong viscous gel when the polymer hydrates in contact with water.^{32,36}

Effect of excipients

Directly compressible excipients have been used to change the size of drug tablets and to enhance their mechanical characteristics and compression.³⁷ Although the mechanical properties of ibuprofen tablets prepared with *Irvingia gabonensis* mucilage were acceptable, the tablets became more friable (friability > 1%) as the drug concentration increased.³⁸ Therefore, 3 direct compressible excipients, namely MCC, lactose and dicalcium phosphate (DCP), were added to the matrix tablet formulation in the drug–polymer–excipient at a ratio of 1:3:1. It was found that the mechanical and drug release properties of the tablets (Table 4) with added excipients were significantly ($p < 0.001$) higher than those without added excipients. The crushing strength and CSFR of the formulations increased, while the friability decreased upon addition of the excipients. There was a significant difference ($p < 0.001$) in the crushing strength, friability and CSFR of matrix tablets that contained the excipients and of those containing the binary mixtures of ibuprofen–polymer. The ranking of the excipient effect on the crushing strength and CSFR was found to be DCP > lactose > MCC. The ranking was reversed for friability. Comparing all of the polymers, the ranking of excipient effect on crushing strength and CSFR was HPMC > xanthan gum > freeze-dried *Irvingia gabonensis* > oven-dried *Irvingia gabonensis* polymer, and it was reversed for friability. Generally, the matrix tablets containing the 3 different excipients had friability values <1%, and thus had enhanced ability

to withstand the rigours involved in transport and handling of the formulations.

The addition of the excipients in the matrix tablet formulations facilitated the release of ibuprofen from the tablets. Lactose and MCC had lower t_{25} values than DCP, although there was no significant difference ($p > 0.05$) in the dissolution time (t_{25} and t_{50} – time for 25% and 50% drug release, respectively) in both oven- and freeze-dried *Irvingia gabonensis* kernel matrices. Lactose is a water-soluble excipient that dissolves upon contact with the dissolution media creating a diffusion pathway for the release of the drug. On the other hand, MCC, though water-insoluble, may have largely acted through its disintegrant property, which could facilitate the breakup of the matrix tablet. Collectively, these properties of MCC could increase the dissolution rate and thus cause a faster release of the drug.³²

Unlike *Irvingia gabonensis* kernel polymer, xanthan gum and HPMC standard polymers containing the excipients facilitated a slower release of ibuprofen, as shown by the higher dissolution times. The t_{25} values of xanthan gum and HPMC matrices that contained the excipients were significantly ($p < 0.001$) higher than the values for *Irvingia gabonensis* kernel matrices with the 3 excipients. Hydrophilic polymers such as HPMC have been shown to facilitate prolonged drug release from matrix tablets due to the formation of a strong viscous gel when the polymer hydrates come into contact with an aqueous medium.^{1,39}

The correlation coefficients from the different dissolution kinetic equations used to determine the drug release kinetics are presented in Table 5. The results showed that drug release from matrix tablets followed the first-order and Korsmeyer kinetic models. The mechanism of drug release depended on the type of polymer and excipient used in the formulation. There appeared to be an interaction between the polymer and excipients, which affected the rate of drug release from the matrix

Table 4. Effect of excipient on the mechanical and drug release properties of ibuprofen matrix tablets

Polymer	Composition (drug:polymer:excipient)	Crushing strength [N]	Friability [%]	CSFR	t_{25} [h]	t_{50} [h]
Oven-dried <i>Irvingia gabonensis</i>	MCC	41.00 ± 0.46	0.40 ± 0.05	102.50	0.50	2.20
	lactose	45.00 ± 0.75	0.36 ± 0.04	125.00	0.55	2.40
	DCP	51.67 ± 0.80	0.35 ± 0.03	147.62	0.85	2.80
Freeze-dried <i>Irvingia gabonensis</i>	MCC	44.00 ± 0.43	0.38 ± 0.03	115.79	0.70	3.15
	lactose	53.00 ± 0.66	0.32 ± 0.04	165.63	0.70	3.30
	DCP	63.33 ± 0.32	0.27 ± 0.02	234.57	2.20	3.50
Xanthan gum	MCC	73.06 ± 0.78	0.21 ± 0.14	347.62	4.75	5.67
	lactose	78.00 ± 0.26	0.18 ± 0.02	433.33	4.70	5.67
	DCP	83.67 ± 0.40	0.14 ± 0.06	597.62	4.80	5.85
HPMC	MCC	87.33 ± 0.85	0.13 ± 0.04	671.77	4.30	5.65
	lactose	90.20 ± 0.76	0.09 ± 0.00	1003.67	4.20	5.75
	DCP	98.67 ± 0.31	0.00 ± 0.00	98.67	4.65	5.85

HPMC – hydroxymethylpropylcellulose; CSFR – crushing strength–friability ratio; MCC – microcrystalline cellulose; DCP – dicalcium phosphate; t_{25} – time for 25% drug release; t_{50} – time for 50% drug release.

Table 5. Drug release parameters of ibuprofen matrix tablets containing different tablet excipients obtained from different release kinetic models

Polymer	Composition (drug:polymer:excipient)	Zero-order		First-order		Higuchi		Hixson–Crowell		Korsmeyer		
		k_0 (h ⁻¹)	R ²	k	R ²	k_H	R ²	k	R ²	k	R ²	n
Oven-dried <i>Irvingia gabonensis</i>	MCC	3.37	0.785	0.08	0.982	22.37	0.950	1.36	0.988	0.49	0.988*	1.49
	lactose	3.47	0.688	0.08	0.946	22.64	0.887	1.36	0.962*	0.49	0.949	1.48
	DCP	3.40	0.698	0.08	0.929	23.20	0.888	1.55	0.954*	0.58	0.946	1.34
Freeze-dried <i>Irvingia gabonensis</i>	MCC	2.77	0.608	0.09	0.941*	17.34	0.828	0.82	0.923	0.26	0.890	1.72
	lactose	3.66	0.652	0.11	0.973*	23.61	0.860	1.34	0.938	0.46	0.915	1.52
	DCP	3.44	0.519	0.95	0.958*	22.09	0.748	1.19	0.861	0.40	0.851	1.58
Xanthan gum	MCC	4.45	0.664	0.06	0.911*	27.93	0.810	2.45	0.872	1.22	0.908	0.60
	lactose	4.69	0.614	0.07	0.843*	29.50	0.754	2.51	0.779	1.22	0.813	0.56
	DCP	4.58	0.588	0.06	0.739	29.01	0.733	2.49	0.782	1.22	0.827*	0.57
HPMC	MCC	4.49	0.625	0.07	0.831	28.46	0.779	2.37	0.877	1.14	0.916*	0.71
	lactose	4.45	0.623	0.08	0.874	28.52	0.793	2.25	0.883	1.01	0.913*	0.86
	DCP	4.54	0.597	0.06	0.756	28.89	0.749	2.38	0.820	1.12	0.864*	0.78

* drug release kinetics with the highest correlation coefficient; MCC – microcrystalline cellulose; DCP – dicalcium phosphate; k_0 – the apparent dissolution rate constant or zero-order release constant; k_H – Higuchi constant.

tablets.¹ The value of release parameters (n) derived from the Korsmeyer kinetics model depended on the excipient. Formulations containing MCC showed the highest values and DCP the lowest. The release mechanism was generally non-Fickian super case II transport for *Irvingia gabonensis* matrix tablets with n values greater than 1. On the other hand, the release from xanthan gum and HPMC matrices was found to be anomalous (non-Fickian) diffusion. This non-Fickian release mechanism implies that drug release is controlled by diffusion or a combination of diffusion and macromolecular chain relaxation

mechanisms. The above indicates that the nature and type of excipients appeared not to alter the release mechanism of formulations.

Effect of polymers

One method for achieving controlled time-independent release is to use a polymer mixture to achieve sustained release over the desired time. If the 2 polymers are carefully chosen and used in appropriate quantities, it should be possible to create a polymer system with

Table 6. Effect of polymer on the mechanical and drug release properties of ibuprofen matrix tablets

Polymer	<i>Irvingia gabonensis</i> polymer	Composition (drug: <i>Irvingia gabonensis</i> : polymer)	Crushing strength [N]	Friability [%]	CSFR	t_{25} [h]	t_{50} [h]	% of drug released after 9 h
HPMC	oven-dried <i>Irvingia gabonensis</i>	2:7:1	25.00 ± 0.40	0.88 ± 0.18	28.41	1.18	4.0	68.96
		2:6:2	14.00 ± 0.60	4.67 ± 0.11	3.00	1.20	4.4	66.16
		2:5:3	12.00 ± 0.80	4.85 ± 0.18	2.47	1.33	6.1	64.95
		2:4:4	17.50 ± 1.66	1.95 ± 0.10	8.97	1.38	6.6	60.93
	freeze-dried <i>Irvingia gabonensis</i>	2:7:1	26.33 ± 0.21	0.83 ± 0.03	31.73	1.10	4.2	67.99
		2:6:2	19.67 ± 0.97	1.97 ± 0.24	9.98	1.30	5.5	66.04
		2:5:3	17.33 ± 0.70	2.19 ± 0.25	7.91	1.40	6.4	61.91
		2:4:4	18.67 ± 0.31	2.03 ± 0.04	9.20	1.55	7.3	58.38
Xanthan gum	oven-dried <i>Irvingia gabonensis</i>	2:7:1	17.00 ± 0.36	0.76 ± 0.00	22.37	1.30	4.4	66.89
		2:6:2	12.33 ± 0.50	1.33 ± 0.14	9.27	1.50	5.4	64.09
		2:5:3	8.00 ± 0.35	0.78 ± 0.02	10.26	1.70	6.5	58.26
		2:4:4	14.67 ± 0.31	1.80 ± 0.17	8.15	1.80	7.2	56.43
	freeze-dried <i>Irvingia gabonensis</i>	2:7:1	18.67 ± 0.15	0.27 ± 0.07	69.14	1.30	5.3	65.92
		2:6:2	13.00 ± 0.40	0.56 ± 0.00	23.21	1.50	5.7	62.92
		2:5:3	10.33 ± 0.25	0.43 ± 0.01	24.03	1.60	7.0	56.07
		2:4:4	15.34 ± 0.57	1.04 ± 0.03	14.74	1.80	7.8	55.34

CSFR – crushing strength–friability ratio; HPMC – hydroxymethylpropylcellulose; t_{25} – time for 25% drug release; t_{50} – time for 50% drug release.

Table 7. Drug release parameters of ibuprofen matrix tablets containing hydroxymethylpropylcellulose (HPMC) and xanthan gum obtained from different release kinetic models

Polymer	<i>Irvingia gabonensis</i> polymer	Composition (drug: <i>Irvingia gabonensis</i> : polymer)	Zero-order		First-order		Higuchi		Hixson–Crowell		Korsmeyer		
			k_0 (h ⁻¹)	R ²	k	R ²	k_h	R ²	k	R ²	k	R ²	n
HPMC	oven-dried <i>Irvingia gabonensis</i>	2:7:1	3.37	0.782	0.05	0.995*	20.01	0.964	1.24	0.993	0.50	0.972	1.37
		2:6:2	3.37	0.805	0.05	0.993	19.81	0.974	1.26	0.997*	0.52	0.974	1.34
		2:5:3	3.40	0.824	0.05	0.993*	19.80	0.976	1.30	0.990	0.55	0.963	1.29
		2:4:4	3.37	0.850	0.05	0.986*	19.34	0.978	1.33	0.977	0.59	0.928	1.24
	freeze-dried <i>Irvingia gabonensis</i>	2:7:1	3.09	0.738	0.04	0.963	18.70	0.943	1.25	0.981*	0.53	0.936	1.34
		2:6:2	3.14	0.759	0.04	0.967	18.81	0.952	1.29	0.988*	0.56	0.951	1.29
		2:5:3	3.12	0.799	0.03	0.964	18.31	0.959	1.28	0.983*	0.56	0.958	1.25
		2:4:4	3.15	0.852	0.03	0.987	18.06	0.981	1.31	0.982*	0.61	0.944	1.18
Xanthan gum	oven-dried <i>Irvingia gabonensis</i>	2:7:1	3.19	0.763	0.04	0.977	19.08	0.957	1.26	0.996*	0.53	0.993	1.32
		2:6:2	3.27	0.803	0.04	0.984	19.19	0.969	1.29	0.991*	0.55	0.974	1.30
		2:5:3	3.23	0.850	0.04	0.992*	18.61	0.983	1.27	0.986	0.56	0.975	1.24
		2:4:4	3.27	0.859	0.03	0.991*	18.69	0.984	1.39	0.987	0.67	0.961	1.12
	freeze-dried <i>Irvingia gabonensis</i>	2:7:1	3.15	0.761	0.04	0.966	18.85	0.954	1.32	0.987*	0.58	0.945	1.27
		2:6:2	3.25	0.790	0.04	0.970	19.14	0.960	1.38	0.984*	0.62	0.951	1.20
		2:5:3	3.21	0.825	0.03	0.980	18.64	0.973	1.40	0.984*	0.66	0.942	1.14
		2:4:4	3.25	0.854	0.03	0.986	18.62	0.980	1.45	0.986*	0.71	0.955	1.07

* drug release kinetics with the highest correlation coefficient; k_0 – the apparent dissolution rate constant or zero-order release constant; k_h – Higuchi constant.

a time-independent release.^{1,40} The mechanical and drug release properties of ibuprofen tablets prepared with a polymer mixture of *Irvingia gabonensis* kernel polymer and standard polymers, xanthan gum and HPMC are shown in Table 6. The results showed that tablets prepared with the drug:*Irvingia gabonensis*:polymer ratio of 2:7:1 exhibited significantly higher ($p < 0.05$) mechanical strength than those containing higher concentrations of the standard polymers. Formulations containing HPMC showed higher mechanical strength than those containing xanthan gum. The amount of ibuprofen released after 9 h ranged from 55.34% w/w to 68.96% w/w. Formulations containing HPMC generally showed a slower drug release. There was no significant ($p > 0.05$) difference in the drug release properties of the formulations.

The parameters obtained from the different drug release kinetic equations (Table 7) showed that the release kinetics from the oven-dried *Irvingia gabonensis* kernel polymer with xanthan gum and HPMC generally followed the first-order release kinetics, whereas the release of ibuprofen from freeze-dried *Irvingia gabonensis* kernel polymer matrices containing HPMC and xanthan gum followed the Hixson–Crowell model. The release parameters (n) derived from the Korsmeyer kinetics model indicated that the drug release from the matrix was super case II, suggesting time-independent release kinetics. Thus, the release kinetics of ibuprofen from the matrix tablets prepared with polymer blends appeared independent of the type and concentration of the standard polymer in the polymer blend.

Conclusions

Our results suggest that *Irvingia gabonensis* polymer is suitable as a directly compressible excipient for the formulation of ibuprofen tablets, comparable to xanthan gum and HPMC. Increasing ibuprofen concentration generally decreased the mechanical and dissolution properties of drug tablets. Inclusion of excipients improved tablet mechanical properties, aided ibuprofen release and altered the release kinetics, which was largely defined by the Korsmeyer–Peppas model. Increasing the proportion of xanthan gum and HPMC in the matrices resulted in a decreased amount of ibuprofen released after 9 h, with xanthan gum having the greatest effect. *Irvingia gabonensis* polymer could be effective for the preparation of controlled release tablets, and the right combination with xanthan gum or HPMC could provide a time-independent release for longer durations.

ORCID iDs

Bernard O. Patani  <https://orcid.org/0000-0002-1312-7022>
 Olufunke Dorothy Akin-Ajani  <https://orcid.org/0000-0002-8790-3653>
 Arul Kumaran  <https://orcid.org/0000-0001-8052-4530>
 Oluwatoyin Adepeju Odeku  <https://orcid.org/0000-0002-0732-1304>

Reference

- Bamiro OA, Odeku OA, Sinha VR, Kumar R. Terminalia gum as a directly compressible excipient for controlled drug delivery. *AAPS PharmSciTech*. 2012;13(1):16–23. doi:10.1208/s12249-011-9712-0
- Abu Fara D, Dadou SM, Rashid I, et al. A direct compression matrix made from xanthan gum and low molecular weight chitosan designed to improve compressibility in controlled release tablets. *Pharmaceutics*. 2019;11(11):603. doi:10.3390/pharmaceutics11110603

3. Zhao H, Zhao L, Lin X, Shen L. An update on microcrystalline cellulose in direct compression: Functionality, critical material attributes, and co-processed excipients. *Carbohydr Polym.* 2022;278:118968. doi:10.1016/j.carbpol.2021.118968
4. Odeku OA, Patani BO. Evaluation of dika nut mucilage (*Irvingia gabonensis*) as binding agent in metronidazole tablet formulations. *Pharm Dev Technol.* 2005;10(3):439–446. doi:10.1081/PDT-54477
5. Varshosaz J, Tavakoli N, Kheirollahi F. Use of hydrophilic natural gums in formulation of sustained-release matrix tablets of tramadol hydrochloride. *AAPS PharmSciTech.* 2006;7(1):E168–E174. doi:10.1208/pt070124
6. Patil SH, Talele GS. Natural gum as mucoadhesive controlled release carriers: Evaluation of cefpodoxime proxetil by D-Optimal design technique. *Drug Deliv.* 2014;21(2):118–129. doi:10.3109/10717544.2013.834416
7. Akin-Ajani O, Odeku O, Babalola Y. Formulation of paediatric paracetamol suppositories using shea butter and dika fat as suppository bases. *Trop J Nat Prod Res.* 2019;3(2):31–36. doi:10.26538/tjnpr/v3i2.2
8. Onyechi JO, Udeala OK. The tableting properties of dika fat lubricant. *Drug Dev Ind Pharm.* 1990;16(7):1203–1216. doi:10.3109/03639049009114937
9. Ofoefule SI, Chukwu A, Okore VC, Ugwah MO. Use of dika fat in the formulation of sustained release frusemide encapsulated granules. *Boll Chim Farm.* 1997;136(10):646–650. PMID:9528173.
10. Isimi CY, Kunle OO, Bangudu AB. Some emulsifying and suspending properties of the mucilage extracted from kernels of *Irvingia gabonensis*. *Boll Chim Farm.* 2000;139(5):199–204. PMID:11213437.
11. Odeku OA, Okunlola A, Lamprecht A. Microbead design for sustained drug release using four natural gums. *Int J Biol Macromol.* 2013;58:113–120. doi:10.1016/j.ijbiomac.2013.03.049
12. Patani BO, Akin-Ajani O, Kumaran A, Odeku O. Material and compressional properties of *Irvingia gabonensis* (O'Rorke) Bail polymers. *J Excipients Food Chem.* 2022;13(2):64–76. <https://jefc.scholasticahq.com/article/36809-material-and-compressional-properties-of-irvingia-gabonensis-o-rorke-bail-polymers>. Accessed September 8, 2022.
13. Odeku OA, Itiola OA. Evaluation of the effects of khaya gum on the mechanical and release properties of paracetamol tablets. *Drug Dev Ind Pharm.* 2003;29(3):311–320. doi:10.1081/DDC-120018205
14. Odeku OA, Itiola OA. Characterization of khaya gum as a binder in a paracetamol tablet formulation. *Drug Dev Ind Pharm.* 2002;28(3):329–337. doi:10.1081/DDC-120002848
15. Akin-Ajani OD, Itiola OA, Odeku OA. Effect of acid modification on the material and compaction properties of fonio and sweet potato starches. *Starch-Stärke.* 2014;66(7–8):749–759. doi:10.1002/star.201300280
16. Sonnergaard JM. A critical evaluation of the Heckel equation. *Int J Pharm.* 1999;193(1):63–71. doi:10.1016/S0378-5173(99)00319-1
17. Kawakita K, Lüdde KH. Some considerations on powder compression equations. *Powder Technol.* 1971;4(2):61–68. doi:10.1016/0032-5910(71)80001-3
18. Heckel R. Density-pressure relationships in powder compaction. *J Trans Metall Soc AIME.* 1961;221(4):671–675. <https://www.semanticscholar.org/paper/Density-Pressure-Relationships-in-Powder-Compaction-R.-Heckel/25aabf88969b3e566248d843bf6291346a1bb930>. Accessed September 8, 2022.
19. Humbert-Droz P, Gurny R, Mordier D, Doelker E. Densification behaviour of drugs presenting availability problems. *J Int J Pharm Tech Prod Mfr.* 1983;4:29–35.
20. Odeku OA, Itiola OA. Evaluation of khaya gum as a binder in a paracetamol tablet formulation. *Pharmacy Pharmacol Commun.* 1998;4(4):183–188. <https://onlinelibrary.wiley.com/doi/abs/10.1111/j.2042-7158.1998.tb00331.x>. Accessed September 8, 2022.
21. Yang L, Fassihi R. Zero-order release kinetics from a self-correcting floatable asymmetric configuration drug delivery system. *J Pharm Sci.* 1996;85(2):170–173. doi:10.1021/js950250r
22. Gibaldi M, Feldman S. Establishment of sink conditions in dissolution rate determinations: Theoretical considerations and application to nondisintegrating dosage forms. *J Pharm Sci.* 1967;56(10):1238–1242. doi:10.1002/jps.2600561005
23. Wagner JG. Interpretation of percent dissolved-time plots derived from in vitro testing of conventional tablets and capsules. *J Pharm Sci.* 1969;58(10):1253–1257. doi:10.1002/jps.2600581021
24. Higuchi T. Rate of release of medicaments from ointment bases containing drugs in suspension. *J Pharm Sci.* 1961;50(10):874–875. doi:10.1002/jps.2600501018
25. Hixson AW, Crowell JH. Dependence of reaction velocity upon surface and agitation. *Ind Eng Chem.* 1931;23(8):923–931. doi:10.1021/ie50260a018
26. Costa P, Sousa Lobo JM. Modeling and comparison of dissolution profiles. *Eur J Pharm Sci.* 2001;13(2):123–133. doi:10.1016/S0928-0987(01)00095-1
27. Kormsmeier RW, Gurny R, Doelker E, Buri P, Peppas NA. Mechanisms of potassium chloride release from compressed, hydrophilic, polymeric matrices: Effect of entrapped air. *J Pharm Sci.* 1983;72(10):1189–1191. doi:10.1002/jps.2600721021
28. Odeku OA. Assessment of *Albizia zygia* gum as a binding agent in tablet formulations. *Acta Pharm.* 2005;55(3):263–276. PMID:16375837.
29. Odeku OA, Fell JT. Effects of the method of preparation on the compression, mechanical, and release properties of khaya gum matrices. *Pharm Dev Technol.* 2006;11(4):435–441. doi:10.1080/10837450600770544
30. Ogunjimi AT, Alebiowu G. Neem gum as a binder in a formulated paracetamol tablet with reference to acacia gum BP. *AAPS PharmSciTech.* 2014;15(2):500–510. doi:10.1208/s12249-014-0079-x
31. Doelker E, Shotton E. The effect of some binding agents on the mechanical properties of granules and their compression characteristics. *J Pharm Pharmacol.* 2011;29(1):193–198. doi:10.1111/j.2042-7158.1977.tb11287.x
32. Odeku OA, Fell JT. Evaluation of khaya gum as a directly compressible matrix system for controlled release. *J Pharm Pharmacol.* 2010;56(11):1365–1370. doi:10.1211/0022357044652
33. Adeoye O, Alebiowu G. Flow, packing and compaction properties of novel coprocessed multifunctional directly compressible excipients prepared from tapioca starch and mannitol. *Pharm Dev Technol.* 2014;19(8):901–910. doi:10.3109/10837450.2013.840843
34. Jamzad S, Tutunji L, Fassihi R. Analysis of macromolecular changes and drug release from hydrophilic matrix systems. *Int J Pharm.* 2005;292(1–2):75–85. doi:10.1016/j.ijpharm.2004.11.011
35. Huang YT, Tsai TR, Cheng CJ, Cham TM, Lai TF, Chuo WH. Formulation design of an HPMC-based sustained release tablet for pyridostigmine bromide as a highly hygroscopic model drug and its in vivo/in vitro dissolution properties. *Drug Dev Ind Pharm.* 2007;33(11):1183–1191. doi:10.1080/03639040701377334
36. Newton AMJ, Lakshmanan P. Effect of HPMC-E15 LV premium polymer on release profile and compression characteristics of chitosan/pectin colon targeted mesalamine matrix tablets and in vitro study on effect of pH impact on the drug release profile. *Recent Pat Drug Deliv Formul.* 2014;8(1):46–62. doi:10.2174/1872211308666140225143926
37. David ST, Augsburger LL. Plastic flow during compression of directly compressible fillers and its effect on tablet strength. *J Pharm Sci.* 1977;66(2):155–159. doi:10.1002/jps.2600660205
38. Mužíková J, Eimerová I. A study of the compaction process and the properties of tablets made of a new co-processed starch excipient. *Drug Dev Ind Pharm.* 2011;37(5):576–582. doi:10.3109/03639045.2010.530270
39. Kim H, Fassihi R. Application of a binary polymer system in drug release rate modulation. 1. Characterization of release mechanism. *J Pharm Sci.* 1997;86(3):316–322. doi:10.1021/js960302s
40. Agarwal V, Nazzal S, Khan MA. Optimization and in vivo evaluation of an oral dual controlled-release tablet dosage form of insulin and duck ovomucoid. *Pharm Dev Technol.* 2008;13(4):291–298. doi:10.1080/10837450802089123

Extracellular product of *Pseudomonas aeruginosa* in growth medium is involved in the pro-inflammatory cytokine response of human oral epithelial cells in vitro

Majid Neamah Ali^{A,B}, Ayaid Khadem Zgair^{A–F}

Department of Biology, College of Science, University of Baghdad, Iraq

A – research concept and design; B – collection and/or assembly of data; C – data analysis and interpretation; D – writing the article; E – critical revision of the article; F – final approval of the article

Polymers in Medicine, ISSN 0370-0747 (print), ISSN 2451-2699 (online)

Polim Med. 2022;52(2):77–82

Address for correspondence

Ayaid Zgair

E-mail: ayaid.zgair@sc.uobaghdad.edu.iq

Funding sources

None declared

Conflict of interest

None declared

Received on June 11, 2022

Reviewed on October 14, 2022

Accepted on October 18, 2022

Published online on November 30, 2022

Abstract

Background. Epithelial cells are the first barrier to any microbial invasion. Finding a safe and affordable substance to stimulate the innate immune response of epithelial cells is one of the main challenges immunologists and vaccine manufacturers are facing.

Objectives. This study aimed to show the comparative effect of sterile bacterial secretion (SBS) and *Pseudomonas aeruginosa* bacterial cell isolates obtained from burn wound infections on the ability of human epithelial cells (HECs) to produce interleukin (IL)-1 β and tumor necrosis factor alpha (TNF- α) in vitro.

Materials and methods. The HEC cultures were exposed to *P. aeruginosa* 8 (Pa 8), Pa 2 and Pa 1 bacterial cells (isolated from burn wound infections). The other 3 groups of HECs were exposed to 50 μ L of sterile, endotoxin-free SBS of Pa 8, Pa 2 and Pa 1. The time course of changes in IL-1 β mRNA, TNF- α mRNA, IL-1 β , and TNF- α was examined.

Results. Moderate ($p < 0.05$) elevations of IL-1 β mRNA in HECs and IL-1 β protein in the supernatant of the HEC culture were observed following exposure to SBS of Pa 8, Pa 2 and Pa 1 at most time points. High elevation ($p < 0.05$) of IL-1 β was seen in the supernatant of the HEC culture that was exposed to bacterial cells (Pa 8, Pa 2 and Pa 1). Similar results were found when TNF- α mRNA was measured in HECs and TNF- α in the supernatant of the HEC cultures after exposure to bacterial cells (Pa 8, Pa 2 and Pa 1) and the SBS of Pa 8, Pa 2 and Pa 1.

Conclusion. This is the first time that the capacity of SBS to generate epithelial cell pro-inflammatory cytokines in vitro has been shown. In other words, SBS enhanced a nonspecific immune response, which opens the door to the possibility of using SBS from *P. aeruginosa* as an adjuvant in the future.

Keywords: human epithelial cells (HECs), interleukin-1, *Pseudomonas aeruginosa*, tumor necrosis factor alpha, sterile bacterial secretion (SBS)

Cite as

Ali MN, Zgair AK. Extracellular product of *Pseudomonas aeruginosa* in growth medium is involved in the pro-inflammatory cytokine response of human oral epithelial cells in vitro. *Polim Med.* 2022;52(2):77–82. doi:10.17219/pim/155849

DOI

10.17219/pim/155849

Copyright

Copyright by Author(s)

This is an article distributed under the terms of the Creative Commons Attribution 3.0 Unported (CC BY 3.0) (<https://creativecommons.org/licenses/by/3.0/>)

Background

Pseudomonas aeruginosa is a highly prevalent pathogen associated with several infectious diseases.¹ Infections with these bacterial isolates have a wide range of illness severity. For the most part, persistent infection with this bacterium creates a distinctive phenotype enclosed by a thick alginate of capsular polysaccharide.² This helps the bacteria survive in the lungs of the host and leads to reduced immune responses against *P. aeruginosa*, which ultimately results in severe respiratory tract infections.³

Pseudomonas aeruginosa has a genetic adaptation that enables it to persist in the body through its ability to evade the immune system and resist antimicrobial agents.⁴ In addition, it was found that a number of *P. aeruginosa* isolates have the ability to secrete substances that enable the bacteria to penetrate the first lines of defense of the respiratory system.⁵ Previous studies have shown that the secretions of bacterial proteolytic enzymes destroy antimicrobial peptides and proteins, which helps the bacteria overcome the host's innate immune system.⁶ Other studies have confirmed the ability of *P. aeruginosa* to stimulate the innate immune system and pro-inflammatory immune system through its structural proteins and surface proteins (i.e., flagella and pili). Further research has shown that bacterial secretions from *P. aeruginosa* may help stimulate the pro-inflammatory immune system.⁷

Epithelial cells are the first barrier in the body in general and in the respiratory system in particular. They protect the body from exposure to chemicals and microorganisms.⁷ These cells work to prevent the entry of pathogenic microorganisms that cause respiratory system infections. Several previous studies have shown the function of human epithelial cells (HECs) in the mucosal innate response of the immune system through their ability to engulf pathogenic microorganisms, as well as secrete mucus substances that contribute to reducing the adhesion of microorganisms and antibacterial substances.⁸ Other studies have shown the ability of these cells to secrete different pro-inflammatory cytokines (interleukin (IL)-1 β and IL-6, and tumor necrosis factor-alpha (TNF- α)) and chemokines (IL-8) after exposure to bacterial cells, which enables the HECs to have a significant effect on the pro-inflammatory immune response.⁹

This study aimed to demonstrate the effect of extracellular secretions from *P. aeruginosa* in growth medium on the ability of epithelial cells to produce pro-inflammatory cytokines in vitro.

Materials and methods

Isolation and identification of bacteria

The standard method developed by Zgair et al. was followed.⁹ Wound swabs were collected from 110 patients suffering from burn wound infections and treated at the Baghdad

Teaching Hospital in Baghdad, Iraq. All individuals gave written informed consent to participate in the study. The patients did not receive any antibiotics for 2 days before sample collection. The swabs were subjected to an asparagine broth enrichment medium to enhance *P. aeruginosa* growth, and incubated for 48 h at 37°C with vigorous shaking at 200 rpm. A loopful of bacterial suspension was streaked onto asparagine plates containing 1.5% agar (HiMedia, Mumbai, India) and incubated at 37°C until colonies developed.⁹ A VITEK 2 DensiCHEK fluorescence instrument system with an ID-GNB card (bioMérieux, Marcy-l'Étoile, France) was used to identify the isolates of *P. aeruginosa*.¹⁰

The study was conducted following approval from the Human Ethical Committee of the University of Baghdad, Iraq (Reference No. HS-212, April 1, 2020).

Preparation of bacterial suspension

Pseudomonas aeruginosa clinical isolates (PAC) isolated from infected wounds were grown in Luria–Bertani (LB) broth (HiMedia) at 37°C for 18 h. Bacterial cell pellets were collected by centrifugation (5000 g for 20 min at 4°C). The collected pellets were washed 3 times with phosphate-buffered saline (PBS) (0.01 M, pH 7.2). The final bacterial counts were adjusted to 2×10^7 colony forming units (CFU)/mL with PBS.¹¹

Preparation of sterile bacterial secretion

The PAC and *P. aeruginosa* environmental isolate (PAE) were grown overnight in LB broth at 37°C (18 h). The supernatants of bacterial growth from the LB broth (sterile bacterial secretion (SBS)) were obtained by centrifugation (5000 g for 20 min at 4°C) and were filtrated using a special Merck Millipore filter (MF-Millipore™ Membrane Filter, 0.22 μ m pore size; Merck Millipore, Waltham, USA). The sterility of the supernatants (SBS) was checked by culturing on LB agar plates.

Oral human epithelial cell culture

The HEC samples were obtained from 4 healthy adult donors (2 females and 2 males) aged 30–35 years. The samples were collected from the oral mucosa by scratching the inner surface of the mouth with sterile sticks. The collected mucus was washed with NaCl (0.15 M, pH 7.1) supplemented with 500 U/mL penicillin and 500 μ g/mL streptomycin (Life Technologies, Carlsbad, USA) at 100 g (10 min, 4°C). The final volume was adjusted to 2 mL with NaCl (0.15 M, pH 7.1). The epithelial cell suspension was placed onto different dilutions of Percoll (Sigma-Aldrich, St. Louis, USA) (30%, 40%, 50%, and 60% of stock isotonic Percoll in the final solution). It was determined using a light microscope (model DM300; Leica Microsystems, Wetzlar, Germany) that the concentration of 40% of the dilute yielded the highest percentage of epithelial cells. Zgair's

standard method was followed to prepare the standard cell culture medium of RPMI 1640 (fetal bovine serum (FBS); Sigma-Aldrich) with all supplements.¹² This medium was used to re-suspend the collected epithelial cell layer. The suspension was washed 3 times with the standard cell culture medium. The number of epithelial cells was adjusted to 5×10^5 cells/mL using the culture medium. The trypan blue dye exclusion method showed that more than 90% of the cells were viable.

Experiment

The standard number of epithelial cells (5×10^5 viable cells/mL) was re-cultured under standard cell culture conditions.¹² The cell cultures were divided into 6 groups of cell culture tubes (Nunc™) (pluriSELECT, Leipzig, Germany). Then, 100 μ L of 10^7 CFU/mL of *P. aeruginosa* 8 (Pa 8), Pa 6 and Pa 1 were added to culture tubes 1, 2 and 3, respectively, while 100 μ L of SBS (Pa 8), SBS (Pa 6) and SBS (Pa 1) were added to culture tubes 4, 5 and 6, respectively. Phosphate-buffered saline was added to the epithelial cell culture as the control subgroup.

Levels of IL-1 β and TNF- α

In a next step, 200 μ L of the supernatants of the tissue cultures of different groups were collected at different time intervals (0 h, 1 h, 6 h, and 24 h) after stimulation with either bacterial cells or bacterial SBS. The collected supernatants were centrifuged at 600 g for 5 min and filtered (MF-Millipore™ Membrane Filter, 0.2 μ m). The prepared supernatants were stored at -20°C until used for enzyme-linked immunosorbent assay (ELISA). The levels of pro-inflammatory cytokines were measured using human TNF- α and human IL-1 β ELISA kits (Koma Biotech Inc., Seoul, South Korea) at a wavelength of 450 nm following the manufacturer's instructions.¹³

IL-1 β and TNF- α mRNA gene expression

Quantitative real-time polymerase chain reaction (RT-PCR) was performed using the ABI Prism 7700 Sequence Detection System (Applied Biosystems, Waltham, USA). RNA was isolated and purified from HECs pelleted from tissue culture at different time intervals (0 h, 1 h, 6 h, 24 h, 48 h, and 72 h) following exposure to either bacterial cells or bacterial SBS using TRIzol reagent (Thermo Fisher Scientific, Waltham, USA). For cDNA synthesis, 1 μ g of total RNA was transcribed with TaqMan Reverse Transcription Reagent (Thermo Fisher Scientific) using random hexamers. The PCR primers of IL-1 β , TNF- α and G3PDH were designed, and RT-PCR was performed as described previously.^{14–17} Quantitative RT-PCR for IL-1 β and TNF- α was performed normalized to the copies of GAPDH mRNA from the same sample. The experiments were conducted in duplicate, and the results were calculated as mean values.

Statistical analyses

Origin 8 software (OriginLab Corporation, Northampton, USA) was used to perform the statistical analyses. The data were expressed as mean \pm standard error ($M \pm SE$). The differences were evaluated using Student's t-test and one-way analysis of variance (ANOVA). The p-values < 0.05 were considered statistically significant.

Results

Pseudomonas aeruginosa isolation and identification

Briefly, 110 infected wound samples were collected from hospitalized patients. Ten isolates of *P. aeruginosa* were isolated and identified. Isolates of Pa 8, Pa 6 and Pa 1 were selected to conduct further experiments, which included evaluating the ability of bacterial cells and their SBS to stimulate epithelial cell cultures to produce IL-1 β and TNF- α .

Pseudomonas aeruginosa and SBS stimulate HECs to produce IL-1 β in vitro

The IL-1 β levels in the HEC cultures after exposure to bacterial cells of *P. aeruginosa* (Pa 8, Pa 6 and Pa 1) and SBS of *P. aeruginosa* (Pa 8, Pa 6 and Pa 1) (test groups) and the HEC culture exposed to PBS (control group) were measured at different time intervals. Figure 1 shows the fold change in mRNA expression of IL-1 β . Significant elevation of IL-1 β expression was seen as early as 1 h after exposure to bacterial cells of *P. aeruginosa* (Pa 8, Pa 6 and Pa 1) and SBS of *P. aeruginosa* (Pa 8, Pa 6 and Pa 1) compared to the IL-1 β expression of the control group (HECs exposed to PBS only). The results indicated that the ability

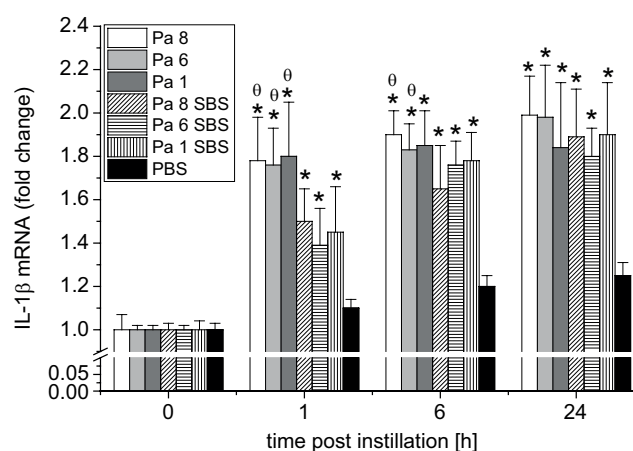


Fig. 1. Time course of changes in interleukin (IL)-1 β mRNA in human epithelial cell (HEC) cultures following exposure to *Pseudomonas aeruginosa* (Pa 8, Pa 6 and Pa 1), and sterile bacterial secretion (SBS) of Pa 8, Pa 6 and Pa 1. Control group: HEC culture exposed to phosphate-buffered saline (PBS; 0.1 M, pH 7.2). [§], p < 0.05 compared to control group A, *, p < 0.05 compared to corresponding SBS

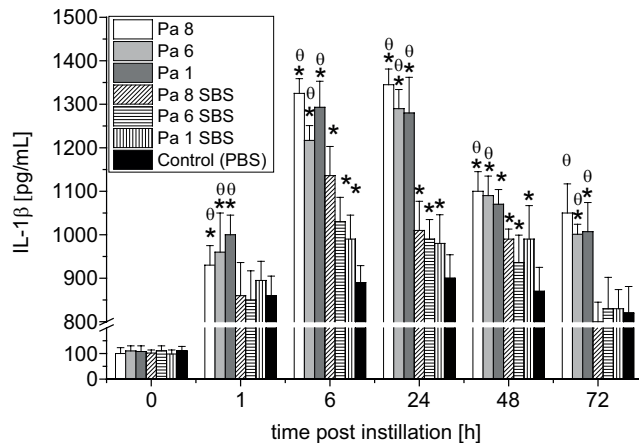


Fig. 2. Time course of changes in interleukin (IL)-1 β [pg/mL] in the supernatant of human epithelial cell (HEC) cultures following exposure to *Pseudomonas aeruginosa* (Pa 8, Pa 6 and Pa 1) and sterile bacterial secretion (SBS) of Pa 8, Pa 6 and Pa 1. Control group: HEC culture exposed to phosphate-buffered saline (PBS; 0.1 M, pH 7.2). θ , $p < 0.05$ compared to control group A, *, $p < 0.05$ compared to corresponding SBS

of bacterial cells to stimulate gene expression was higher than the ability of their SBS to stimulate IL-1 β expression 1 h and 6 h post-exposure.

Figure 2 shows the level of IL-1 β post-exposure to either bacterial cells or bacterial SBS. A significant elevation of IL-1 β was seen as early as 1 h after exposure to bacterial cells of *P. aeruginosa* (Pa 8, Pa 6 and Pa 1) and SBS of *P. aeruginosa* (Pa 8, Pa 6 and Pa 1) compared to the IL-1 β level of the control group (HECs exposed to PBS only) ($p < 0.05$). The results indicated that the IL-1 β level in the HEC culture that was exposed to bacterial cells was higher than the IL-1 β level post-exposure to bacterial SBS ($p < 0.01$) at all time points. The highest levels of IL-1 β were observed 6 h and 24 h after exposure to bacterial cells. The maximum concentrations of IL-1 β in the HEC culture post-exposure to SBS were observed 6 h, 24 h and 48 h post-exposure, with only slight differences related to which bacterial strain the SBS was prepared from. The IL-1 β levels declined over time; the lowest IL-1 β level was observed 72 h post-exposure to bacterial cells and their SBS. At 72 h, the IL-1 β levels in the supernatants of the HEC cultures that were exposed to bacterial cells were higher ($p < 0.05$) than the concentrations of IL-1 β in the supernatants of the HEC cultures that were exposed to SBS and PBS (control). At 72 h, there was no significant difference between the concentrations of IL-1 β in the HEC cultures that were stimulated with SBS and the IL-1 β levels in the HEC culture that was stimulated with PBS ($p > 0.05$).

Pseudomonas aeruginosa and SBS stimulate HECs to produce TNF- α in vitro

Similarly, the TNF- α levels in the oral HEC cultures following exposure to bacterial cells of *P. aeruginosa* (Pa 8, Pa 6 and Pa 1) (test group), SBS of *P. aeruginosa* (Pa 8, Pa 6 and Pa 1) (test group) and PBS (control group) at different

time intervals were measured. Figure 1 shows the fold change in TNF- α mRNA expression. A significant rise in TNF- α expression was observed as early as 1 h post-exposure to *P. aeruginosa* bacterial cells (Pa 8, Pa 6 and Pa 1) and SBS of *P. aeruginosa* (Pa 8, Pa 6 and Pa 1) compared to the TNF- α expression in the control group (HEC culture exposed to PBS only). The results showed that the ability of bacterial cells to stimulate TNF- α gene expression was higher than the ability of their SBS to stimulate TNF- α gene expression 1 h and 6 h post-exposure (Fig. 3).

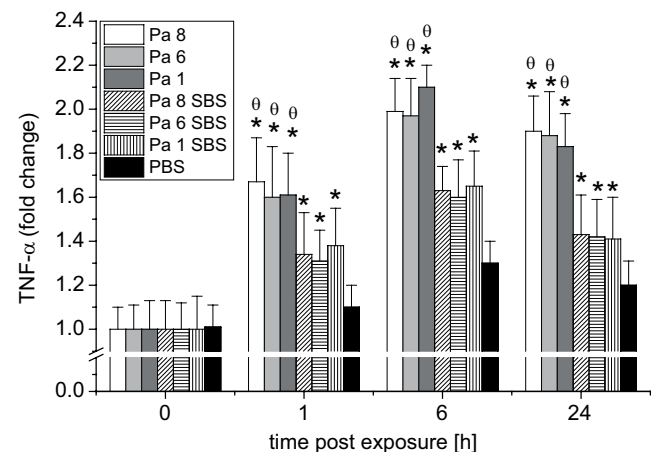


Fig. 3. Time course of changes in tumor necrosis factor alpha (TNF- α) mRNA in human epithelial cell (HEC) cultures following exposure to *Pseudomonas aeruginosa* (Pa 8, Pa 6 and Pa 1) and sterile bacterial secretion (SBS) of Pa 8, Pa 6 and Pa 1. Control group: HEC culture exposed to phosphate-buffered saline (PBS; 0.1 M, pH 7.2). θ , $p < 0.05$ compared to control group A, *, $p < 0.05$ compared to corresponding SBS

The TNF- α levels in the HEC cultures following exposure to either bacterial cells or bacterial SBS were evaluated. Figure 4 illustrates that significant production of TNF- α was seen as early as 1 h after exposure compared to the TNF- α level in the control group HEC culture (exposed to PBS only).

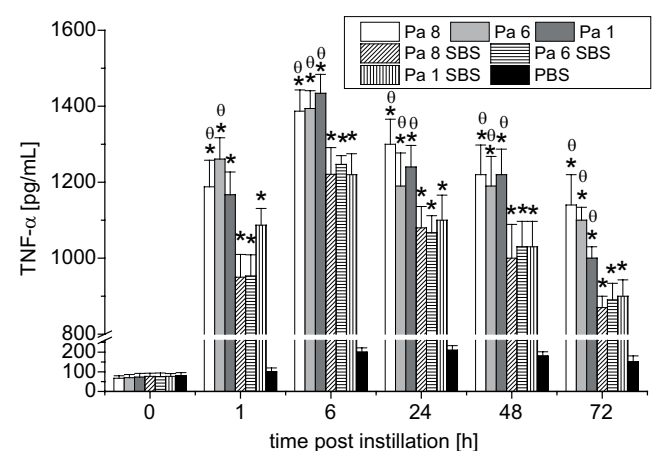


Fig. 4. Time course of changes in tumor necrosis factor alpha (TNF- α) in the supernatant of human epithelial cell (HEC) cultures following exposure to *Pseudomonas aeruginosa* (Pa 8, Pa 6 and Pa 1) and sterile bacterial secretion (SBS) of Pa 8, Pa 6 and Pa 1. Control group: HEC culture exposed to phosphate-buffered saline (PBS; 0.1 M, pH 7.2). θ , $p < 0.05$ compared to control group A, *, $p < 0.05$ compared to corresponding SBS

At that time point, significant ($p < 0.05$) elevations of TNF- α were found in the HEC cultures stimulated with bacterial cells (Pa 8 and Pa 6) compared to the TNF- α levels of the HEC cultures exposed to SBS of Pa 8 and Pa 6. The maximum production of TNF- α was observed at 6 h; after that, TNF- α levels declined dramatically with time. The lowest TNF- α levels were seen 72 h post-exposure to either bacterial cells (Pa 8, Pa 6, and Pa 1) or their SBS. This study demonstrated that *P. aeruginosa* bacterial cells have a higher ability to stimulate HECs to produce TNF- α than their SBS.

Discussion

This study highlights one of the most important type of cells that contribute to the innate immune response. In addition to being a major barrier that prevents the entry of pathogenic microorganisms, HECs play a pivotal role in the primary immune response, as well as in the inflammatory immune response and phagocytosis.¹² Moreover, HECs have a strong ability to produce antibacterial agents (antimicrobial peptides) that prevent pathogenic bacteria from invading the respiratory system.¹⁸

This study involved isolating epithelial cells from healthy donors and then culturing them in RPMI medium and exposing them to 3 *P. aeruginosa* bacterial isolates, as well as stimulating them in vitro with SBS from 3 *P. aeruginosa* isolates. The study showed for the first time that secretions (SBS) of a bacteria (*P. aeruginosa*) in growth medium stimulated oral HECs to produce IL-1 β and TNF- α . However, the ability of SBS to stimulate the epithelial cells to secrete pro-inflammatory cytokines was limited and less pronounced than the ability of *P. aeruginosa* cells to stimulate epithelial cells. This supports the notion that bacterial extracts may be used to stimulate the inflammatory immune response and thereby contribute to enhancing the innate immune response against external pathogens nonspecifically.

The ability of *P. aeruginosa* to stimulate a pro-inflammatory immune response depends on the ability of its surface proteins, as well as flagella and pili, to enhance the immune response of epithelial cells by stimulating them to produce pro-inflammatory cytokines.⁷ The surface receptors of epithelial cells (i.e., Toll-like receptors (TLRs)) have a role in stimulating these cells to respond to bacterial cell proteins. The TLRs bind to pathogen-associated molecular patterns (PAMPs) and thus are one of the pattern recognition receptors. Toll-like receptor 4 (TLR4) binds to flagellin (the structural protein of flagella), which stimulates the cascades of epithelial cell immune responses that ultimately produce pro-inflammatory cytokines.⁸ A similar process occurs when epithelial cells are stimulated by other proteins and other materials produced during *P. aeruginosa* growth in vitro. Molecules that are produced or secreted from bacterial cells or produced when bacterial cells are destroyed, such as nucleic acids and cell membrane lipopolysaccharides, and other enzymes that are produced

by bacterial cells during bacterial growth (PAMPs), activate the innate immune system by binding with specific TLRs. This activates different pathways to produce different pro-inflammatory cytokines and ultimately activates the non-specific immune response against external pathogens.²⁰ Secretions from bacterial cells in growth medium consist of different compounds, and these compounds can stimulate epithelial cells to respond to them. A previous study reported that both intracellular and extracellular sensing play important roles in stimulating the pro-inflammatory immune response via activation of macrophages and other innate immune response arms. This happens through activation of the cellular activation pathway of human cells.²¹

The results of this study are very interesting, as SBS could be used to stimulate the pro-inflammatory immune response, which may lead to a specific immune response when used with a particular vaccine. The study opens the door to the possibility of using SBS as an adjuvant, which would be better than using the whole bacterial body because the bacterial body can cause severe and prolonged inflammatory responses that have negative effects on lung tissue.²² In contrast, in this study, SBS stimulated the pro-inflammatory immune response in a moderate manner and for a limited period, which is what is required to develop a specific immune response when it combines with a particular antigen. This may help improve the immune response against high-risk pathogens (viruses and bacteria). Our laboratory is conducting several experiments concerning the possibility of using this extract to develop a specific immune response against pathogens. We have also conducted several experiments to determine the ability of SBS to stimulate a nonspecific and pro-inflammatory immune response in an animal model. The positive results we have obtained demonstrate that SBS has the ability to stimulate the mucosal innate immune response in mouse lungs (data not yet published). Several previous studies have highlighted the important role of molecules produced during bacterial growth (i.e., quorum-sensing bacteria produce and release chemical signal molecules called autoinducers). These molecules play a central role in biofilm formation and also play a role in the regulation of virulence bacterial factors.²³ In contrast, other studies have shown that nitric oxide produced by *P. aeruginosa* during bacterial growth negatively affected biofilm structure, which helped it dispose of biofilm mass.²⁴

Conclusions

It can be concluded that the extracellular products released in the growth medium after inoculation with *P. aeruginosa* successfully promoted pro-inflammatory cytokine production by HECs in vitro. This phenomenon could be implemented by researchers to yield a safe, effective and affordable pro-inflammatory stimulant that could help augment the immune response against external pathogens, both specifically and nonspecifically.

ORCID iDs

Majid Neamah Ali  <https://orcid.org/0000-0001-7607-0839>

Ayaid Khadem Zgair  <https://orcid.org/0000-0002-2356-3338>

References

- Lyczak JB, Cannon CL, Pier GB. Lung infections associated with cystic fibrosis. *Clin Microbiol Rev.* 2002;15(2):194–222. doi:10.1128/CMR.15.2.194-222.2002
- Govan JR, Deretic V. Microbial pathogenesis in cystic fibrosis: Mucoid *Pseudomonas aeruginosa* and *Burkholderia cepacia*. *Microbiol Rev.* 1996;60(3):539–574. doi:10.1128/mr.60.3.539-574.1996
- Jones AM, Horsley A, Denning DW. What is the importance of classifying Aspergillus disease in cystic fibrosis patients? *Expert Rev Respir Med.* 2014;8(4):389–392. doi:10.1586/17476348.2014.915751
- Odeniyi M, Olusomoka E, Odeniyi O, Adebayo-Tayo B. Design and evaluation of antimicrobial properties of Ackee seed extract-silver nanoparticles film formulations. *Polim Med.* 2020;50(2):65–73. doi:10.17219/pim/130388
- Phuong MS, Hernandez RE, Wolter DJ, Hoffman LR, Sad S. Impairment in inflammasome signaling by the chronic *Pseudomonas aeruginosa* isolates from cystic fibrosis patients results in an increase in inflammatory response. *Cell Death Dis.* 2021;12(3):241. doi:10.1038/s41419-021-03526-w
- Zhang LJ, Gallo RL. Antimicrobial peptides. *Curr Biol.* 2016;26(1):R14–R19. doi:10.1016/j.cub.2015.11.017
- Groeger S, Meyle J. Oral mucosal epithelial cells. *Front Immunol.* 2019;10:208. doi:10.3389/fimmu.2019.00208
- Sharma L, Feng J, Britto CJ, Dela Cruz CS. Mechanisms of epithelial immunity evasion by respiratory bacterial pathogens. *Front Immunol.* 2020;11:91. doi:10.3389/fimmu.2020.00091
- Zgair AK, Jabbar H, Ghafil JA. Biosorption of Pb and Ni from aqueous solution by *Staphylococcus aureus*, *Pantoea* and *Pseudomonas aeruginosa*. *Iraqi J Sci.* 2019;60(4):739–744. <https://ijs.uobaghdad.edu.iq/index.php/eijs/article/view/766>. Accessed April 1, 2022.
- Funke G, Monnet D, deBernardis C, von Graevenitz A, Frenay J. Evaluation of the VITEK 2 system for rapid identification of medically relevant Gram-negative rods. *J Clin Microbiol.* 1998;36(7):1948–1952. doi:10.1128/JCM.36.7.1948-1952.1998
- Zgair AK, Chhibber S. *Stenotrophomonas maltophilia* flagellin restricts bacterial colonization in BALB/c mouse lung in vivo. *FEMS Immunol Med Microbiol.* 2012;66(2):191–200. doi:10.1111/j.1574-695X.2012.00999.x
- Zgair AK. The effect of high temperature on the kinetics of lipopolysaccharide (LPS)-induced human monocytes activity in vitro. *Cell Immunol.* 2012;275(1–2):55–60. doi:10.1016/j.cellimm.2012.03.001
- Zgair AK, Al-Adressi AMH. *Stenotrophomonas maltophilia* fimbrin stimulates mouse bladder innate immune response. *Eur J Clin Microbiol Infect Dis.* 2013;32(1):139–146. doi:10.1007/s10096-012-1729-0
- Jang CH, Choi JH, Byun MS, Jue DM. Chloroquine inhibits production of TNF- α , IL-1 β and IL-6 from lipopolysaccharide-stimulated human monocytes/macrophages by different modes. *Rheumatology.* 2006;45(6):703–710. doi:10.1093/rheumatology/kei282
- Lee EH, Rikihisa Y. Absence of tumor necrosis factor alpha, interleukin-6 (IL-6), and granulocyte-macrophage colony-stimulating factor expression but presence of IL-1beta, IL-8, and IL-10 expression in human monocytes exposed to viable or killed *Ehrlichia chaffeensis*. *Infect Immun.* 1996;64(10):4211–4219. doi:10.1128/iai.64.10.4211-4219.1996
- Yamamura M, Uyemura K, Deans R, et al. Defining protective responses to pathogens: Cytokine profiles in leprosy lesions. *Science.* 1991;254(5029):277–279. doi:10.1126/science.254.5029.277
- Kagari T, Doi H, Shimozato T. The importance of IL-1 β and TNF- α , and the noninvolvement of IL-6, in the development of monoclonal antibody-induced arthritis. *J Immunol.* 2002;169(3):1459–1466. doi:10.4049/jimmunol.169.3.1459
- Uehara A, Fujimoto Y, Fukase K, Takada H. Various human epithelial cells express functional Toll-like receptors, NOD1 and NOD2 to produce anti-microbial peptides, but not proinflammatory cytokines. *Mol Immunol.* 2007;44(12):3100–3111. doi:10.1016/j.molimm.2007.02.007
- Sasai M, Yamamoto M. Pathogen recognition receptors: Ligands and signaling pathways by Toll-like receptors. *Int Rev Immunol.* 2013;32(2):116–133. doi:10.3109/08830185.2013.774391
- Greenhalgh DG, Green TL, Lim D, Cho K. Bacterial pathogen-associated molecular patterns (PAMPs) upregulate human glucocorticoid receptor expression in peripheral blood mononuclear cells [published online as ahead of print on September 26, 2022]. *Shock.* 2022. doi:10.1097/SHK.0000000000002004
- Periselneris J, Ercoli G, Pollard T, et al. Relative contributions of extracellular and internalized bacteria to early macrophage proinflammatory responses to *Streptococcus pneumoniae*. *mBio.* 2019;10(5):e02144-19. doi:10.1128/mBio.02144-19
- Uderhardt S, Martins AJ, Tsang JS, Lämmermann T, Germain RN. Resident macrophages cloak tissue microlesions to prevent neutrophil-driven inflammatory damage. *Cell.* 2019;177(3):541–555.e17. doi:10.1016/j.cell.2019.02.028
- Kim H, Cha E, Ham S, et al. Linoleic acid inhibits *Pseudomonas aeruginosa* biofilm formation by activating diffusible signal factor-mediated quorum sensing. *Biotechnol Bioeng.* 2021;118(1):82–93. doi:10.1002/bit.27552
- Neufeld BH, Reynolds MM. Critical nitric oxide concentration for *Pseudomonas aeruginosa* biofilm reduction on polyurethane substrates. *Biointerphases.* 2016;11(3):031012. doi:10.1116/1.4962266

Talinum triangulare (Jacq.) Willd. mucilage and pectin in the formulation of ibuprofen microspheres

Olufunke Dorothy Akin-Ajani^{A,C-F}, Temiloluwa Mary Hassan^{B,C,F}, Oluwatoyin Adepeju Odeku^{C,E,F}

Department of Pharmaceutics and Industrial Pharmacy, University of Ibadan, Nigeria

A – research concept and design; B – collection and/or assembly of data; C – data analysis and interpretation; D – writing the article; E – critical revision of the article; F – final approval of the article

Polymers in Medicine, ISSN 0370-0747 (print), ISSN 2451-2699 (online)

Polim Med. 2022;52(2):83–92

Address for correspondence

Olufunke Dorothy Akin-Ajani
E-mail: oakinajani@yahoo.com

Funding sources

None declared

Conflict of interest

None declared

Acknowledgements

The authors would like to thank the University of Potsdam, Golm Campus, Germany, for the use of their scanning electron microscope during O.D. Akin-Ajani and O.A. Odeku's research visit.

Received on July 8, 2022

Reviewed on July 13, 2022

Accepted on September 5, 2022

Published online on October 21, 2022

Abstract

Background. Mucilage and pectin are both natural polymers with the advantages of availability and biodegradability. Microspheres made from biodegradable polymers can break down naturally after performing their tasks.

Objectives. The study aimed to use mucilage and pectin from the leaves of *Talinum triangulare* (Jacq.) Willd. as polymer matrices for the formulation of microspheres, with ibuprofen as the model drug.

Materials and methods. Both polymers were examined under a microscope and evaluated using measurements of viscosity, density, flow properties, swelling power, elemental analysis, Fourier-transform infrared spectroscopy (FTIR), and the degree of esterification (DE) for pectin. The microspheres were prepared using the ionotropic gelation method and alginate:mucilage/pectin at ratios of 1:1 and 1:2. They were assessed for swellability, drug entrapment effectiveness and drug release profile.

Results. The mucilage particles were ovoid while pectin particles were irregularly shaped. Pectin had higher particle, bulk and tapped densities than mucilage, while mucilage had a higher swelling power and a better flow than pectin. *Talinum triangulare* pectin is a low-methoxyl pectin with a DE of 7.14%. The FTIR spectra showed no interaction between the polymers and ibuprofen. The surface morphology of the microspheres without ibuprofen was smooth, while those with ibuprofen revealed a spongy-like mesh. The swelling power of the microspheres was higher in phosphate buffer with a pH of 7.2 than in distilled water. The entrapment efficiency ranged within 39.57–60.43% w/w, with microspheres containing alginate:mucilage/pectin ratio of 1:1 having higher entrapment efficiency. Microspheres with polymer at a ratio of 1:1 provided a longer release (>2 h), while microspheres with polymer blend of 1:2 provided an immediate release of ibuprofen.

Conclusions. The polymers of *T. triangulare* could be used as matrices in microsphere formulations.

Key words: *Talinum triangulare*, microspheres, polymers, pectins, ibuprofen

Cite as

Akin-Ajani OD, Hassan TM, Odeku OA. *Talinum triangulare* (Jacq.) Willd. mucilage and pectin in the formulation of ibuprofen microspheres. *Polim Med.* 2022;52(2):83–92. doi:10.17219/pim/153520

DOI

10.17219/pim/153520

Copyright

Copyright by Author(s)

This is an article distributed under the terms of the Creative Commons Attribution 3.0 Unported (CC BY 3.0) (<https://creativecommons.org/licenses/by/3.0/>)

Introduction

Mucilage and pectin are natural polymers used in the pharmaceutical and food industries, with the advantages of chemical inertness and biodegradability.^{1,2} While mucilages are polysaccharides that produce monosaccharides upon hydrolysis as well as sugars such as arabinose and galactose, they do not readily dissolve in water, but rather form slimy masses.³ Pectin, on the other hand, is mostly formed from citrus fruit peels, but is also found in potato pulp and cocoa husk. Pectin is a ionic polysaccharide (heteropolysaccharide chains form esterified D-galacturonic acid (1,4-linked-D-galacturonic acid)) naturally occurring in terrestrial plant cell walls, that undergoes chain-chain association and produces hydrogels when divalent cations are introduced.^{2,4-8} One crucial factor used to categorize the various forms of pectin is the degree of esterification (DE), or the proportion of carboxyl groups that are esterified and present in the structure of the pectin.⁹ According to Giacomazza et al., high-methoxyl pectin (HMP) with DE > 50% is primarily used in the food industry as a thickening and gelling agent.¹⁰ Low-methoxyl pectin (LMP), which is typically produced by the de-esterification of HMP, exhibits DE < 50%.¹¹

Waterleaf, or *Talinum triangulare* (Jacq) Willd., belongs to the Portulacaceae family. Waterleaf is also known as talinum, Ceylon spinach, Philippine spinach, etc., and locally in Nigeria, as Efo Gbure (Yoruba), Mgbolodi (Igbo), Alenruwa (Hausa), and Ebe-dondon (Edo).¹² *Talinum* has about 40 known species and is particularly abundant in tropical Africa, USA and Mexico.¹³ It is used as an ornamental plant in southern Asia and to make vegetable soup in the southern parts of Nigeria and other parts of West and Central Africa.^{14,15} The average annual yield of talinum has continued to increase as more farmers have begun to plant it.^{13,16} *Talinum*, like most vegetables, has a short life cycle and is highly perishable; the shoots may start withering within a few hours of harvesting. It has, however, been shown that the dried leaves retain most of their nutritive value, even when sun-dried.^{13,17} *Talinum triangulare* has antitumor, anti-inflammatory, antioxidant, and tyrosinase-inhibitory properties.¹⁸⁻²³ The hypoglycemic and antianemic effects of *T. triangulare* are most pronounced in pregnant women and small children.^{24,25} Waterleaf is also known to be a rich source of phenolic antioxidants, vitamin C, sugar, magnesium, phosphorus, etc.²⁶

Mucilage and pectin from *T. triangulare* have been extracted to determine their quality and nutritional and antioxidant properties, as well as the effect of season on its production.^{15,26,27} However, no studies have investigated *T. triangulare* mucilage and pectin in drug formulation. In the present study, mucilage and pectin extracted from the leaves of *T. triangulare* have been used as polymer matrices for the formulation of microspheres, with ibuprofen as the model drug.

Materials and methods

Materials

The materials used include: ibuprofen (a gift from Bond Chemicals Nig. Ltd., Awe, Nigeria), sodium alginate (S.D. Fine Chem, Mumbai, India), zinc chloride (QFC Fine Chem, Mumbai, India), acetone (CDH Fine Chemical, New Delhi, India), diethyl ether, phosphate buffer (VWR Chemicals, Leuven, Belgium), and waterleaf (*T. triangulare* locally harvested from farmlands around the University of Ibadan, Nigeria).

Extraction of mucilage from *Talinum triangulare*

Fresh leaves of *T. triangulare* were separated from the stalk, weighed and cleaned with distilled water. The juice was extracted manually with a muslin cloth, and the mucilage was precipitated with ethanol (96%). Before filtering, the precipitated mucilage was cleaned with diethyl ether. After drying in a hot air oven (Laboratory Oven TT-9083; Techmel & Techmel, Venaville, USA) at 50°C, the mucilage was milled, sieved with a 250- μ m mesh sieve and stored in a dry container.²⁸

Extraction of pectin from *Talinum triangulare*

The dried leaves of *T. triangulare* (150 g) were put in a 2-liter beaker holding 500 mL of distilled water, and the mixture was allowed to boil for 45 min. The mixture was filtered using a muslin cloth, and 200 mL of 95% acetone was added to the filtrate in aliquots with continuous stirring to allow the pectin to precipitate.²⁹

Particle size and morphology determination

Using an optical microscope (model 312545; Olympus Corp., Tokyo, Japan), the mucilage and pectin particle sizes of *T. triangulare* were determined. Under the microscope, the diameters of 100 different particles were measured to calculate the mean projected diameter in meters. The Motic Software (Motic MC2000 Image Capture Module; Motic China Group Co., Ltd., Xiamen, China) was used to take photomicrographs.

Density determinations

The bulk and tapped densities of the polymers were calculated as described previously by Ajala et al.²⁸ Particle densities of the polymers were determined with the liquid pycnometer method using xylene as the displacement fluid.

Hausner ratio and Carr's index

Hausner ratio was calculated by dividing the initial bulk volume by the tapped volume. The tapped volume was determined by applying 100 taps at a standardized rate of 38 taps per min to 5 g of polymer in a graduated cylinder.³⁰

Equation 1 was used to calculate the Carr's index³¹:

$$\text{Carr's index (\%)} = \frac{(\text{tapped density} - \text{bulk density})}{\text{tapped density}} \times 100 \quad (1)$$

Angle of repose

The polymer (5 g) was poured through a funnel into an open-ended cylinder positioned on a cone with a 2.8-cm diameter, and the cylinder was gently lifted vertically while the powder formed a mound. The angle of repose was calculated using the height (h) and radius (r) measurements (Equation 2):

$$\tan(\theta) = \frac{h}{r} \quad (2)$$

Swelling power

The polymer (0.5 g) was put into a measuring cylinder with a capacity of 10 mL, and the heights were recorded (h1). The polymer was mixed with phosphate buffer or distilled water to the 10 mL mark, and the resulting slurry was stirred for 5 min. The sedimentation height (h2) was measured after letting the suspension sit for 24 h. Next, the swelling power was determined³⁰ (Equation 3):

$$\text{swelling power} = \frac{v_2}{v_1} \quad (3)$$

where v1 and v2 are volumes derived from h1 and h2, respectively.

Characterization of pectin

The Ranganna's method was used to compute the equivalent weight of pectin.³² In a 250-mL conical flask, pectin (0.5 g), ethanol (5 mL), sodium chloride (1 g), and distilled water (100 mL) were combined. This was titrated against 0.1 N NaOH using phenol red as an indicator. The endpoint was indicated by a change in color to purple. The equivalent weight of pectin was calculated using Equation 4, and the methoxyl content was determined using the neutralized solution²:

$$\text{equivalent weight} = \frac{\text{weight of sample} \times 1000}{\text{volume of alkali} \times \text{normality of alkali}} \quad (4)$$

The neutralized solution produced by the titration with equivalent weight was mixed with sodium hydroxide (25 mL of 0.25 N). After thoroughly stirring the mixture,

it was allowed to stand at room temperature for 30 min. The mixture was then titrated against 0.1 N NaOH using 25 mL of 0.25-N hydrochloric acid.³² Equation 5 was used to determine the methoxyl content of pectin²:

$$\text{methoxyl content (\%)} = \frac{\text{volume of alkali} \times \text{normality of alkali} \times 3.1}{\text{weight of sample}} \quad (5)$$

Equation 6 was used to calculate the total anhydrouronic acid (AUA) of pectin²:

$$\text{AUA (\%)} = \frac{176 \times 0.1z \times 100}{w \times 1000} + \frac{176 \times 0.1y \times 100}{w \times 1000} \quad (6),$$

where the molecular weight of 1 unit of AUA is 176 g, z is the titer volume (mL) of NaOH is determined by equivalent weight, and y is the titer volume (mL) of NaOH is determined by methoxyl content determination, while w is the weight of the pectin sample.

The degree of esterification was calculated from the percentage of methoxyl content (MeO) (Equation 5) and % AUA (Equation 6) using Equation 7:

$$\text{DE (\%)} = \frac{176 \times \% \text{MeO}}{31 \times \% \text{AUA}} \times 100 \quad (7)$$

An atomic absorption spectrophotometer (AAS, Model 2500; Torontech Inc., Toronto, Canada) was used to evaluate the pectin and mucilage for 10 elements.³³

The Fourier-transform infrared spectroscopy (FTIR) spectra of dried powders of mucilage, pectin, alginate, and ibuprofen, as well as their mixes formed in potassium bromide (KBr) discs, were determined using an FTIR system (Spectrum BX 273; PerkinElmer, Waltham, USA), with a scanning range of 350–4400 cm⁻¹.

The viscosity of mucilage and pectin blends with sodium alginate was evaluated using a viscometer (model RVVDV-II +P; Brookfield Engineering Laboratories Inc., Middleboro, USA) with a spindle size of 4 at 50 rpm and 100 rpm.

Preparation of microspheres

Ibuprofen-loaded microspheres were created using the ionotropic gelation technique. Different batches of sodium alginate alone, as well as the polymer blends of different concentrations of alginate with mucilage and alginate with pectin in ratios 1:1 and 1:2, were prepared. Ibuprofen (1 g) was incorporated into various blends at a polymer-to-drug ratio of 2:1. The microspheres were prepared with 10% w/v zinc chloride as the crosslinking agent. The polymer mixture was extruded using a 21-G needle and a 5-mL syringe at a dropping rate of 2 mL/min and a stirring speed of 300 rpm. To begin the curing process, the microspheres were immersed in zinc chloride for 10 min. Then, they were filtered, rinsed 3 times with distilled water, dried at ambient temperature for 24 h, and further dried for 6 h at 40°C in a hot air oven (laboratory oven TT-9083; Techmel & Techmel).

Evaluation of polymeric microspheres

Scanning electron microscope (SEM) was used to determine the size (diameter) and shape of the polymeric microspheres.³⁴ Briefly, microspheres were applied to double-sided carbonated adhesive stills affixed to SEM stubs, and images were taken at 1 kV with $\times 5000$ magnification in a SEM (Zeiss Ultra Plus; Carl Zeiss AG, Jena, Germany). The swelling index of the microspheres was also determined.

Ibuprofen-loaded microspheres (50 mg) were crushed with a mortar and pestle, and then suspended in a 10 mL of phosphate buffer with a pH of 7.2 and filtered after 24 h. The phosphate buffer was then used to dilute the filtrate before it was examined at 221 nm with a spectrophotometer. The following formula was used to compute the drug entrapment efficiency (Equation 8):

$$\text{entrapment (\%)} = \frac{\text{actual drug content}}{\text{theoretical drug content}} \times 100 \quad (8)$$

The paddle method was used in the in vitro dissolution tests with rotating at 100 rpm in 900 mL of 7.2 phosphate buffer at $37 \pm 0.5^\circ\text{C}$; 200 mg of ibuprofen was used as a model. Then, at regular intervals, 5-mL samples were removed and replaced with an equivalent volume of the new phosphate buffer. After the samples were diluted, the amount of ibuprofen released at 221 nm was measured using a ultraviolet-visible (UV/VIS) spectrophotometer (Spectrumlab 752s UV-VIS spectrophotometer; Wincom Company Ltd., Shanghai, China). To determine the mechanism of drug release, the dissolution data (i.e., the first 60% of drug release data) were fitted to the Korsmeyer–Peppas equation with DD Solver (Microsoft Excel 2016; Microsoft Corp., Redmond, USA).^{35,36}

Results and discussion

Characterization of *Talinum triangulare* mucilage and pectin

The pectin of *T. triangulare* had a DE of 7.14% w/w, which suggests that *T. triangulare* is a low-methoxyl weight pectin. While LMP does not require a lot of sugar or acidity (low pH) to gel, it does require the presence of divalent cations.²⁹

The elemental composition of the mucilage and pectin of *T. triangulare* is presented in Table 1. The highest elemental content in mucilage was sodium, whereas it was potassium in pectin. Copper, cadmium and lead were

Table 1. Elemental properties of *Talinum triangulare* mucilage and pectin

Elements	Mucilage [mg/g]	Pectin [mg/g]
Ca	3.5760	7.8800
Fe	0.5332	0.8368
Na	20.3082	50.7970
Mg	17.5200	31.0000
K	10.8234	56.1130
Cd	0.0002	0.0017
Cu	0.0267	0.0823
Cr	0.0097	0.0658
Ni	0.0076	0.0309
Pb	0.0077	0.0623

present in the polymers in minute, permissible quantities. According to The World Health Organization/The Food and Agriculture Organization of the United Nations (WHO/FAO), the permissible limits for copper, cadmium and lead are 40 mg/kg, 0.2 mg/kg and 0.3 mg/kg, respectively.³⁷ The presence of heavy metals has been previously reported in this plant.³⁸

The FTIR spectra shown in Fig. 1 indicate that the spectra for sodium alginate, pectin and mucilage of *T. triangulare* were distinct from that of ibuprofen, which had characteristic peaks at $1708\text{--}1729\text{ cm}^{-1}$ and 2955 cm^{-1} . The polymers showed no interaction with ibuprofen, even at the different ratios used, as indicated by the distinct fingerprint region ($1500\text{--}500\text{ cm}^{-1}$) of ibuprofen showing the aromatic ring and isobutyl moiety.³⁹ However, this was not the case with sodium alginate – the fingerprint region of ibuprofen was not clearly defined.

The mucilage particles were ovoid while pectin particles were irregularly shaped (Fig. 2) with *T. triangulare* mucilage having a smaller mean particle size than pectin (Table 2). Particles with smaller sizes and irregular shapes have better cohesiveness compared to oval and spherical particles; additionally, large particle sizes reduce cohesiveness and prevent particle packing.⁴⁰

Packing behavior of a powder during various unit operations is described by its bulk density. The particle, bulk and tapped densities of pectin exceeded those of mucilage, according to the results shown in Table 2. This indicates that greater packing would be achieved with pectin than with mucilage, which would be important where shipping and packaging or low volume dosage forms are required.

The Hausner ratio and Carr's index are used to determine the flowability and compressibility of powders. A lower Carr's index indicates better flow and less compressibility,

Table 2. Material properties of *Talinum triangulare* mucilage and pectin

Polymer nature	Particle size [μm]	Particle density [g/cm^3]	Bulk density [g/cm^3]	Tapped density [g/cm^3]	Hausner ratio	Carr's index [%]	Angle of repose ($^\circ$)	Swelling power [%]
Mucilage	85.0 ± 33.1	1.288	0.705	0.874 ± 0.012	1.239	19.28	49.7	1.16
Pectin	197.0 ± 78.3	1.569	0.711	0.882 ± 0.014	1.240	19.38	48.0	1.09

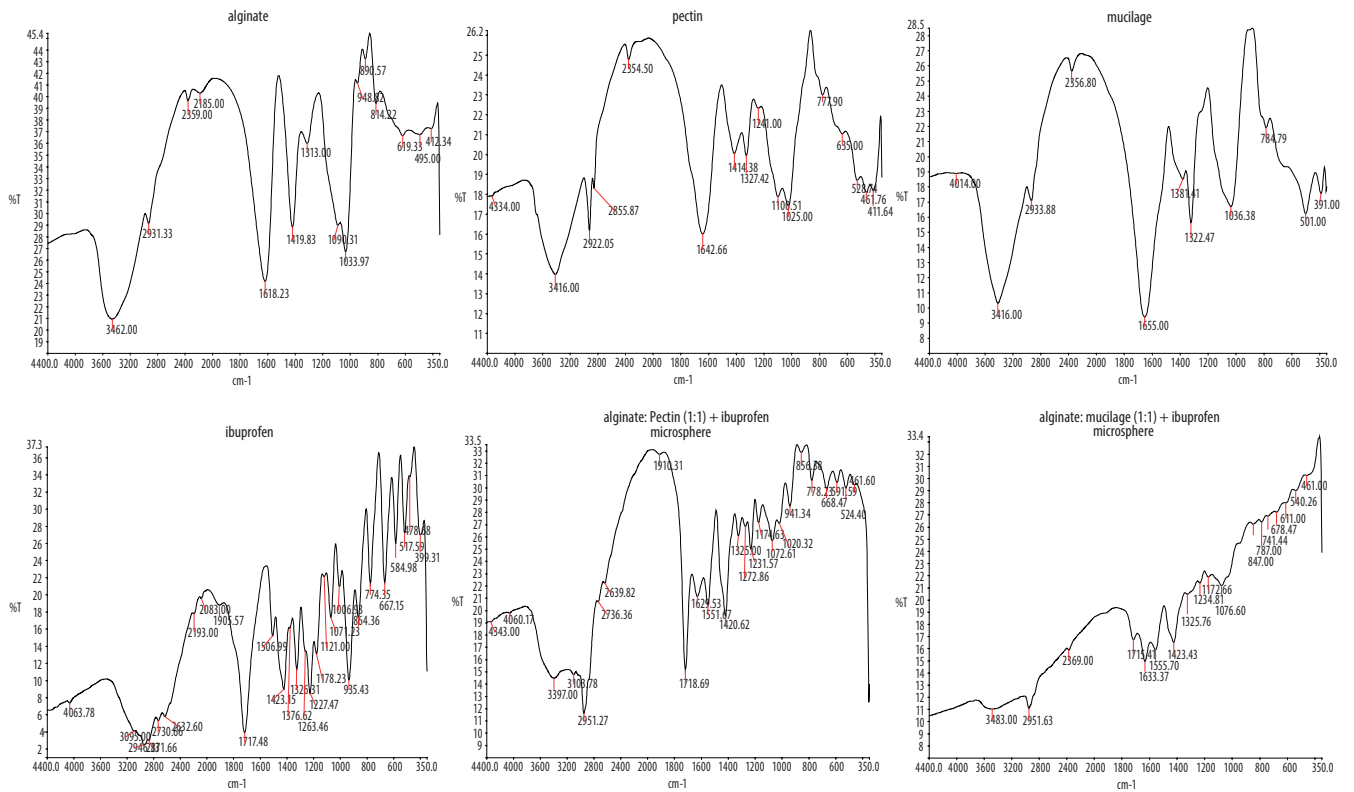


Fig. 1. Fourier-transform infrared spectroscopy (FTIR) spectra of polymers, ibuprofen and microspheres

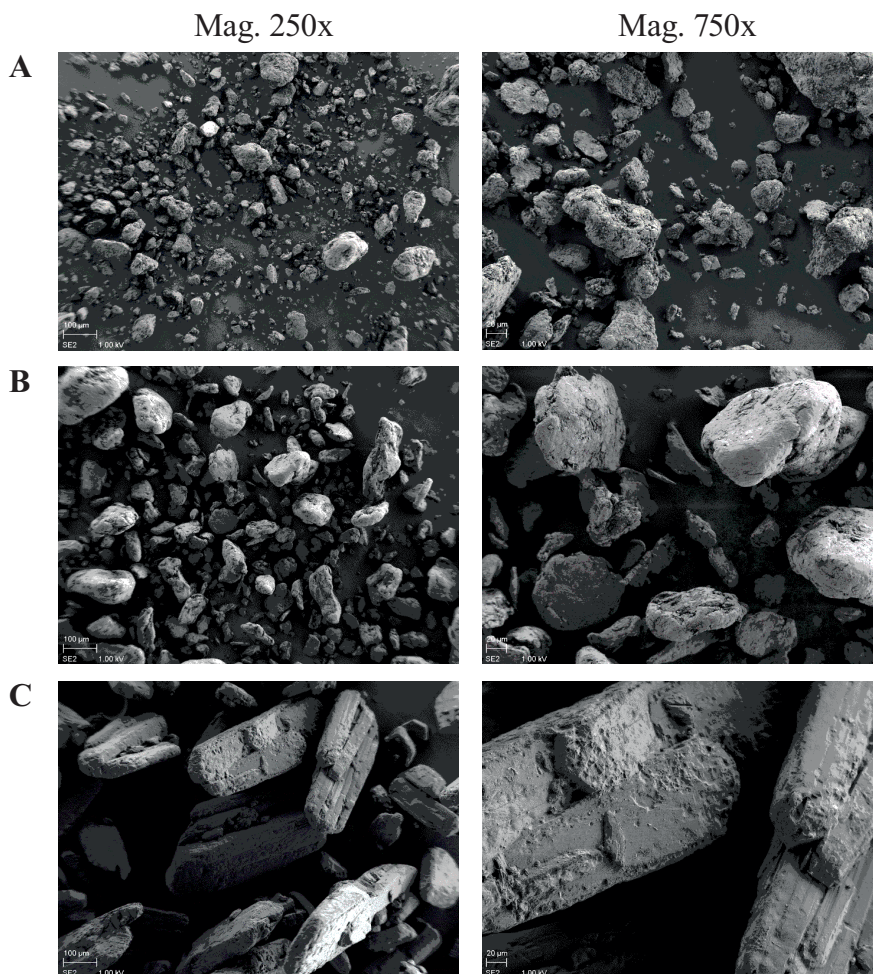


Fig. 2. Scanning electron microscope (SEM) images of (A) mucilage, (B) pectin polymers and (C) ibuprofen

while a higher Carr's index indicates less flow but better compression, implying a greater cohesiveness.³¹ The Hausner ratio is related to the inter-particle friction: values greater than 1.25 signify that the material flow is passable, those greater than 1.35 indicate poor flow, while those greater than 1.5 indicate cohesiveness.⁴¹ Our results show that *T. triangulare* mucilage has a better flowability than pectin, possibly due to the shape of the mucilage particles compared with the irregularly shaped pectin particles.

The angle of repose is used to measure the inter-particle force as well as the cohesiveness of materials. The rougher and more irregular the surface of the particles, the higher the angle of repose will be.⁴² The angle of repose obtained for mucilage was higher than that of pectin, although pectin showed lower flow than mucilage.

Swelling power indicates the ability of a substance to hold fluid and its absorption behavior. It has generally been used to demonstrate differences between various types of materials.⁴³ The swelling power of mucilage was higher than that of pectin (Table 2).

Viscosity is the measure of fluid resistance to flow and a measure of the gradual deformation to shear or tensile stress.⁴⁴ The polymer blends exhibited non-Newtonian behavior in that their viscosity decreased with increasing shear rate for 1:1 blends and increased with increasing shear rate for 1:2 blends (Table 3). An increase in the concentration of either mucilage or pectin, with or without drugs, led to a decrease in the viscosity of the blends. Polymer blends with drug-containing pectin had higher viscosity than those containing mucilage at both ratios. There was no difference in the viscosity of the polymer blends at a ratio of 1:2 without the drug. Microspheres containing sodium alginate alone with or without drugs had the highest viscosity.

Properties of ibuprofen microspheres

The photomicrographs of the microspheres showed spherical to ovoid shapes at different ratios, with the microspheres with the ratio of 1:1 being more spherical (Fig. 3). This could

Table 3. Viscosity analysis of polymeric blends

Polymer ratio [%]			Ibuprofen [%]	Viscosity [cP] 50 rpm
Sodium alginate	mucilage	pectin		
100	–	–	–	19.28 ±7.30
50	50	–	–	1.98 ±2.30
50	–	50	–	1.96 ±4.00
34	66	–	–	0.62 ±2.30
34	–	66	–	0.62 ±2.30
33	33	–	34	1.70 ±2.80
33	–	33	34	2.40 ±0.00
22	44	–	34	0.42 ±2.80
22	–	44	34	0.74 ±2.80
66	–	–	34	24.85 ±8.30

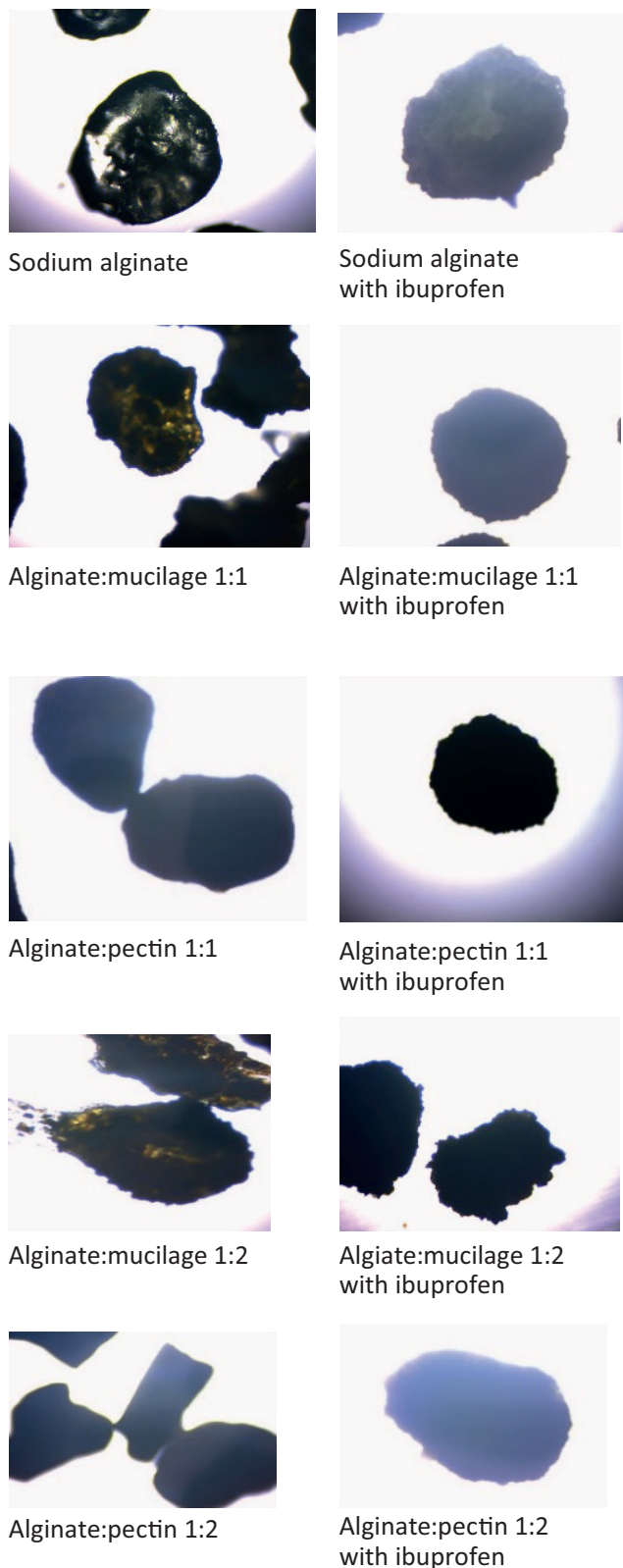


Fig. 3. Photomicrograph of all microspheres (×40 magnification)

be due to the decreased viscosity displayed at increased polymer concentrations, as compared to the viscosity of alginate. Therefore, increasing the concentration of the mucilage or pectin decreased the capacity of the polymer blend to form spheres. The surface morphology of the microspheres shown

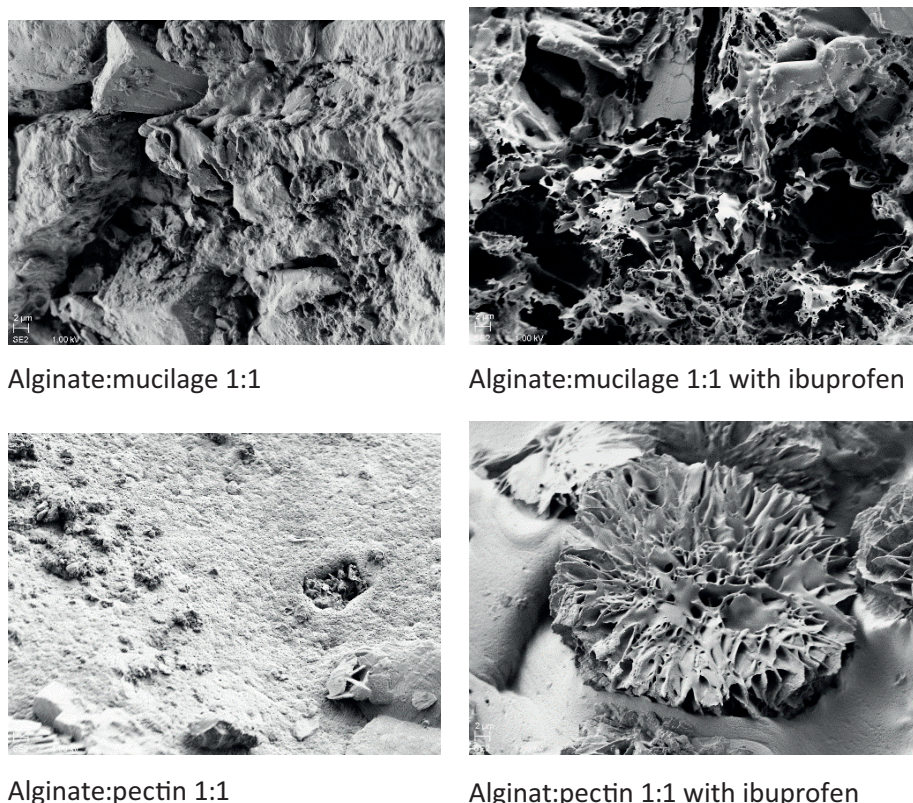


Fig. 4. Scanning electron microscope (SEM) images of microsphere surfaces of polymer ratios 1:1 without and with drug (x5000 magnification)

in Fig. 4 indicates that the microspheres generally had rough surfaces, which is in agreement with previous studies.^{33,45} Microspheres with polymer ratio of 1:1 showed smoother surface morphology. However, upon closer inspection with SEM, the surface revealed a spongy-like mesh for microspheres containing ibuprofen, while those without ibuprofen remained largely smooth. The microsphere sizes ranged within 929.4–1479.9 μm for mucilage and within 952.4–1652.6 μm for pectin (Table 4). In summary, the pectin-containing microspheres were generally larger.

Swelling power is described as the ability of the polymer matrix to absorb fluid and form a protective matrix. The swelling power (Table 4) of the microspheres was significantly higher ($p < 0.001$) in phosphate buffer at pH of 7.2

than in distilled water (pH 5.8). This indicated a greater absorption of fluid into the microspheres in the alkaline medium than in acidic medium, which suggests a greater effectiveness of the microspheres in the duodenum than in the stomach.⁴⁶

Entrapment efficiency

Entrapment efficiency is the amount of drug entrapped or encapsulated within a matrix; it is an important parameter that describes the ability of the polymer blend or matrix to trap or hold drugs within it. Microspheres containing alginate:mucilage/pectin at a ratio of 1:1 had a greater entrapment of ibuprofen compared to a ratio

Table 4. Sizes and swelling index of all microspheres

Polymer ratio [%]			Microsphere size [μm]	Swelling [%]	
Sodium alginate	mucilage	pectin		phosphate buffer	distilled water
100	–	–	1311.9 \pm 120.3	349.5 \pm 91.2	2.0 \pm 0.0
50	50	–	1136.7 \pm 161.1	396.0 \pm 73.5	20.0 \pm 1.4
50	–	50	1276.4 \pm 269.2	71.0 \pm 65.0	27.0 \pm 5.65
34	66	–	1246.5 \pm 228.4	323.5 \pm 61.5	35.5 \pm 3.5
34	–	66	1083.8 \pm 131.4	51.0 \pm 0.0	2.5 \pm 0.7
33	33	–	1208.8 \pm 161.7	316.0 \pm 2.8	50.5 \pm 0.7
33	–	33	1090.4 \pm 115.4	284.5 \pm 43.1	24.0 \pm 2.8
22	44	–	1153.7 \pm 224.3	263.5 \pm 21.9	70.5 \pm 0.7
22	–	44	1400.9 \pm 251.7	142.0 \pm 26.8	22.0 \pm 1.4
66	–	–	1518.5 \pm 122.7	207.6 \pm 42.6	6.5 \pm 2.5

Table 5. Entrapment efficiency and dissolution time of ibuprofen in microspheres

Polymer ratio [%]			Shape of microsphere	Yield [%]	Entrapment efficiency [%]	Dissolution time [min]	
Sodium alginate	mucilage	pectin				t ₅₀	t ₈₀
50	50	–	spherical	77.37	55.71	45.0	98.0
50	–	50	spherical	99.67	60.43	66.0	–
34	66	–	irregular	69.10	45.94	32.0	66.0
34	–	66	oblong	88.63	39.57	31.0	37.8
100	–	–	spherical	97.93	48.64	68.0	100.0

of 1:2 (Table 5), thus indicating that an increase in the concentration of either mucilage or pectin did not enhance the entrapment of the drug. The entrapment efficiency of the alginate:mucilage/pectin ratio 1:1 was also higher than the alginate microspheres alone. Overall, the microspheres had an entrapment efficiency that ranged from 39.57% to 60.43%.

Release studies

The dissolution profiles of ibuprofen microspheres shown in Fig. 5 indicated different release properties based on the concentration of the pectin and mucilage present. The microspheres with a polymer blend of 1:1 had a longer release, whereas microspheres with a polymer blend of 1:2 had an immediate release, with the alginate:pectin blend of 1:2 having a faster release than the alginate:mucilage blend of 1:2. Microspheres containing a ratio of 1:1 of alginate:pectin had the slowest release rate, probably due to its higher viscosity, and a sustained release of over 2 h. All of the ibuprofen-loaded microspheres had t₅₀ within the range of 31–68 min and t₈₀ within the range of 37–100 min (Table 5), except for microspheres containing alginate:pectin at a ratio of 1:1, which failed to attain 80% drug release at 120 min. Fitting the microsphere dissolution data to the Korsmeyer–Peppas

equation yielded correlation coefficients $R^2 \geq 0.977$ and $n > 0.89$. The drug release mechanism for all of the microspheres, irrespective of polymer or ratio, was the super case II transport (relaxation) mechanism.^{47,48}

Conclusions

The *T. triangulare* pectin particles displayed larger particle size and greater packing behavior than the mucilage, and were found to be low in methoxyl pectin. Interestingly, the mucilage particles showed better flow and swellability. The FTIR spectra showed no interaction of ibuprofen with the test polymers. Ibuprofen-loaded microspheres had significantly greater swelling in an alkaline medium. Polymer blends of pectin with ibuprofen had higher viscosity, and at a ratio of 1:1 had the slowest release of ibuprofen. Ibuprofen-loaded microspheres with polymer blends of 1:1 had a longer release of ibuprofen, whereas microspheres with polymer blends of 1:2 had immediate release of ibuprofen, even though they were all transported by the super case II transport mechanism. Therefore, the polymers of *T. triangulare* have use as matrices in microspheres depending on the type of drug release required.

ORCID iDs

Olufunke Dorothy Akin-Ajani  <https://orcid.org/0000-0002-8790-3653>
Temiloluwa Mary Hassan  <https://orcid.org/0000-0003-2550-9615>
Oluwatoyin Adepeju Odeku  <https://orcid.org/0000-0002-0732-1304>

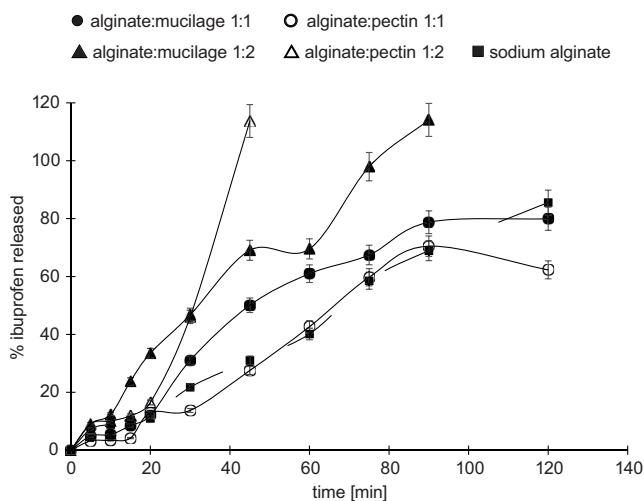


Fig. 5. Plots of the percentage of ibuprofen released against time [min] for alginate

References

- Reddy M, Manjunath K. Pharmaceutical applications of natural gums, mucilages and pectins: A review. *Int J Pharm Chem Sci.* 2013;2(3): 1233–1239. <https://www.researchgate.net/publication/267329407>. Accessed April 30, 2022.
- Azad AKM. Isolation and characterization of pectin extracted from lemon pomace during ripening. *J Food Nutr Sci.* 2014;2(2):30. doi:10.11648/j.jfns.20140202.12
- Paynel F, Pavlov A, Ancelin G, et al. Polysaccharide hydrolases are released with mucilages after water hydration of flax seeds. *Plant Physiol Biochem.* 2013;62:54–62. doi:10.1016/j.plaphy.2012.10.009
- Levigne S, Ralet MC, Thibault JF. Characterisation of pectins extracted from fresh sugar beet under different conditions using an experimental design. *Carbohydr Polym.* 2002;49(2):145–153. doi:10.1016/S0144-8617(01)00314-9
- Mollea C, Chiampo F, Conti R. Extraction and characterization of pectins from cocoa husks: A preliminary study. *Food Chem.* 2007;107(3): 1353–1356. doi:10.1016/j.foodchem.2007.09.006

6. Czurzyńska A, Lenart A, Karwosińska J. Effect of quantity of low-methoxyl pectin on physical properties of freeze-dried strawberry jellies. *Pol J Food Nutr Sci.* 2015;65(4):233–241. doi:10.2478/pjfn-2013-0020
7. Yang JS, Mu TH, Ma MM. Extraction, structure, and emulsifying properties of pectin from potato pulp. *Food Chem.* 2018;244:197–205. doi:10.1016/j.foodchem.2017.10.059
8. Akin-Ajani O, Okunlola A. Pharmaceutical applications of pectin. In: Masuelli MA, ed. *Pectins: The New-Old Polysaccharides*. London, UK: IntechOpen; 2022. ISBN:978-1-83969-597-1.
9. Mellinas C, Ramos M, Jiménez A, Garrigós MC. Recent trends in the use of pectin from agro-waste residues as a natural-based biopolymer for food packaging applications. *Materials (Basel).* 2020;13(3):673. doi:10.3390/ma13030673
10. Giacomazza D, Bulone D, San Biagio PL, Marino R, Lapasin R. The role of sucrose concentration in self-assembly kinetics of high methoxyl pectin. *Int J Biol Macromol.* 2018;112:1183–1190. doi:10.1016/j.ijbiomac.2018.02.103
11. Wu C, Pan LL, Niu W, et al. Modulation of gut microbiota by low methoxyl pectin attenuates type 1 diabetes in non-obese diabetic mice. *Front Immunol.* 2019;10:1733. doi:10.3389/fimmu.2019.01733
12. Alozie YE, Ene-Obong HN. Recipe standardization, nutrient composition and sensory evaluation of waterleaf (*Talinum triangulare*) and wild spinach (*Gnetum africanum*) soup “afang” commonly consumed in south Nigeria. *Food Chem.* 2018;238:65–72. doi:10.1016/j.foodchem.2016.12.071
13. Fontem D, Schippers R. *Talinum triangulare* (Jacq.) Willd: Record from PROTAbase. 2004. [https://www.prota4u.org/database/protav8.asp?g=pe&p=Talinum+triangulare+\(Jacq.\)+Willd](https://www.prota4u.org/database/protav8.asp?g=pe&p=Talinum+triangulare+(Jacq.)+Willd). Accessed May 27, 2022.
14. Enete A, Okon U. Economics of waterleaf (*Talinum triangulare*) production in Akwa Ibom State, Nigeria. *Field Actions Sci Rep.* 2010;4:1–12. <https://journals.openedition.org/factsreports/438?file=1>. Accessed April 30, 2022.
15. Adetuyi F, Dada I. Nutritional, phytoconstituent and antioxidant potential of mucilage extract of Okra (*Abelmoschus esculentus*), water leaf (*Talinum triangulare*) and Jew's mallow (*Corchorus olitorius*). *Int Food Res J.* 2014;21(6):2345–2353. [http://www.ifrj.upm.edu.my/21%20\(06\)%202014/41%20IFRJ%2021%20\(06\)%202014%20Adetuyi%20128.pdf](http://www.ifrj.upm.edu.my/21%20(06)%202014/41%20IFRJ%2021%20(06)%202014%20Adetuyi%20128.pdf). Accessed April 30, 2022.
16. Nya EJ, Okorie NU, Eka MJ. An economic analysis of *Talinum triangulare* (Jacq.) production/farming in southern Nigeria. *Trends Agricult Econ.* 2010;3(2):79–93. doi:10.3923/tae.2010.79.93
17. Oluwalana I, Ayo J, Idowu M, Malomo S. Effect of drying methods on the physicochemical properties of waterleaf (*Talinum triangulare*). *Int J Biol Chem Sci.* 2011;5(3):880–889. doi:10.4314/ijbcs.v5i3.72167
18. Ikewuchi CC, Ikewuchi JC, Ifeanchio MO. Bioactive phytochemicals in an aqueous extract of the leaves of *Talinum triangulare*. *Food Sci Nutr.* 2017;5(3):696–701. doi:10.1002/fsn3.449
19. Kelechi A, Dorothy T. Economic study of tropical leafy vegetables in South-East of Nigeria: The case of rural women farmers. *Am J Agric Sci.* 2015;2(2):34–41. <http://article.aascit.org/file/pdf/8920737.pdf>. Accessed May 18, 2022.
20. Liao DY, Chai YC, Wang SH, Chen CW, Tsai MS. Antioxidant activities and contents of flavonoids and phenolic acids of *Talinum triangulare* extracts and their immunomodulatory effects. *J Food Drug Anal.* 2015;23(2):294–302. doi:10.1016/j.jfda.2014.07.010
21. Oliveira Amorim A, Campos de Oliveira M, de Azevedo Amorim T, Echevarria A. Antioxidant, iron chelating and tyrosinase inhibitory activities of extracts from *Talinum triangulare* leaf stem. *Antioxidants.* 2013;2(3):90–99. doi:10.3390/antiox2030090
22. Oluwole O, Obote O, Elemo G, Ibekwe D, Adesioye T. Anti-inflammatory and anti-cancer properties of selected green leafy vegetables: A review. *Nutr Food Process.* 2021;4(8):1–5. <https://www.auctoresonline.org/article/anti-inflammatory-and-anti-cancer-properties-of-selected-green-leafy-vegetables---a-review>. Accessed May 18, 2022.
23. Swarna J, Lokeswari TS, Smita M, Ravindhran R. Characterisation and determination of in vitro antioxidant potential of betalains from *Talinum triangulare* (Jacq.) Willd. *Food Chem.* 2013;141(4):4382–4390. doi:10.1016/j.foodchem.2013.06.108
24. Biona K, Shen C, Ragasa C. Chemical constituents of *Talinum triangulare*. *Res J Pharm Biol Chem Sci.* 2015;6(1):167–171. https://www.researchgate.net/publication/268575472_Chemical_constituents_of_Talinum_triangular. Accessed April 30, 2022.
25. Lara-Espinoza C, Carvajal-Millán E, Balandrán-Quintana R, López-Franco Y, Rascón-Chu A. Pectin and pectin-based composite materials: Beyond food texture. *Molecules.* 2018;23(4):942. doi:10.3390/molecules23040942
26. Andarwulan N, Faridah DN, Prabekti YS, et al. Dietary fiber content of waterleaf (*Talinum triangulare* (Jacq.) Willd) cultivated with organic and conventional fertilization in different seasons. *Am J Plant Sci.* 2015;6(2):334–343. doi:10.4236/ajps.2015.62038
27. Sanda M. Evaluation of quality and cholesterol level of eggs of laying hens placed on drinking water fortified with waterleaf (*Talinum triangulare*) mucilage. *Am Acad Sci Res J Eng Technol Sci.* 2015;13(1):81–87. <https://core.ac.uk/download/pdf/235049679.pdf>. Accessed April 30, 2022.
28. Ajala TO, Akin-Ajani OD, Ihuoma-Chidi C, Odeku OA. *Chrysophyllum albidum* mucilage as a binding agent in paracetamol tablet formulations. *J Pharm Invest.* 2016;46(6):565–573. doi:10.1007/s40005-016-0266-8
29. Okunlola A, Akindele O. Application of response surface methodology and central composite design for the optimization of metformin microsphere formulation using tangerine (*Citrus tangerina*) pectin as copolymer. *Br J Pharm Res.* 2016;11(3):1–14. doi:10.9734/BJPR/2016/25095
30. Akin-Ajani OD, Itiola OA, Odeku OA. Effect of acid modification on the material and compaction properties of fonio and sweet potato starches. *Starch-Stärke.* 2014;66(7–8):749–759. doi:10.1002/star.201300280
31. Carr R. Evaluating flow properties of solids. *Chem Eng.* 1965;18:163–168.
32. Ranganna S. *Handbook of Analysis and Quality Control for Fruits and Vegetable Products.* 2nd ed. New Delhi, India: Tata McGraw Hill; 2007. ISBN:978-0-07-451851-9.
33. Akin-Ajani O, Ikehin M, Ajala T. Date mucilage as co-polymer in metformin-loaded microbeads for controlled release. *J Excip Food Chem.* 2019;10(1):3–12. <https://jefc.scholasticahq.com/article/8440-date-mucilage-as-co-polymer-in-metformin-loaded-microbeads-for-controlled-release>. Accessed April 30, 2022.
34. Odeku OA, Aderogba AA, Ajala TO, Akin-Ajani OD, Okunlola A. Formulation of floating metronidazole microspheres using cassava starch (*Manihot esculenta*) as polymer. *J Pharm Invest.* 2017;47(5):445–451. doi:10.1007/s40005-017-0319-7
35. Ahmed L, Atif R, Eldeen T, Yahya I, Omara A, Eltayeb M. Study the using of nanoparticles as drug delivery system based on mathematical models for controlled release. *Int J Latest Tech Eng Manag.* 2019;8(5):52–56. <https://www.ijltemas.in/DigitalLibrary/Vol.8Issue5/52-56.pdf>. Accessed May 25, 2022.
36. Peppas NA, Sahlin JJ. A simple equation for the description of solute release. III. Coupling of diffusion and relaxation. *Int J Pharm.* 1989;57(2):169–172. doi:10.1016/0378-5173(89)90306-2
37. Elbagermi MA, Edwards HGM, Alajtal AI. Monitoring of heavy metal content in fruits and vegetables collected from production and market sites in the Misurata area of Libya. *ISRN Anal Chem.* 2012;2012(1–3):827645. doi:10.5402/2012/827645
38. Ukpabi C, Akubugwo E, Agbafor K, Wogu C, Chukwu H. Phytochemical and heavy metal composition of *Telfairia occidentalis* and *Talinum triangulare* grown in Aba, Nigeria, and environmental health implications. *Am J Biochem.* 2013;3(3):67–73. <http://article.sapub.org/10.5923.j.ajb.20130303.01.html>. Accessed April 30, 2022.
39. Dinte E, Bodoki E, Leucuta S, Iuga C. Compatibility studies between drugs and excipients in the preformulation phase of buccal mucoadhesive systems. *Farmacia.* 2013;61:703–712. <https://farmaciajournal.com/wp-content/uploads/2013-04-art.09.dinte-703-712.pdf>. Accessed April 30, 2022.
40. Okunlola A, Odeku OA. Effects of water yam and corn starches on the interacting variables influencing the disintegration of chloroquine phosphate tablets. *Dhaka Univ J Pharm Sci.* 2012;10(1):21–28. doi:10.3329/dujps.v10i1.10011
41. Staniforth J. Powder flow. In: Aulton ME, Cooper JW, eds. *Pharmaceuticals: The Science of Dosage Form Design*. Edinburgh, UK-New York, USA: Churchill Livingstone; 1988. ISBN:978-0-443-03643-9.
42. Teixeira AZA. Compaction characteristics of the powder from the seed coat of tingui (*Magonia pubescens*). *Estud Biol.* 2007;29(68/69):277–282. doi:10.7213/rev.v29i68/69.22778

43. Kaur N, Garg T, Goyal AK, Rath G. Formulation, optimization and evaluation of curcumin- β -cyclodextrin-loaded sponge for effective drug delivery in thermal burns chemotherapy. *Drug Deliv.* 2016;23(7): 2245–2254. doi:10.3109/10717544.2014.963900
44. Ekolu S, Dundu M, Gao X. *Construction Materials and Structures: Proceedings of the First International Conference on Construction Materials and Structures*. Washington, USA: IOS Press; 2014. ISBN:978-1-61499-465-7.
45. Odeku OA, Okunlola A, Lamprecht A. Microbead design for sustained drug release using four natural gums. *Int J Biol Macromol.* 2013;58: 113–120. doi:10.1016/j.ijbiomac.2013.03.049
46. Sriamornsak P, Thirawong N, Korkerd K. Swelling, erosion and release behavior of alginate-based matrix tablets. *Eur J Pharm Biopharm.* 2007;66(3):435–450. doi:10.1016/j.ejpb.2006.12.003
47. Dash S, Murthy PN, Nath L, Chowdhury P. Kinetic modeling on drug release from controlled drug delivery systems. *Acta Pol Pharm.* 2010; 67(3):217–223. PMID:20524422.
48. Ghumman SA, Noreen S, Tul Muntaha S. *Linum usitatissimum* seed mucilage-alginate mucoadhesive microspheres of metformin HCl: Fabrication, characterization and evaluation. *Int J Biol Macromol.* 2020; 155:358–368. doi:10.1016/j.ijbiomac.2020.03.181

Effect of glaze and chlorhexidine on physical and mechanical properties of bis-acryl resin: An in situ study

Betina Chairelo Commar^{1,B,D}, Marcelle Danelon^{2,B}, Paulo Augusto Panitente^{1,C,E}, Emily Vivianne Freitas da Silva^{1,B,C}, Sandro Basso Bitencourt^{1,E}, Valentim Adelino Ricardo Barão^{3,D,E}, Clóvis Lamartine de Moraes Melo Neto^{1,D–F}, Marcelo Coelho Goiato^{1,A,F}, Daniela Micheline dos Santos^{1,A,D,F}

¹ Department of Dental Materials and Prosthodontics, São Paulo State University (UNESP), School of Dentistry, Araçatuba, Brazil

² Department of Preventive and Restorative Dentistry, São Paulo State University (UNESP), School of Dentistry, Araçatuba, Brazil

³ Department of Prosthodontics and Periodontology, State University of Campinas (UNICAMP), School of Dentistry, Piracicaba, Brazil

A – research concept and design; B – collection and/or assembly of data; C – data analysis and interpretation;

D – writing the article; E – critical revision of the article; F – final approval of the article

Polymers in Medicine, ISSN 0370-0747 (print), ISSN 2451-2699 (online)

Polim Med. 2022;52(2):93–99

Address for correspondence

Marcelo Coelho Goiato
E-mail: m.goiato@unesp.br

Funding sources

FAPESP (São Paulo Research Foundation) financial support (process No. #2017/11803-8) provided to the first author.

Conflict of interest

None declared

Received on August 29, 2022

Reviewed on November 14, 2022

Accepted on November 24, 2022

Published online on December 12, 2022

Abstract

Background. Temporary prosthesis protects the oral tissues, in addition to providing aesthetic look and masticatory function until a definitive prosthesis is manufactured.

Objectives. To evaluate the effect of glaze and 0.12% chlorhexidine (CHX) on the physical and mechanical properties of bis-acryl, and to evaluate the antimicrobial efficacy of CHX.

Materials and methods. Eighty specimens of bis-acryl resin were made. Over 40 of them the glaze was applied. One specimen with and 1 specimen without glaze were placed in niches of an appliance manufactured for each patient. Each of the 20 volunteers received 2 devices. Initially, the volunteers used one device and treated it with sucrose for 7 days (control), and later they used the other device and treated it with sucrose and CHX for 7 days (test). Color, microhardness, roughness, surface energy, and insoluble extracellular polysaccharides (EPS) tests were performed. All results were submitted to the Tukey's test, with the exception of the EPS results, which were submitted to the Student's t test.

Results. The Δ^{E00} of the unglazed control group was significantly higher than that of the unglazed test group. In all groups, a significant decrease in microhardness occurred over time. At both times, the glaze significantly increased the microhardness of the specimens (in all the glazed groups). At the final time, the test glaze group showed significantly higher microhardness compared with the control glaze group. Roughness in the groups without glaze increased significantly with CHX treatment over time. At both times, the glaze generated a significant reduction in roughness in the control and test groups. There was a significant reduction in surface energy over time in all groups. In most comparisons, the glazed groups showed significantly higher surface energy values compared with the unglazed control group. At the final time point, the unglazed test group showed a significantly higher surface energy value than the unglazed control group; and the glazed test group showed a significantly higher surface energy value compared with the glazed control group. The resins that received CHX had a significantly lower amount of biofilm.

Conclusions. Color values were clinically acceptable in all tested groups. At both time points, the roughness values were clinically acceptable only in the glazed groups. Glaze increased the microhardness of the specimens. Microhardness and surface energy were reduced over time in all groups. Chlorhexidine can help prevent microhardness degradation. Glaze and CHX can increase surface energy. Chlorhexidine reduced the amount of bacterial biofilm.

Keywords: bacterial adhesion, surface property, temporary dental restorations, dental biofilm

Cite as

Chairelo Commar B, Danelon M, Panitente PA, et al. Effect of glaze and chlorhexidine on physical and mechanical properties of bis-acryl resin: An in situ study. *Polim Med.* 2022;52(2):93–99. doi:10.17219/pim/156868

DOI

10.17219/pim/156868

Copyright

Copyright by Author(s)

This is an article distributed under the terms of the Creative Commons Attribution 3.0 Unported (CC BY 3.0) (<https://creativecommons.org/licenses/by/3.0/>)

Background

Temporary restorations (or provisional prostheses) can be used for long periods of time to enable the evaluation the results of periodontal and endodontic treatment, and during the phases of making a porcelain crown.^{1,2} They have the function of protecting periodontal and dental tissues, in addition to restoring chewing, aesthetics and, in many cases, phonetics.¹ Materials such as acrylic resins and bis-acryl resins can be used to manufacture temporary restorations.¹⁻³ In addition, it is worth mentioning that bis-acryl resins have excellent aesthetics, a relevant factor for patients.

Mouthwashes are widely used in the prevention and control of caries and periodontal diseases, even without a prescription from a dentist.^{3,4} Chlorhexidine (CHX) is a widely used mouthwash due to its antimicrobial action.^{3,5} However, it has the potential to stain restorations, in addition to affecting other factors such as microhardness, roughness and surface free energy.^{3,6}

Color stability is the property of a material to retain its color for a period of time in a given environment.⁷ The color change can be influenced by the surface degradation of the polymeric material, as the degraded areas can serve as deposits of pigments present in various substances, such as CHX.^{3,7,8} Adequate microhardness is also important because it is related to the wear resistance of the material, which in turn is important for preserving its surface integrity over time.⁷ Regarding the surface roughness of a material, it is always recommended that it be as small as possible to avoid microbial adhesion.^{1,9} A rough surface can facilitate the adhesion of the microbial biofilm due to a larger contact surface.³ In addition to roughness, surface energy has an considerable impact on bacterial adhesion, as a material with high surface energy attracts more bacteria to its surface than one with low surface energy.^{1,10} Moreover, surface energy is related to the material's ability to repel or attract water (thus, the higher the surface energy value of a material, the more water it will attract).³ It is worth mentioning that a material that easily attracts water can also absorb it, and this can cause degradation of such material over time.³

In the oral cavity, most bacteria can only survive if they adhere to hard surfaces.¹ To reduce biofilm retention on the temporary restoration, it must be properly ground and polished before installing it on the tooth. Mechanical polishing materials (e.g., abrasive burs with different grits) are used to increase the smoothness of polymer surfaces, thus decreasing bacterial adhesion on them.⁷ It is noteworthy that liquid polishing with light curing sealants is also available to obtain smooth surface of a provisional restoration.⁷

There is a lack of studies that evaluate the alteration of the properties of bis-acryl resins *in situ* with and without glaze in association with the use of antimicrobial solutions. Therefore, the objective of this research was to evaluate

the influence of glaze and 0.12% CHX on the color, microhardness, roughness, and surface energy of the bis-acryl resin. The 2nd objective was to evaluate the antimicrobial efficacy of 0.12% CHX. The null hypotheses were that 1) the analyzed properties would not be altered by the use of 0.12% CHX and glaze application, and that 2) CHX would not have anti-biofilm capacity.

Materials and methods

This study was approved by the Ethics Committee for Research with Human Beings of the Araçatuba Dental School, São Paulo State University, Brazil (process No. 71186117-0-0000-5420). Participants received and signed an informed consent form. This study also followed the guidelines of the Declaration of Helsinki.

Twenty volunteers aged between 18 and 25 years were included in this study.³ Inclusion criteria were: good oral health; good oral hygiene; and absence of gingivitis, periodontitis, carious lesions, systemic diseases, and diseases in the salivary glands.³ In addition, participants who wore any type of dental prosthesis, or orthodontic appliances, or used medications that may alter salivary flow, were excluded.³

Eighty specimens (10 mm in diameter, 2 mm in thickness)³ were made using bis-acryl resin (Protemp 4; 3M ESPE, Two Harbors, USA). The preparation of the specimens followed the manufacturer's recommendations. Protemp 4 is composed of an organic resin system (dimethacrylate polymer and bis-GMA) and inorganic fillers (zirconia silica, fumed silica, silane, and pigments).

The making of the specimens was carried out in metallic matrix according to the method described by Commar et al.³ After polymerization, the surfaces of all specimens ($n = 80$) were polished. This polishing was performed in a semiautomatic polishing machine at a speed of 300 rpm under constant irrigation (Ecomet 300PRO; Buhler, Lake Bluff, USA). In this equipment, 2 sandpapers were used to polish the specimens (400 and 800 grit sandpaper; Buehler).^{3,7} Each specimen had its thickness measured using a digital caliper (500-171-20B; Mitutoyo, Tokyo, Japan) to establish the correct dimensions (10 mm in diameter, 2 mm in thickness)³.

Half of the specimens ($n = 40$) were polished with light curing glaze (Megadenta, Radeberg, Germany).^{3,7} The application of the glaze was carried out with the aid of a brush (KG Brush; KG Sorensen, São Paulo, Brazil).⁷ After 20 s, the glaze layer was photoactivated for 180 s (Strobolux; EDG Equipamentos, São Carlos, Brazil).^{3,7} Thus, the bis-acryl specimens were divided into 2 groups (without and with glaze).

For each volunteer, 2 palatal appliances were made. One device was for control condition analysis and the other was for test condition analysis. The devices were made from chemically activated acrylic resin (Jet; Clássico, São

Paulo, Brazil), and each contained 2 niches in the palatal region with dimensions of 10×2 mm.³ For each device, 1 unglazed specimen was placed in one niche and 1 glazed specimen was placed in the other niche.³ The specimens were fixed in these niches with sticky wax (Kota, São Paulo, Brazil), and covered with a plastic mesh, which was positioned at a distance of 1 mm from the specimens.³ These procedures were performed to avoid displacement of the specimens from their position.³

Initially, the subjects used the first device with the specimens (control group) for 7 days and applied, with a dropper, a drop of 30% sucrose solution on the specimens 6 times a day (sucrose diluted in distilled water was made in a compounding pharmacy (Pharmacy Manipullis, Araçatuba, Brazil)).³ After applying the solution, each volunteer waited 5 min before repositioning the device in their oral cavity. During this 5-minute period, the device was not rinsed and excess solution was not removed from the device.³ After using the device for 7 days (control group), each volunteer did not use any other device for another 7 days (“rest period”). Then, each volunteer started to use their other device containing the test group specimens.³ The period of use of this other device (test group) was 7 days.³ A drop of 30% sucrose was dispensed over the specimens 6 times a day (test group).³ One minute after the 3rd and 6th sucrose application, the specimens (test group) received a drop of 0.12% CHX without dye and alcohol (Pharmacy Manipullis).³ Each volunteer then waited 4 min to place the device (test group) in their oral cavity.³

The volunteers received guidance on cleaning the palatal device with a soft brush and specific toothpaste (Colgate Máxima Proteção Anti-cáries; Colgate Brazil, São Paulo, Brazil) 3 times a day.³ Volunteers were also instructed how to remove the device during meals and clean the oral cavity, and regarding specimen surface treatment protocol.³ All these procedures were performed with the palatal device outside the mouth, but with the specimens properly positioned in their niches.

All specimens (control and test) were submitted to color change, microhardness, roughness, and surface free energy tests before and after the in situ period, corresponding to 7 days. After this period, biofilm collection was also performed on test and control specimens for subsequent insoluble extracellular polysaccharides (EPS) analysis. In all analyses, the plastic mesh was removed and the specimens were removed from their niches.

The color stability (ΔE_{00}) test was performed using a spectrophotometer (UV-2450; Shimadzu, Kyoto, Japan).^{3,9} The ΔE_{00} was calculated using the CIEDE2000 system and the following formula:

$$\Delta E_{00} = \{[\Delta L'/(K_L S_L)]^2 + [(\Delta C'/(K_C S_C)]^2 + [\Delta H'/(K_H S_H)]^2 + R_T[\Delta C'/(K_C S_C) \times [\Delta H'/(K_H S_H)]]\}^{1/2}.^{3,9}$$

The microhardness (Knoop) of the specimens was measured using a microdurometer (HMV-2T; Shimadzu).³ Three penetrations with a load of 25 g for 10 s were made

on the surface of each specimen with 500 μ m of distance between each penetration.³ The values were recorded in Knoop hardness number (KHN). The average of the 3 results obtained was calculated.³

Surface roughness was measured in micrometers with a profilometer (Mitutoyo SJ-400; Mitutoyo) using the cut-off of 500 μ m for 12 s to obtain average roughness (Ra).³ One reading was taken over the center of the specimen and then 2 more readings were taken to the right and to the left of the initial reading.⁹ Then, the average of the 3 results obtained was calculated.

The surface free energy was calculated based on the contact angle.³ Contact angle values were obtained using a goniometer (Krüss DSA20E Easy Drop Goniometer; Krüss Optronic GmbH, Hamburg, Germany) employing the Owens–Wendt–Rabel–Kaelble (OWRK) technique.^{3,11}

For EPS analysis, formed dental biofilm was collected from all specimens using beveled plastic spatulas.¹² To carry out this test, 1.0 mol/L of NaOH (0.1 mL/10 mg dry weight of biofilm) was added to the biofilm precipitate. The EPS analysis was performed by the phenol-sulfuric method. Thus, 25 μ L of 80% phenol and 125 μ L of 95.5% sulfuric acid were added to the biofilm specimens.¹²

The values obtained in the analysis of color change were evaluated with two-way analysis of variance (ANOVA). The values for other tests were submitted to three-way repeated measures ANOVA. All results were submitted to the Tukey’s test ($p < 0.05$), with the exception of the EPS results, which were submitted to the Student’s t-test ($p < 0.001$).

Results

Regarding color evaluation, ANOVA showed that there was a statistical significance for the disinfection factor ($p = 0.013$) (Table 1). The ΔE_{00} value in the unglazed control group was significantly higher than in the unglazed test group (Fig. 1).

Regarding microhardness, ANOVA showed that the glaze ($p < 0.001$) and time ($p < 0.001$) factors, and the interaction between the glaze and disinfection ($p = 0.007$) and time and disinfection ($p = 0.040$) were statistically significant (Table 2). In all groups (Fig. 2), a statistically significant decrease in microhardness was observed over time. At each time point (initial and final), the groups with the glaze showed a significantly higher microhardness than the groups without the glaze (Fig. 2). At the final time point, the test glaze group showed significantly higher microhardness compared with the control glaze group (Fig. 2).

When analyzing surface roughness, ANOVA showed that the interaction between time and glaze factors showed statistical significance ($p = 0.033$) (Table 3). The roughness values in the groups without glaze (control and test) increased significantly over time (Fig. 3). In addition, at both

Table 1. Two-way ANOVA of color change of test and control resins with and without glaze

Factors	SS	df	MS	F	p-value
Glaze	0.043	1	0.043	0.047	0.829
Disinfection	5.836	1	5.836	6.422	0.013*
Glaze × Disinfection	0.933	1	0.933	1.026	0.314
Error	65.433	72	0.909	–	–
Total	301.369	76	–	–	–

* represents statistical significance. ANOVA – analysis of variance; df – degrees of freedom; MS – mean squares; SS – sum of squares

Table 2. Three-way repeated measures ANOVA of microhardness of test and control resins with and without glaze

Factors	SS	df	MS	F	p-value
Glaze	6961.005	1	6961.005	492.332	<0.001*
Disinfection	26.090	1	26.090	1.845	0.179
Glaze × Disinfection	108.059	1	108.059	7.643	0.007*
Between specimens	1017.996	72	14.139	–	–
Time	1238.575	1	1238.575	154.369	<0.001*
Time × Glaze	14.107	1	14.107	1.758	0.189
Time × Disinfection	35.034	1	35.034	4.366	0.040*
Time × Glaze × Disinfection	27.308	1	27.308	3.403	0.069
Intra-specimen	577.692	72	8.023	–	–

* represents statistical significance. ANOVA – analysis of variance; df – degrees of freedom; MS – mean squares; SS – sum of squares.

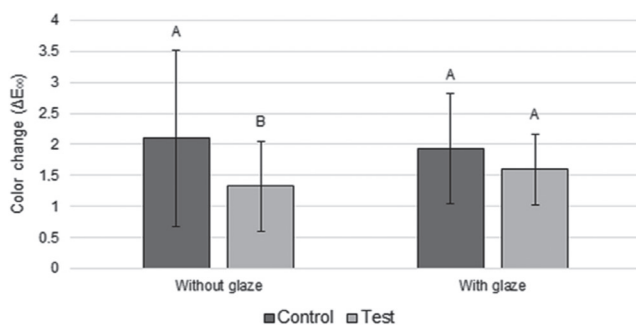


Fig. 1. Tukey's test results ($p < 0.05$). Mean values of color change (ΔE_{00}). Different capital letters between the same glaze group (presence or absence of glaze) indicate a statistically significant difference

time points, the glazed groups showed significantly lower roughness than the unglazed ones (Fig. 3).

Regarding surface free energy, ANOVA showed that the interaction between time and glaze ($p < 0.001$) and time and disinfection ($p = 0.026$) were statistically significant (Table 4). Figure 4 shows that there was a significant reduction in surface energy over time in all groups. At the initial time point, the glazed control group showed significantly higher surface energy value compared with the unglazed control group (Fig. 4). At the final time point, the glazed groups showed significantly higher surface energy values than the unglazed ones (Fig. 4). In addition, at the final time point, the unglazed test group showed a significantly higher surface energy value than the unglazed control group; and the glazed test group showed a significantly

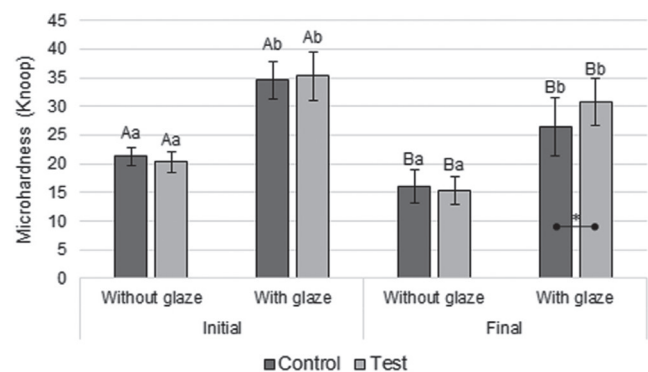


Fig. 2. Tukey's test results ($p < 0.05$). Mean values of microhardness (Knoop hardness number (KHN)). When time points are compared (final compared to initial), mean values with the same capital letter do not differ significantly in the same glaze and resin group. Within each time point (individually), mean values with the same lowercase letter do not differ significantly in the same resin group (control or test). At the same time point, (*) represents a significant difference between the control group and the test group time point the presence or absence of glaze

higher surface energy value compared to the glazed control group (Fig. 4).

For the EPS analysis, more biofilm volume was required than the glazed and unglazed groups could provide separately, so there was no other possibility but to merge the groups with and without glaze in order to perform the EPS test. Perhaps the time period of 7 days was not enough to form more biofilm. Thus, resins that received 0.12% CHX treatment had a significantly lower amount of biofilm compared with resins that did not receive such treatment.

Table 3. Three-way repeated measures ANOVA of roughness of test and control resins with and without glaze

Factors	SS	df	MS	F	p-value
Glaze	1.883	1	1.883	987.436	<0.001*
Disinfection	0.000	1	0.000	0.064	0.800
Glaze × Disinfection	0.000	1	0.000	0.143	0.707
Between specimens	0.137	72	0.002	–	–
Time	0.016	1	0.016	18.576	<0.001*
Time × Glaze	0.004	1	0.004	4.704	0.033*
Time × Disinfection	0.000	1	0.000	0.389	0.535
Time × Glaze × Disinfection	0.001	1	0.001	1.186	0.280
Intra-specimen	0.061	72	0.001	–	–

* represents statistical significance. ANOVA – analysis of variance; df – degrees of freedom; MS – mean squares; SS – sum of squares.

Table 4. Three-way repeated measures ANOVA of surface energy of test and control resins with and without glaze

Factors	SS	df	MS	F	p-value
Glaze	1451.373	1	1451.373	118.618	<0.001*
Disinfection	166.134	1	166.134	13.578	<0.001*
Glaze × Disinfection	3.508	1	3.508	0.287	0.594
Between specimens	880.971	72	12.236	–	–
Time	5693.926	1	5693.926	460.118	<0.001*
Time × Glaze	597.208	1	597.208	48.260	<0.001*
Time × Disinfection	63.844	1	63.844	5.159	0.026*
Time × Glaze × Disinfection	11.011	1	11.011	0.890	0.349
Intra-specimen	890.995	72	12.375	–	–

* represents statistical significance. ANOVA – analysis of variance; df – degrees of freedom; MS – mean squares; SS – sum of squares.

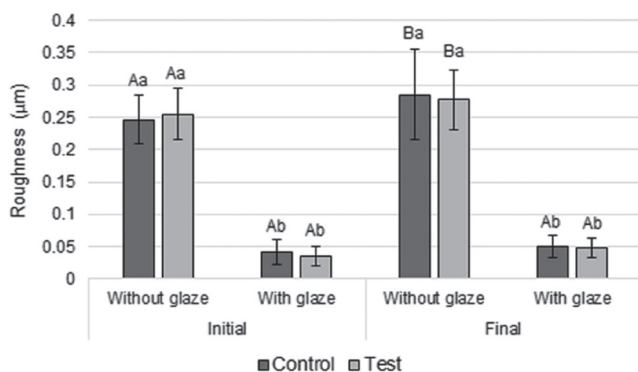


Fig. 3. Tukey's test ($p < 0.05$). Mean values of roughness [μm]. When time points are compared (final compared to initial), mean values with the same capital letter do not differ significantly in the same glaze and resin group. Within each time point (individually), mean values with the same lowercase letter do not differ significantly in the same resin group (control or test). At the same time point, (*) represents a significant difference between the control group and the test group regarding the presence or absence of glaze

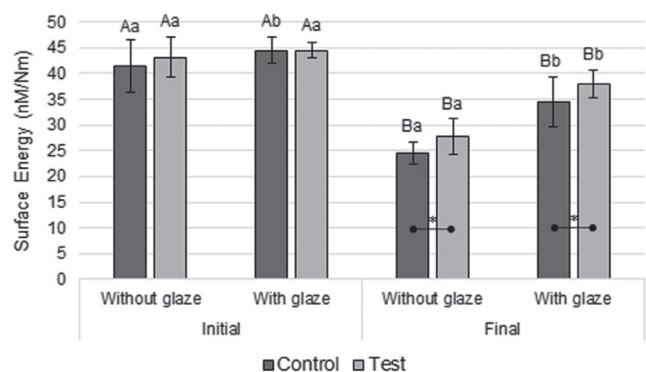


Fig. 4. Tukey's test ($p < 0.05$). Mean values of surface free energy. When time points are compared (final compared to initial), mean values with the same capital letter do not differ significantly in the same glaze and resin group. Within each time point (individually), mean values with the same lowercase letter do not differ significantly in the same resin group (control or test). At the same time point, (*) represents a significant difference between the control group and the test group regarding the presence or absence of glaze

Discussion

The tested null hypotheses were rejected since the properties of the tested material showed changes due to the use of 0.12% CHX and glaze. In addition, 0.12% CHX showed anti-biofilm capacity on the resin.

Bis-acryl resins have a heterogeneous chemical composition formed by an organic and inorganic matrix and a bonding agent.⁷ The chemical composition of a material influences the water sorption (absorption and adsorption) and solubility processes that occur with it, causing a material, for example, to absorb more water than another.⁹

These processes can change the color of the restoration (degradation) due to the exit of water with particles and chemical compounds from the material, as well as the entry of water with particles of different colors and chemical compounds in the material.^{7,9} Chlorhexidine has been widely used in oral diseases due to its antimicrobial effect; despite this, it is worth mentioning that it has the potential to stain polymers.^{6,13} However, in this study, the unglazed group that received the CHX treatment (without dye) showed significantly lower color change values compared with the unglazed group that did not receive such treatment (Fig. 1). This result may be associated with the influence of other extrinsic factors, such as acquired pellicle formation¹³ and more intensive deposition of microorganisms when CHX was not applied.¹⁴ It is worth mentioning that a greater amount of biofilm may result in a greater amount of its toxins that degrade and, consequently, stain the resin.¹⁴ Despite this, all groups showed clinically acceptable levels of ΔE_{00} ($\Delta E_{00} \leq 2.1$; Fig. 1).^{3,9}

Microhardness is related to the wear resistance of materials.⁷ Microhardness significantly decreased in all groups over time (Fig. 2), possibly due to water absorption by the resin, which resulted in hydrolytic degradation between the inorganic particles and the organic matrix.⁷ In addition, at the final time point, the glazed test group exhibited significantly higher microhardness than the glazed control group, probably because 0.12% CHX reduced the amount of biofilm on the surface of the resin used, thus decreasing the amount of toxins generated by the biofilm and, consequently, helping to prevent the degradation of this material. It is worth remembering that the mouthwash used did not contain alcohol in its composition; alcohol would prevent the recognition of the individual effect of CHX on the specimens, as alcohol can degrade the polymer matrix and cause changes in its physical and mechanical properties.^{3,4}

The groups that received the glaze exhibited a significantly higher microhardness than the groups that did not receive it (Fig. 2), presumably because the glaze applied to the surface layer of the specimens had a higher microhardness than the surface of the tested material.⁷ As the tip of the microdurometer measures microhardness only on the surface of the specimens, it is likely that the reading was taken only on the glaze surface and not on the resin.

Adequate surface smoothness is important for a temporary restorative material because it helps to prevent the accumulation of biofilm on the material, which consequently limits its degradation over time, in addition to preventing gingival inflammation.^{1,9,15} In this study, all specimens that received glaze application showed significantly lower roughness values compared with specimens that did not receive glaze (Fig. 3). This may have happened because the glaze has the function of filling microdefects and microcracks present on the surface of the resin, which may remain even after mechanical polishing of the surface of this material.⁷ In addition, there was a significant

increase in roughness over time in all unglazed groups – unlike glazed groups, which did not show a significant increase in roughness values over time (Fig. 3). Thus, the glaze likely protected the specimen surfaces from being significantly roughened over time. It is worth noting that, due to the greater microhardness (higher wear resistance) of the glaze layer compared with the bis-acryl resin, the surface smoothness of this layer was not significantly changed over time (Fig. 3).

Bacterial adhesion on the surface of a material is facilitated when its surface roughness is greater than $0.2 \mu\text{m}$.^{9,15} Thus, it is possible to observe that the groups with glaze showed clinically acceptable roughness $\leq 0.05 \mu\text{m}$ (Fig. 3). On the other hand, all unglazed groups showed clinically unacceptable roughness ($>0.2 \mu\text{m}$; Fig. 3). Therefore, the application of a glaze layer on bis-acryl resin restorations is clinically indicated.

The surface free energy is related to the material's ability to repel or attract water.³ At both times, the glazed groups had significantly higher surface energy values than the unglazed ones ($p < 0.05$), except for the test conditions at initial time ($p > 0.05$; Fig. 4), probably because the glaze has a higher surface energy compared with the bis-acryl resin. As previously reported, a material with high surface energy attracts more bacteria to its surface than a material with low surface energy.^{1,10} Despite this, at both times, the surface roughness was clinically acceptable only in the groups with glaze, helping to prevent bacterial adhesion to the surface of the material.^{9,15} It is worth remembering that the surface energy was significantly reduced over time in all groups (Fig. 4). Thus, the application of glaze over the bis-acryl resin is indicated.

At the final time point, the test groups showed significantly higher surface energy values than their respective control groups (Fig. 4). This may be related to the positive ionic charge present in CHX,^{6,13} which can lead it to the phosphate groups on the surface of the resin, resulting in an increase in the surface energy of the material.³ Thus, although CHX increased the surface energy of the tested material due to its deposition on it, CHX is also bacteriostatic and bactericidal (factors that prevent the increase in the amount of biofilm).

Oral biofilm is the main etiological factor for the development of periodontitis and peri-implantitis.¹⁶ Resins that received 0.12% CHX treatment had a significantly lower amount of biofilm compared to resins that did not receive this treatment. This reduction in the amount of biofilm with CHX treatment can be explained, as CHX penetrates the biofilm, altering its formation (bacteriostatic effect) or having a bactericidal effect.¹⁶ According to Solderer et al., "as the bacterial cell is negatively charged, the cationic CHX molecule binds to its surface. The integrity of the bacterial cell is thus altered in such a way that CHX can penetrate its inner cell membrane leading to an increase in the permeability of this membrane. This results in leakage phenomena of low molecular weight

components from the bacterial cell. At this point, the antimicrobial action is still in the bacteriostatic stage and it can be reversed if the CHX is removed and the bacterial cell is able to recover. If CHX treatment is continued, this may lead to irreversible damage to the bacterial cell (bactericidal effect).¹⁶

The authors of the present study recommend further studies of this nature.

Conclusions

Color values were clinically acceptable in all tested groups. At both time points, the roughness values were clinically acceptable only in the glazed groups. Glaze increased the microhardness of the specimens. Microhardness and surface energy were reduced over time in all groups. Chlorhexidine can help prevent microhardness degradation. Glaze and CHX can increase surface energy. Chlorhexidine reduced the amount of bacterial biofilm.

ORCID iDs

Betina Chiarello Commar  <https://orcid.org/0000-0003-3828-7679>
 Marcelle Danelon  <https://orcid.org/0000-0002-4117-5080>
 Paulo Augusto Panitente  <https://orcid.org/0000-0003-1064-1170>
 Emily Viavianne Freitas da Silva  <https://orcid.org/0000-0002-0164-1788>
 Sandro Basso Bitencourt  <https://orcid.org/0000-0001-9140-7516>
 Valentim Adelino Ricardo Barão  <https://orcid.org/0000-0002-6391-9917>
 Clóvis Lamartine de Moraes Melo Neto  <https://orcid.org/0000-0003-1477-2055>
 Marcelo Coelho Goiato  <https://orcid.org/0000-0002-3800-3050>
 Daniela Micheline dos Santos  <https://orcid.org/0000-0001-6297-6154>

References

1. Şen D, Göller G, İşsever H. The effect of two polishing pastes on the surface roughness of bis-acryl composite and methacrylate-based resins. *J Prosthet Dent.* 2002;88(5):527–532. doi:10.1067/mpr.2002.129335
2. Mickeviciute E, Ivanauskienė E, Noreikiene V. In vitro color and roughness stability of different temporary restorative materials. *Stomatologija.* 2016;18(2):66–72. PMID:27649722.
3. Commar BC, da Silva EVF, Penitente PA, et al. Influence of light-curing glaze and chlorhexidine gluconate in the acrylic resin properties: An in situ study [published online as ahead of print on August 2, 2022]. *Eur J Prosthodont Restor Dent.* 2022. doi:10.1922/EJPRD_2281 Commar07
4. Miranda de A, Bertoldo CE, Aguiar FH, Lima DA, Lovadino JR. Effects of mouthwashes on Knoop hardness and surface roughness of dental composites after different immersion times. *Braz Oral Res.* 2011; 25(2):168–173. doi:10.1590/S1806-83242011000200012
5. Brambilla E, Ionescu A, Gagliani M, Cochis A, Arciola CR, Rimondini L. Biofilm formation on composite resins for dental restorations: An in situ study on the effect of chlorhexidine mouthrinses. *Int J Artif Organs.* 2012;35(10):792–799. doi:10.5301/ijao.5000165
6. Cal E, Güneri P, Kose T. Digital analysis of mouthrinses' staining characteristics on provisional acrylic resins. *J Oral Rehabil.* 2007;34(4):297–303. doi:10.1111/j.1365-2842.2007.01727.x
7. Santos DMD, Commar BC, da Rocha Bonatto L, et al. Surface characterization of polymers used in fabrication of interim prostheses after treatment with photopolymerized glaze. *Mater Sci Eng C Mater Biol Appl.* 2017;71:755–763. doi:10.1016/j.msec.2016.10.059.
8. Soheilifar S, Khodadadi H, Naghdi N, Farhadian M. Does a diluted chlorhexidine-based orthodontic mouthwash cause less discoloration compared to chlorhexidine mouthwash in fixed orthodontic patients? A randomized controlled trial. *Int Orthod.* 2021;19(3):406–414. doi:10.1016/j.ortho.2021.05.001.
9. Paulini MB, Micheline dos Santos D, de Moraes Melo Neto CL, et al. Analysis of physical properties of facial silicones with different pigmentations submitted to nonthermal plasma treatment and accelerated aging. *J Prosthet Dent.* 2020;124(6):815.e1–815.e7. doi:10.1016/j.prosdent.2020.05.034
10. Ahn HB, Ahn SJ, Lee SJ, Kim TW, Nahm DS. Analysis of surface roughness and surface free energy characteristics of various orthodontic materials. *Am J Orthod Dentofacial Orthop.* 2009;136(5):668–674. doi:10.1016/j.jado.2007.11.032
11. Valverde GB, Coelho PG, Janal MN, et al. Surface characterisation and bonding of Y-TZP following non-thermal plasma treatment. *J Dent.* 2013;41(1):51–59. doi:10.1016/j.jdent.2012.10.002
12. Takeshita EM, Danelon M, Castro LP, Sasaki KT, Delbem ACB. Effectiveness of a toothpaste with low fluoride content combined with trimetaphosphate on dental biofilm and enamel demineralization in situ. *Caries Res.* 2015;49(4):394–400. doi:10.1159/000381960
13. Sheen S, Banfield N, Addy M. The effect of unstimulated and stimulated whole saliva on extrinsic staining in vitro: A developmental method. *J Dent.* 2002;30(7-8):365–369. doi:10.1016/S0300-5712(02)00053-2
14. Sousa RP, Zanin ICJ, Lima JPM, et al. In situ effects of restorative materials on dental biofilm and enamel demineralisation. *J Dent.* 2009;37(1):44–51. doi:10.1016/j.jdent.2008.08.009
15. Perez CR, Hirata R, Silva AHMFT, Sampaio EM, Miranda MS. Effect of a glaze/composite sealant on the 3-D surface roughness of esthetic restorative materials. *Oper Dent.* 2009;34(6):674–680. doi:10.2341/08-014-L
16. Solderer A, Kaufmann M, Hofer D, Wiedemeier D, Attin T, Schmidlin PR. Efficacy of chlorhexidine rinses after periodontal or implant surgery: A systematic review. *Clin Oral Invest.* 2019;23(1):21–32. doi:10.1007/s00784-018-2761-y

Spray drying and nano spray drying as manufacturing methods of drug-loaded polymeric particles

Suszenie rozpyłowe i nanosuszenie rozpyłowe jako metody sporządzania cząstek polimerowych z substancjami leczniczymi

Dominik Strojewski^{A–D}, Anna Krupa^{A,E,F}

Department of Pharmaceutical Technology and Biopharmaceutics, Jagiellonian University Medical College, Kraków, Poland

A – research concept and design; B – collection and/or assembly of data; C – data analysis and interpretation; D – writing the article; E – critical revision of the article; F – final approval of the article

Polymers in Medicine, ISSN 0370-0747 (print), ISSN 2451-2699 (online)

Polim Med. 2022;52(2):101–111

Address for correspondence

Anna Krupa
E-mail: a.krupa@uj.edu.pl

Funding sources

This review was prepared in the frame of SONATA BIS grant No. DEC-2019/34/E/NZ7/00245, financed by the National Science Centre in Kraków, Poland.

Conflict of interest

None declared

Received on June 12, 2022

Reviewed on July 13, 2022

Accepted on July 20, 2022

Published online on August 12, 2022

Abstract

In this review, benefits and drawbacks of the process of spray drying and nano spray drying with regard to the manufacturing of polymeric particles for pharmaceutical applications are discussed. Spray drying has been used for many years in the food, chemical and pharmaceutical industries for converting liquids into solids, in order to form products of uniform appearance. The construction of spray dryer enables to atomize the liquid into small droplets, which ensures a large surface area for heat and mass transfer, and significantly shortens the processing. Each droplet dries to an individual solid microparticle of characteristic features that can be tailored by optimizing formulation variables and critical process parameters. Since spray drying technology is easy to scale up and can be used for drying almost any drug in a solution or suspension, there are numerous examples of products in clinical use, in which this process has been successfully applied to improve drug stability, enhance bioavailability or control its release rate. In recent years, nano spray drying technology has been proposed as a method for lab-scale manufacturing of nanoparticles. Such an approach is of particular interest at early stages of drug development, when a small amount of new chemical entities is available. Here, the nebulization technique is used for feed atomization, while laminar gas flow in the drying chamber ensures gentle drying conditions. Moreover, electrostatic collectors have gradually replaced cyclone separators, ensuring high effectiveness in producing solid nanoparticles, even if a small volume of the sample is processed.

Key words: nano spray drying, spray drying, polymeric particles, microparticles, nanoparticles

Cite as

Strojewski D, Krupa A. Spray drying and nano spray drying as manufacturing methods of drug-loaded polymeric particles. *Polim Med.* 2022;52(2):101–111. doi:10.17219/pim/152230

DOI

10.17219/pim/152230

Copyright

Copyright by Author(s)

This is an article distributed under the terms of the Creative Commons Attribution 3.0 Unported (CC BY 3.0) (<https://creativecommons.org/licenses/by/3.0/>)

Streszczenie

W artykule omówiono zalety i wady procesu suszenia rozpyłowego i nanosuszenia rozpyłowego w odniesieniu do wytwarzania cząstek polimerowych do zastosowań farmaceutycznych. Suszenie rozpyłowe jest procesem stosowanym od wielu lat w przemyśle spożywczym, chemicznym i farmaceutycznym. Służy do przekształcania próbek ciekłych w jednorodne ciała stałe. Konstrukcja suszarki rozpyłowej umożliwia rozpylenie cieczy na drobne krople, co zapewnia dużą powierzchnię suszenia i prowadzi do skrócenia tego procesu. Właściwości stałych mikrocząstek można projektować przez optymalizację zmiennych, zależnych od receptury i krytycznych parametrów procesu. Ponieważ technologia suszenia rozpyłowego jest łatwa do zastosowania w skali przemysłowej i może być stosowana do suszenia niemal każdej substancji leczniczej w postaci roztworu lub zawiesiny, istnieje wiele przykładów zarejestrowanych produktów leczniczych opracowanych przy użyciu tej metody. Dzięki zastosowaniu suszenia rozpyłowego możliwe było zwiększenie trwałości i biodostępności lub kontrola szybkości uwalniania wielu substancji leczniczych. W ostatnich latach zaproponowano technologię suszenia nanorozpyłowego jako metodę przeznaczoną do wytwarzania stałych nanocząstek w skali laboratoryjnej. Takie podejście jest szczególnie interesujące na wczesnych etapach opracowywania nowych leków, gdy są one dostępne w ograniczonej ilości. W tej metodzie technika nebulizacji jest wykorzystywana do atomizacji cieczy, natomiast laminarny przepływ gazu w komorze zapewnia łagodne warunki procesu suszenia. Z kolei separatory cyklonowe zastąpiono kolektorem elektrostatycznym, co zapewnia wysoką wydajność procesu wytwarzania stałych nanocząstek, nawet w przypadku małych próbek.

Słowa kluczowe: nanosuszenie rozpyłowe, suszenie rozpyłowe, cząstki polimerowe, mikrocząstki, nanocząstki

Introduction

Spray drying is a well-known industrial technology that is used to transform liquids into powders.^{1,2} Due to the fact that both aqueous and organic solvents can be used for such processing, this technology is suitable for combining compounds of different physicochemical properties with the aim of enhancing their functionality. The opportunity to design the particle size, shape, surface roughness, and surface composition of the final product by optimizing critical process parameters and formulation variables makes spray drying a suitable method of modifying unfavorable properties of both drugs and excipients. Importantly, spray drying is a one-step, continuous, cost-effective, and easy-to-scale process that can be used for manufacturing various polymeric drug delivery systems, including aseptic formulations.^{3,4}

Advantages of spray drying

Multiple studies provided evidence that upon spray drying, it is possible to transform crystalline drugs into amorphous microparticles. A reduction of particle size followed by an increase of specific surface area, together with the modification of the physical form may translate into better solubility of the drug in water and, finally, in the enhancement of bioavailability.^{5,6} Hence, the combination of drugs with polymers allows for manufacturing complex polymeric drug delivery systems that can control drug release, which remains stable for a long period of time.^{7,8} Furthermore, the preparation of spherical particles may improve the flowability of the powder bed, which is an important factor in compaction or capsules filling.^{9,10} In turn, the porous surface of spray-dried particles may be crucial

in ensuring compactibility, facilitating mechanical interlocking of particles upon compaction and, as a result, ensuring a high mechanical strength of tablets. Importantly, such processing can be used even for thermolabile compounds, as their exposition to high temperature is very short.³ Thus, the spray drying process is used for the encapsulation of labile compounds with the aim of improving their stability in contact with water vapor, oxygen, ultraviolet (UV) radiation, incorrect pH, or other incompatible compounds.

Therefore, during the last 2 decades, the spray drying process has been used in manufacturing of several drug products for both systemic and topical drug delivery. These products are mainly administered orally, by inhalation or via parenteral route.^{11,12} Due to the fact that the spray drying process is considered one of the most commonly used industrial methods of ASD manufacturing, among the examples of commercially available spray-dried drug products there are formulations loaded with polymeric amorphous solid dispersions (ASD), e.g., immunosuppressive Prograf (tacrolimus, Astellas Pharma, 1994) and Zortress (everolimus, Novartis, 2010).¹³ Recently, several fixed-dose combination drugs with polymeric ASD composed of 2 or 3 active pharmaceutical ingredients (API) have also been launched, such as Orkambi (lumacaftor/ivacaftor, Vertex, 2015), Zepatier (elbasvir/grazoprevir, Merck, 2016), Trikafta (elexacaftor/tezacaftor/ivacaftor, Vertex, 2019), and Symdeko (tezacaftor/ivacaftor, Vertex, 2019).^{14,15} The spray drying process is also suitable for preparing protein formulations, e.g., inhaled insulin powder Exubera (Pfizer Inc./Nektar Therapeutics, 2006) or Afrezza (MannKind Corp., 2015), microsphere suspension loaded with lanreotide acetate for intramuscular injections Somatuline (Ipsen, 2013), or a powder fibrin sealant Raplixa for topical bleeding control during surgery (fibrinogen/thrombin, Nova Laboratories, 2016).^{3,16,17}

Spray drying technology in a nutshell

The spray drying process consists of 3 main phases, namely atomization, evaporation of the solvent and collection of particles.¹⁸ Atomization is the process of turning a liquid into a fine spray. For this purpose, 3 kinds of atomizers can be used, i.e., rotary atomizers, hydraulic nozzles or pneumatic nozzles.¹⁸ The size of the droplets formed is controlled by the type of nozzle, as well as surface tension, viscosity and density of the fluid.¹⁹ To prepare feed solutions water, organic solvents and their mixtures are used. Table 1 shows the characteristics of organic solvents that are often utilized in spray drying, while a scheme of a spray drier is shown in Fig. 1A. The atomized droplets pass through a drying chamber flushed with drying gas.

The droplet–drying gas contact can be of countercurrent, cocurrent or mixed flow type. Cocurrent contact systems are widely used for pharmaceutical purposes.²⁰ Atmospheric air, previously filtered and preheated, is usually applied as drying gas.² However, if flammable organic solvents are used or compounds are prone to oxidation, the air in the drying chamber is replaced by inert gases, i.e., nitrogen. In this way, the level of oxygen can be considerably reduced, which limits the risk of chemical degradation or explosion. In such cases, the drying is carried out in tightly close systems (loops), where an aspirator is used for the circulation of the inert gas. The vapors of organic solvents are condensed in a refrigerator and collected in a closed receiver. The cleaned gas stream is preheated and flows back to the spray dryer. It is worth mentioning that modern spray dryers are also equipped with

Table 1. Characteristics of organic solvents used in spray drying and nano spray drying

Solvent name	Methanol	Acetone	Acetonitrile	Ethanol	Dichloromethane
Structure	CH ₃ OH	CH ₃ COCH ₃	CH ₃ CN	CH ₃ CH ₂ OH	CH ₂ Cl ₂
Density at 20°C [g/cm ³]	0.792	0.784	0.786	0.789	1.33
Freezing point [°C]	−98	−94.8	−45.7	−114	−95
Boiling point [°C]	65	56.1	81.6	78	40
Flammability	highly flammable liquid and vapor				non-combustible danger of explosion with: alkali metals, nitric acid, aluminum, amines, nitrogen oxides (NO _x) exothermic reaction with: alkaline earth metal, metal powder, strong alkali
Auto-ignition temperature [°C]	455	465	524	455	605
Lower (LEL) and upper (UEL) explosion limits [vol. %]	5.5–44	2.6–12.8	4.4–16	2.5–13.5	13–22
Solubility in water at RT [g/L]	freely soluble	freely soluble	1	freely soluble	≈20
Viscosity at RT [mPas]	0.60	0.32	0.39	0.54–0.59	0.43
ICH solvent class	2	3	2	3	2

ICH – International Council for Harmonisation of Technical Requirements for Registration of Pharmaceuticals for Human Use; RT – room temperature.

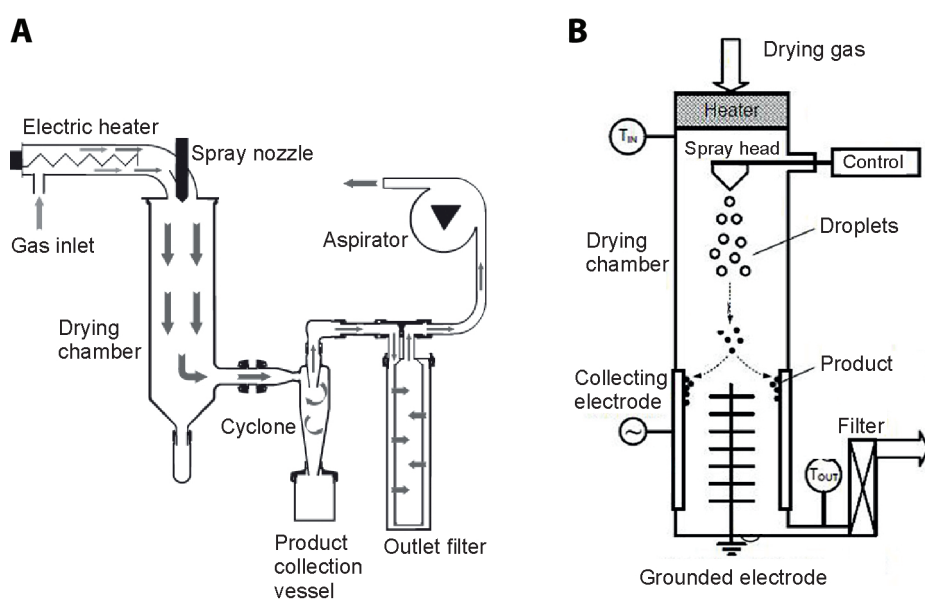


Fig. 1. The comparison of a spray dryer (A) and a nano spray dryer (B)

dehumidifiers. For water-organic solvents, strict control of the drying gas inside the drying chamber ensures robust process conditions and uniform product characteristics, and prevents the deposition of the product on the walls of the drying chamber.²¹

The size of the drying chamber determines the drying time, which is of particular importance for aqueous feed solutions. Two types of drying chambers of different height-to-diameter ratio (5:1 for tall and 2:1 for small chambers) are used.^{18,22} Since the drying time is longer in large chambers than in small chambers, the former are recommended for aqueous fluids.^{1,23}

To separate dry solid particles from the air stream, centrifugal separators in the form of cyclone units are commonly used. The drying gas enters the cyclone at the top and is set in a circular, spiraling motion. In consequence, solid particles moving in the gas stream under the influence of centrifugal force are thrown against the cyclone walls and fall down into the receiver, where they are collected. In turn, the exhaust gas is filtered and removed from the chamber. Unfortunately, particles can also settle on the walls of the drying chamber or cyclone, reducing the efficiency of the process. To prevent the product from being deposited on the walls and to protect it from the mechanical scraping, nonstick coatings and the receivers of cone-shaped bottoms can be applied.^{23,24} It should be stressed that a significant limitation of cyclone is its inability to separate particles smaller than 2 μm from drying gas. If high-performance cyclones are used, particles bigger than 1.4 μm can be separated, but if submicrometer particles are formed, they are removed from the chamber in the exhaust gas.^{25–27}

Optimizing spray drying process

The quality of the spray-dried product is determined by critical process parameters and formulation variables. Therefore, the application of the quality by design (QbD) approach together with process analytical technology (PAT) considerably shortens the transfer of this technology from the laboratory scale to the production plant.²³ Since there are many parameters that can be controlled in such a processing, the relationships between them are complex and sometimes difficult to predict. Therefore, a risk analysis is often combined with statistical tools such as design of experiment (DoE), with the aim to effectively optimize the properties of the spray-dried product, e.g., the morphology of particles.²⁸ In general, particles obtained in this process can be in the shape of spheres with surrounded cores, spheres with empty cores, porous solid foams, microparticles consisting of nanoparticles, composite shells, nanocomposites, or particles with irregular shapes.^{29,30} Until now, multiple research studies have shown that the particle engineering is possible

by tuning the value of critical process parameters (CPPs) to finally meet previously defined critical quality attributes (CQA).³¹

One of the most important CPPs is the inlet temperature of the drying gas. In conventional spray driers, it can be regulated up to 220°C. High inlet temperature ensures a high solvent evaporation rate, which has an impact on the particle formation process and the stability of the final product. Particles formed at high temperatures are bigger than those prepared at low temperatures, because of the agglomeration of primary microparticles. The surface of such particles may also be rough. Moreover, the solvent evaporation rate determines the kinetics of nucleation, which is crucial when amorphous forms are prepared. If the inlet temperature is too high, the solvent evaporates immediately and crystallizing solids may clog the nozzle, not to mention the risk of thermal degradation of thermally sensitive compounds.²³ Yet, it should be noted that the transition from the droplet to the particle takes milliseconds, which limits the risk of thermal degradation of compounds.²³

In turn, the outlet temperature of the drying gas cannot be regulated directly by an operator, because its value depends on solvent vaporization enthalpy, solid load in the feed, inlet temperature, and flow rate of the drying gas. In theory, this is the highest temperature at which the compound can be heated without stability concerns. For amorphous systems, the outlet temperature should not be higher than the temperature of the glass transition, due to the risk of recrystallization. Furthermore, under such conditions, the particles become sticky and easily form deposits on the walls of the drying chamber, which has a negative impact on the yield.³² The outlet temperature influences the level of residual organic solvents or the moisture in the spray-dried product. If its content is too high, an additional drying procedure might be necessary. Attention should be paid to spray-dried biomolecules, as organic solvents or their mixture with water may cause rigidification of their conformation, aggregation, dehydration, and even damage to their molecular structure.¹⁷

An important formulation variable that has an impact on the product morphology is the viscosity of the feed.³³ In conventional spray drying, the atomization of liquids that have viscosity lower than 300 mPas is possible.³⁰ The higher the viscosity, the more difficult it is for droplets to form, and finally, the more energy is needed for atomization. Since the viscosity value is usually related to the solid content in the feed, it is estimated that for a proper droplet formation, it should be below 30%. Moreover, the grade and the concentration of the polymeric carrier are other important factors. In turn, adding surfactants to the feed reduces the surface tension, leading to a small droplet size. The velocity of these droplets is high, and, consequently, a wide spray pattern is obtained.^{1,2,29,33}

Polymeric drug carriers used for spray drying

Table 2 presents the examples of polymers used as carriers for various drugs in order to prepare microparticulates in the spray drying process. They are derivatives of the following:

- cellulose – hydroxypropylmethylcellulose (HPMC)³⁴, hydroxypropylmethylcellulose acetate succinate (HPMCAS)³⁵;
- aminopolysaccharides – chitosan³⁶;
- vinylpyrrolidone – polyvinylpyrrolidone (PVP),³⁷ copolymer of polyvinylpyrrolidone and vinyl acetate (PVPVA)³⁸;
- poly(methacrylic) acid – Eudragit³⁹;
- poly(vinyl) alcohol (PVA)^{40,41};
- poly(ethylene oxide) – Macrogols^{29,42};
- aliphatic polyesters – poly(lactide) acid (PLA),⁴³ poly(lactide-co-glycolide acid) (PLGA).⁴⁴

In recent years, the application of aliphatic polyesters to form drug delivery systems in the spray drying technique has been widely investigated because of the reputation of biocompatible, biodegradable and bioabsorbable drug carriers. The Food and Drug Administration (FDA) and European Medicines Agency (EMA) have approved the use of PLGA in humans in various ratios and molecular weights.⁴⁵ Different forms of this polymer can be obtained by manipulating the ratio of lactide to glycolide during polymerization. The glass transition temperature (T_g) of PLGA ranges from 43°C to 55°C and decreases as the amount of glycolide increases. The grades with low molecular weight and high glycolide content are characterized by high hydrophilicity and amorphousness, which reduces the degradation time.⁴⁶ All aliphatic polyesters are prone to hydrolysis in contact with water or water vapor. As a result, hydroxycarboxylic acids are formed, e.g., PLGA is hydrolyzed to lactic and glycolic acid.⁴⁷ Importantly, the degradation rate of PLGA in vivo can be controlled by tuning the physicochemical properties of the polymer, i.e., crystallinity, hydrophobicity, copolymer ratio, and molecular weight.⁴⁶ The results of multiple studies provided evidence stating that PLGA are suitable for the manufacturing of diverse drug delivery systems composed of microparticles formed in the spray drying process, as they are soluble in many organic solvents, e.g., chloroform, ethyl acetate, ethyl formate, or dichloromethane (DCM).⁴⁸ The latter has a low boiling point (40°C, Table 1), which facilitates processing and prevents polymer agglomeration at high temperatures.^{49,50} The size of PLGA microparticles ranges from 1.3 µm to 15 µm, whereas the yield can be up to 75%. The drug release rate is mainly governed by the content of individual monomers in the copolymer.⁵¹ When hydrophilic excipients such as trehalose, sucrose or PVA are combined with PLGA, proteins and enzymes can be successfully transformed into stable dry powder.^{48,52,53} Therefore, while using PLGA, the development of controlled release

drugs suitable for various routes of administration, including long-acting parenteral drugs, is possible.

Principles of nano spray drying technology

In 2009, Büchi Labortechnik AG (Flawil, Switzerland) launched the first nano spray drier (B-90) that enables the preparation of nanoparticles (understood here as the particles < 1 µm) of a precisely tailored morphology and a narrow particle size distribution.⁵⁴ Importantly, such processing can be performed with high efficiency (up to 96%) and while using a small amount of the drug (10 mg (2.7 g)).¹⁶ The construction of a nano spray dryer can be compared with that of a conventional spray dryer in Fig. 1, while the comparison of the most important features of a spray dryer and a nano spray dryer is presented in Table 3. Briefly, this technology enables nanosizing of drugs, their nanoencapsulation, structural change (crystalline-to-amorphous transition), or preparing nano spray-dried dispersions in matrix-forming excipients.^{55,56}

In contrast to conventional spray dryers, where nozzles of various kinds can be used, a nebulizer mounted on the spray head is responsible for creating tiny aerosol droplets in a nano spray dryer. Importantly, the construction of the nebulizer based on vibrating mesh technology ensures droplet formation with a high precision and reproducibility with regard to its size.⁵⁷ As a result, the particle size distribution of the final product is narrow. Essentially, the feed is circulating over the surface of a thin, perforated metal plate with laser-drilled holes of 4.0 µm, 5.5 µm or 7.0 µm in diameter. Under high-frequency vibrations of a piezoelectric actuator, the spray mesh moves rapidly upwards and downwards, ejecting droplets through the cylindrical holes into the drying chamber (Fig. 1B).^{30,42} The laminar flow of drying gas directs droplets, and then solid particles, into the lower part of the drying chamber, where the latter are electrostatically charged in a high electrostatic field, created between a star-shaped discharge electrode (cathode) and a cylindrical collecting electrode (anode).^{60,61} A high voltage (15–17 kV) at the collecting electrode ensures high efficiency of separation of submicron particles from the drying (up to 99%), even for small samples.^{16,59,60,62} Interestingly, such a separation method is gentle and can be used for collecting even brittle nanoparticles without destroying them. In the end, the dried powder is removed from the surface of the collecting electrode using a scraper.¹⁶

Similarly to the conventional spray drying process, it is possible to adjust the properties of the nano spray-dried product, optimizing both formulation variables and critical process parameters.^{16,18} In general, the particle size of nano spray-dried products ranges between 0.2 µm and 5 µm. Thus, the manufacturing of nanoparticles or microparticles is possible. The most important variables

Table 2. Examples of polymers used as carriers for preparing spray-dried formulations

Drug and route of administration	Carrier	Drug:carrier ratio (w/w)	Solvent	Process parameters	Yield [%]	Particle size [μm]	Particle morphology	Advantages
Carbamazepine ³⁴ for oral administration	Chitosan HPMC	1:1 7:3 9:1	for crude drug: ethanol 96% for samples loaded with HPMC: ethanol/water 2:3 (v/v) for samples loaded with chitosan: 0.5% acetic acid	inlet temperature: 120°C outlet temperature: 75°C spray flow rate: 0.25 L/h air flow rate: 700 N \times L/h	~30	~3	Spherical microspheres	drug amorphization; faster drug release from chitosan-HPMC composite microparticles than those made of HPMC; sustained drug release possible
Andrographolide ³⁷ for oral administration	PVP	1:2 1:3 1:4	methanol	inlet temperature: 60°C outlet temperature: 45°C feed rate: 6–8 mL/min atomization air pressure: 2 kg/cm ²	60–70	2.8–3.6	spherical microparticles	micronization; drug amorphization; stabilizing effect of hydrogen bonds; 5-fold solubility increase
Felodipine ³⁸ for oral administration	PVPVA	1:4	acetone	inlet temperature: 72–184°C outlet temperature: 32–61°C feed rate: 110–188 g/min atomization air pressure: 2.11 kg/cm ² cyclone: 10.2 cm or 15.2 cm two-fluid nozzle or pressure swirl nozzle	66–90	4–115	intact, collapsed or fractured hollow spheres	drug amorphization; flowability of amorphous solid dispersions suitable for compaction; high mechanical resistance of tablets
Diltiazem ³⁹ for oral administration	Eudragit RS & Eudragit RL	1:2 1:4 1:8	DCM	inlet temperature: 70°C outlet temperature: 57–60°C feed rate: 2–5 mL/min spray-flow: 700 N \times L/h 0.5 mm nozzle	N/A	1–9	smooth microspheres	narrow particle size distribution; drug amorphization; high drug load results in faster release rate
Caffeine or progesterone ⁴³	PLA	for progesterone: 10:90 20:80 35:65 50:50 for caffeine: 25:75 40:60 60:40 75:25	DCM	inlet temperature: 70°C outlet temperature: 40–45°C spray flow: 600 N \times L/h 0.5 mm nozzle	N/A	<5	microparticles with progesterone: spherical; those loaded with caffeine: needle-shaped	drug micro-encapsulation; retarded drug release
Vancomycin ⁷ for topical ocular delivery	PLGA	1:2 1:3 1:4	for drug: water for polymer: DCM	inlet temperature: 80–85°C outlet temperature: 68–70°C spray rate: ~10 mL/min 0.7 mm nozzle	<55	10.96–11.75	almost spherical particles with smooth surface, agglomerates visible	controlled drug release; enhanced pharmacokinetic parameters of drug from aqueous suspensions of microspheres shown in rabbit model

DCM – dichloromethane; HPMC – hydroxypropylmethylcellulose; PVP – poly(vinyl)pyrrolidone; PVPVA – poly(vinyl)pyrrolidone/vinyl acetate; PLA – poly(lactic) acid; PLGA – poly(D,L-lactide-co-glycolide); N/A – not available.

that are crucial in particle engineering using a nano spray dryer are listed in Table 3. The majority of nano spray-dried particles are spherical, but they can be wrinkled

or doughnut-like in shape as well. Their internal structure may be hollow, solid or porous. With regard to the feed composition, the same solvents can be used as in spray

Table 3. Differences between spray drying and nano spray drying technology with critical process parameters (CPPs) of nano spray drying

Characteristics	Spray dryer	Nano spray dryer	CPPs in nano spray drying
Feed kind	solution suspension emulsion	solution nanosuspension nanoemulsion	<ul style="list-style-type: none"> • feed type and composition • viscosity max. 10 mPas • surface tension • sample volume • circulation pump rate • inlet temperature • chamber length • drying gas type (air, N₂/CO₂) • drying gas humidity • drying gas flow • aspirator speed • vibration frequency • spray rate intensity • spray mesh size • electric field
Solvents	water; organic solvents, water–organic mixtures		
Minimal sample volume [mL]	30	2	
Maximal drying temperature [°C]	220	120	
Particle size [µm]	2–100	0.2–5	
Particle size distribution	broad	narrow	
Drying gas flow	turbulent	laminar	
Nozzle type	hydraulic, pneumatic, ultrasonic	piezoelectric spray head	
Particle separation	cyclone	high voltage collecting electrode (15 kV)	
Yield [%]	50–70	70–90	
Processing scale	lab [g], pilot [kg], industrial [t]	lab [g]	

drying, yet when organic solvents are used, the outlet temperature is higher than that typical of the aqueous feed. Taking into account the mechanism of nebulization, attention should be paid to the particle size of the solids in dispersed feed systems, the solid load and the viscosity of this liquid formulation. Only solutions, nanosuspensions or nanoemulsions can be applied in nano spray drying, because the coarse particles dispersed in suspensions would block the mesh of the nebulizer.^{50,62–65} If the solid concentration in the feed increases, the particles of the final product become larger, the yield may be higher, and at the same time, the feed rate and the process are longer. Thus, it is recommended that the optimal viscosity of the feed should be less than 10 mPas. This value is twenty times lower than that of the maximal viscosity of the feed suitable for spray drying. If the viscosity of the feed is high, doughnut-like particles can form.^{30,66} When smooth surface is preferable, the addition of a surfactant into the feed can give favorable results, as the reduction of the particle size is observed.^{60,62,63} Similarly, organic solvents combined with surfactants promote hollow particles.⁶⁷

In terms of CPPs, slow drying results in more compact particles, whereas fast drying generates hollow particles.⁶⁸ When the mesh size is increased, the droplet size also increases, and then the particle size of the final product increases as well. Therefore, the application of the mesh with the biggest holes (7 µm) requires a higher feed rate during processing. A high spray rate intensity results in lower outlet temperature, which may be favorable for amorphous drugs. However, in such a process, slightly larger particles are formed, and their stability can be low. Additionally, when the drying gas flow rate increases, the outlet temperature increases as well, and the solvent content in the product is reduced. Yet, if the humidity of the drying gas is high, the moisture level and the outlet temperature increase, and the yield may decrease.

Applications of nano spray drying

Throughout the last 2 decades, nano spray drying technology has been applied for the manufacturing of nanocrystals, amorphous nanoparticles, and amorphous or crystalline solid dispersions of various drugs in polymeric, protein or carbohydrate carriers (Table 4).⁵⁶ It is worth mentioning that not only nanoparticles, but also microparticles can be formed upon such a processing. They can be used for systemic or topical drug delivery. Moreover, there are reports stating that combining microparticles formed in conventional spray drying with nanoparticles prepared using nano spray drying technology can be an interesting option in the development of modern therapies. Thus, multiple studies proved that nano spray drying can be a powerful method that enables the formation of complex systems destined for oral, inhalation, nasal, intravenous, ophthalmic, or dermal administration.^{16,69,70} Their application can be useful in the treatment of pulmonary,⁷¹ oncological⁷² and immune diseases,⁵⁰ as well as mental disorders.⁷³ They can help control cerebral vasospasm⁷⁴ and coat medical implants with the aim of making them biocompatible.^{75,76}

Baba and Nishida developed nanocrystals of calpain inhibitors that prevent programmed cell apoptosis and can be used in the therapy of Alzheimer's disease and Parkinson's disease.⁷⁷ Moreover, they reported that an aqueous dispersion of these nanocrystals could be applied in the form of eye drops for the treatment of Fuchs' endothelial dystrophy of the cornea. To prepare nanocrystals, the ethanolic feed solution loaded with 0.05% or 0.5% of the drug was prepared using 3 types of mesh sizes available (4.0 µm, 5.5 µm and 7.0 µm), and 2 gas flow rates (100 L/min or 150 L/min). The results showed that the particle size of the nanocrystals increased along with an increasing mesh size. Interestingly, the inlet temperature and the high gas flow rate did not influence the particle size. The same relationship was found for dexamethasone or fluorometholone (Table 4).⁷⁸

Table 4. Examples of nano spray-dried drugs, protein and polymeric formulations with process parameters

Drug/year	Carrier	Drug:carrier ratio (w/w)	Solid concentration/ solvent/ in feed	Process parameters	Particle size [μm]	Particle morphology	Product properties
Calpain inhibitors ⁷⁷ 2012	–	–	0.05% 0.50% ethanol solution	inlet temperature: 50°C outlet temperature: 35°C feed rate: 25 mL/h frequency: 60 kHz drying gas: N ₂ /CO ₂ gas flow rate: 100 L/min or 150 L/min mesh size: 4.0; 5.5; 7.0 μm	0.38–0.85	spherical smooth surface	nanocrystals
Dexamethasone, Fluorometholone ⁷⁸ 2013	–	–	for dexamethasone: 1% for fluorometholone: 0.1% ethanol solution	inlet temperature: 50°C outlet temperature: 35°C feed rate: 25 mL/h frequency: 60 kHz drying gas: N ₂ /CO ₂ gas flow rate: 100 L/min mesh size: 4.0; 5.5; 7.0 μm	for dexamethasone: 0.83–1.34 for fluorometholone: 0.60–0.86	spherical shape; smooth surface	nanocrystals; particle size increases with increasing mesh size and solid concentration
Vildagliptin ⁷⁹ 2015	Gelatin	1:1	0.5% (0.25% of drug) solution in water	inlet temperature: 120°C outlet temperature: 27°C gas flow rate: 100–110 L/min mesh size: 4.0 μm	0.45	spherical shape, smooth but undulated surface	mucoadhesive nanospheres of gastroretentive properties
Cyclosporin A, Dexamethasone ⁵⁰ 2012	PLGA	1:5	0.5–2% of solids in DCM and ethanol mixture (70:30)	inlet temperature: 29–32°C outlet temperature: 28–32°C feed rate: 25 mL/h frequency: 60 kHz drying gas: N ₂ /CO ₂ gas flow rate: 102–132 L/min spray rate: 50–100% pressure: 36–51 mbar mesh size: 4.0; 5.5 μm	0.90–2.23	spherical micro- and nanoparticles; narrow particle size	cyclosporin A molecularly dispersed in PLGA; dexamethasone in crystalline form dispersed in PLGA
Sildenafil ⁸⁰ 2015	PLGA	1:9	1–10% of solids in acetone solution	inlet temperature: 45°C outlet temperature: 25–30°C frequency: 60 kHz drying gas: N ₂ /CO ₂ gas flow rate: 100 L/min mesh size: 4.0; 5.5 μm	4–11	spherical particles, agglomerates visible	prolonged drug delivery to lungs; mesh size and solid load determine particle size
Simvastatin ⁷² 2018	PLGA	1:10	O/W emulsion O: 0.25% of drug & 2.5% of PLGA in DCM W: 1% PVA aqueous solution emulsion diluted 3 times with water before processing	N/A apart from the mesh size: 7.0 μm	0.26	spherical particles	polymeric nanoparticles for breast cancer treatment

N/A – not available; DCM – dichloromethane; PLGA – poly(D,L-lactide-co-glycolide); O/W – oil-in-water; PVA – poly(vinyl alcohol).

Furthermore, it was stated that when the concentration was increased 10 times, the nanocrystals were 2 times larger than those prepared with a low-concentrated feed solution.

Harsha et al. prepared mucoadhesive nanospheres with vildagliptin, using aminated gelatin to form the matrix.⁷⁹ These nanoparticles were developed to improve the oral treatment of diabetes by creating a gastroretentive formulation. Both compounds were dissolved in water and the solution of 0.5% was nano spray-dried at 120°C. As a result, a narrow particle size distribution and a high yield (over 80%) were obtained. In vitro drug release studies showed a slower release of vildagliptin from the gelatin nanoparticles compared to the crude drug. Drug release was controlled by diffusion. The results of the wash-off

test showed that after 8 h, more than 85% of the formulation remained at the application site. These findings were confirmed in a rat model where 98.2% of the formulation was retained after 12 h. In addition, these nanospheres were stable for 12 months after storage at room conditions.

Among polymeric carriers, PLGA are universal matrix-forming or encapsulating excipients not only in conventional spray drying but also in nano spray drying technology (Table 4). They have been used for manufacturing of nano spray-dried particles loaded with, e.g., cyclosporine A, dexamethasone,⁵⁰ nimodipine,⁷⁴ simvastatin,⁷² and sildenafil.⁸⁰ Importantly, the majority of these formulations ensure a controlled drug release.

An interesting application of PLGA in the nano spray drying process was described by Amsalem et al.⁸¹ They developed solid nano-in-nanoparticles (double nano carriers in the form of powder) loaded with siRNA. These nanoparticles could be a model platform for systemic delivery of nucleic acids. As a rule of thumb, the encapsulation of biomolecules, such as siRNA, proteins and peptides, provides the opportunity to enhance their stability, reduce their toxicity and achieve targeted drug delivery (PEGylated surface). In this study, smooth surface spherical nanoparticles with particle size ranging from 580 nm to 772 nm were prepared with the aim to treat genetic disorders. The primary nanoparticles consisted of siRNA-loaded cross-linked human serum albumin. They were coated with an organic solution of PLGA or PLGA combined with PEG (1:1) during nano spray drying. Such an approach enabled co-processing at low temperatures (30–60°C). As a result, the activity of siRNA was preserved, processing using small amount of siRNA was possible, and the yields higher than 60% were achieved. Then, in vitro studies confirmed a controlled release of siRNA from solid nano-in-nanoparticles for 12 h or 24 h. Finally, cellular safety and uptake were also shown for PEGylated nanoparticles.


Conclusions

Spray drying and nano spray drying can be used as complementary technologies.⁶¹ Due to its low efficiency in producing particles below 2 µm, standard spray drying is incapable of producing nanoparticles. In this case, nano spray drying allows to achieve submicrometer particle sizes with narrow particle size distribution.⁸² The engineering of the polymeric particles is possible by modifying the formulation variables and process parameters. Moreover, spray drying yields are typically maximum 70% and nano spray drying yields are around 90%, even for small sample volumes. However, it should be noted that nano spray drying is difficult to scale up, which is not a problem with traditional spray drying. Another advantage of spray drying is a much higher viscosity of fluids that can be used compared to nano spray drying. Among dispersed systems, only nanosuspensions or nanoemulsions can be processed; otherwise, mesh blockage can occur.

Despite these limitations, several research studies show the potential of nano spray drying in the manufacturing of polymeric nanoparticles, especially in the field of targeted drug delivery or controlled drug release.

ORCID iDs

Dominik Strojewski  <https://orcid.org/0000-0003-3283-8521>

Anna Krupa  <https://orcid.org/0000-0002-0603-512X>

References

- Kemp IC. Fundamentals of energy analysis of dryers. In: Tsotsas E, Mujumdar AS, eds. *Modern Drying Technology*. Hoboken, USA: Wiley-Blackwell; 2011:1–45. doi:10.1002/9783527631681.ch1
- Mujumdar AS, ed. *Handbook of Industrial Drying*. 3rd ed. Boca Raton, USA: CRC Press; 2006. doi:10.1201/9781420017618
- Sollohub K, Cal K. Spray drying technique. II. Current applications in pharmaceutical technology. *J Pharm Sci*. 2010;99(2):587–597. doi:10.1002/jps.21963
- Patel BB, Patel JK, Chakraborty S. Review of patents and application of spray drying in pharmaceutical, food and flavor industry. *Recent Pat Drug Deliv Formul*. 2014;8(1):63–78. doi:10.2174/1872211308666140211122012
- Li DX, Yan YD, Oh DH, et al. Development of valsartan-loaded gelatin microcapsule without crystal change using hydroxypropylmethylcellulose as a stabilizer. *Drug Deliv*. 2010;17(5):322–329. doi:10.3109/10717541003717031
- Wong SM, Kellaway IW, Murdan S. Enhancement of the dissolution rate and oral absorption of a poorly water soluble drug by formation of surfactant-containing microparticles. *Int J Pharm*. 2006;317(1):61–68. doi:10.1016/j.ijpharm.2006.03.001
- Gavini E, Chetoni P, Cossu M, Alvarez MG, Saettone MF, Giunchedi P. PLGA microspheres for the ocular delivery of a peptide drug, vancomycin using emulsification/spray-drying as the preparation method: In vitro/in vivo studies. *Eur J Pharm Biopharm*. 2004;57(2):207–212. doi:10.1016/j.ejpb.2003.10.018
- Takeuchi H, Yasuji T, Yamamoto H, Kawashima Y. Spray-dried lactose composite particles containing an ion complex of alginate-chitosan for designing a dry-coated tablet having a time-controlled releasing function. *Pharm Res*. 2000;17(1):94–99. doi:10.1023/A:1007530927887
- Chiou D, Langrish TAG, Brahm R. The effect of temperature on the crystallinity of lactose powders produced by spray drying. *J Food Eng*. 2008;86(2):288–293. doi:10.1016/j.jfoodeng.2007.10.005
- Takeuchi H, Yasuji T, Hino T, Yamamoto H, Kawashima Y. Spray-dried composite particles of lactose and sodium alginate for direct tableting and controlled releasing. *Int J Pharm*. 1998;174(1–2):91–100. doi:10.1016/S0378-5173(98)00248-8
- Davis M, Walker G. Recent strategies in spray drying for the enhanced bioavailability of poorly water-soluble drugs. *J Control Release*. 2018; 269:110–127. doi:10.1016/j.jconrel.2017.11.005
- Malamataris M, Charisi A, Malamataris N, Kachrimanis K, Nikolakakis I. Spray drying for the preparation of nanoparticle-based drug formulations as dry powders for inhalation. *Processes*. 2020;8(7):788. doi:10.3390/pr8070788
- Vasconcelos T, Marques S, das Neves J, Sarmento B. Amorphous solid dispersions: Rational selection of a manufacturing process. *Adv Drug Deliv Rev*. 2016;100:85–101. doi:10.1016/j.addr.2016.01.012
- Bhujbal SV, Mitra B, Jain U, et al. Pharmaceutical amorphous solid dispersion: A review of manufacturing strategies. *Acta Pharm Sin B*. 2021;11(8):2505–2536. doi:10.1016/j.apsb.2021.05.014
- Jermain SV, Brough C, Williams RO. Amorphous solid dispersions and nanocrystal technologies for poorly water-soluble drug delivery: An update. *Int J Pharm*. 2018;535(1–2):379–392. doi:10.1016/j.ijpharm.2017.10.051
- Arpagaus C. Pharmaceutical particle engineering via nano spray drying: Process parameters and application examples on the laboratory-scale. *Int J Med Nano Res*. 2018;5(1). doi:10.23937/2378-3664.1410026
- Pinto JT, Faulhammer E, Dieplinger J, et al. Progress in spray-drying of protein pharmaceuticals: Literature analysis of trends in formulation and process attributes. *Dry Technol*. 2021;39(11):1415–1446. doi:10.1080/07373937.2021.1903032
- Cal K, Sollohub K. Spray drying technique. I. Hardware and process parameters. *J Pharm Sci*. 2010;99(2):575–586. doi:10.1002/jps.21886
- Mizoe T, Ozeki T, Okada H. Preparation of drug nanoparticle-containing microparticles using a 4-fluid nozzle spray drier for oral, pulmonary, and injection dosage forms. *J Control Release*. 2007;122(1):10–15. doi:10.1016/j.jconrel.2007.06.001
- Zbicinski I, Strumillo C, Delag A. Drying kinetics and particle residence time in spray drying. *Dry Technol*. 2002;20(9):1751–1768. doi:10.1081/DRT-120015412
- Goula AM, Adamopoulos KG. Spray drying of tomato pulp in dehumidified air. I. The effect on product recovery. *J Food Eng*. 2005;66(1):25–34. doi:10.1016/j.jfoodeng.2004.02.029
- Bordón MG, Alasino NPX, Tesoriero MVD, et al. Spray-air contact in tall and short-type spray dryers affects important physicochemical properties of microencapsulated chia seed oil. In: *The 2nd International Conference of la ValSe-Food Network*. MDPI; 2020:19. doi:10.3390/proceedings2020053019

23. Singh A, Van den Mooter G. Spray drying formulation of amorphous solid dispersions. *Adv Drug Deliv Rev.* 2016;100:27–50. doi:10.1016/j.addr.2015.12.010
24. Carpenter JF, Chang BS, Garzon-Rodriguez W, Randolph TW. Rational design of stable lyophilized protein formulations: Theory and practice. In: Carpenter JF, Manning MC, eds. *Rational Design of Stable Protein Formulations*. Boston, USA: Springer US; 2002:109–133. doi:10.1007/978-1-4615-0557-0_5
25. Bowen M, Turok R, Maa YF. Spray drying of monoclonal antibodies: Investigating powder-based biologic drug substance bulk storage. *Dry Technol.* 2013;31(13–14):1441–1450. doi:10.1080/07373937.2013.796968
26. Maltesen MJ, Bjerregaard S, Hovgaard L, Havelund S, van de Weert M. Quality by design: Spray drying of insulin intended for inhalation. *Eur J Pharm Biopharm.* 2008;70(3):828–838. doi:10.1016/j.ejpb.2008.07.015
27. Chan HK, Kwok PCL. Production methods for nanodrug particles using the bottom-up approach. *Adv Drug Deliv Rev.* 2011;63(6):406–416. doi:10.1016/j.addr.2011.03.011
28. Patel RP. Spray drying technology: An overview. *Indian J Sci Technol.* 2009;2(10):44–47. doi:10.17485/ijst/2009/v2i10.3
29. Vehring R. Pharmaceutical particle engineering via spray drying. *Pharm Res.* 2008;25(5):999–1022. doi:10.1007/s11095-007-9475-1
30. Arpagaus C, John P, Collenberg A, Rütli D. Nanocapsules formation by nano spray drying. In: Jafari SM, ed. *Nanoencapsulation Technologies for the Food and Nutraceuical Industries*. Cambridge, USA: Academic Press; 2017:346–401. doi:10.1016/B978-0-12-809436-5.00010-0
31. Almansour K, Ali R, Alheibshy F, et al. Particle engineering by nano spray drying: Optimization of process parameters with hydroethanolic versus aqueous solutions. *Pharmaceutics.* 2022;14(4):800. doi:10.3390/pharmaceutics14040800
32. Maury M, Murphy K, Kumar S, Shi L, Lee G. Effects of process variables on the powder yield of spray-dried trehalose on a laboratory spray-dryer. *Eur J Pharm Biopharm.* 2005;59(3):565–573. doi:10.1016/j.ejpb.2004.10.002
33. Santos D, Maurício AC, Sencadas V, Santos JD, Fernandes MH, Gomes PS. Spray drying: An overview. In: Pignatello R, Musumeci T, eds. *Biomaterials – Physics and Chemistry – New Edition*. IntechOpen; 2018. doi:10.5772/intechopen.72247
34. Filipović-Grčić J, Perissutti B, Moneghini M, Voinovich D, Martinac A, Jalšenjak I. Spray-dried carbamazepine-loaded chitosan and HPMC microspheres: Preparation and characterisation. *J Pharm Pharmacol.* 2003;55(7):921–931. doi:10.1211/0022357021503
35. Friesen DT, Shanker R, Crew M, Smithey DT, Curatolo WJ, Nightingale JAS. Hydroxypropyl methylcellulose acetate succinate-based spray-dried dispersions: An overview. *Mol Pharm.* 2008;5(6):1003–1019. doi:10.1021/mp8000793
36. Aranaz I, Paños I, Peniche C, Heras Á, Acosta N. Chitosan spray-dried microparticles for controlled delivery of venlafaxine hydrochloride. *Molecules.* 2017;22(11):1980. doi:10.3390/molecules22111980
37. Bothiraja C, Shinde MB, Rajalakshmi S, Pawar AP. Evaluation of molecular pharmaceutical and in-vivo properties of spray-dried isolated andrographolide–PVP. *J Pharm Pharmacol.* 2009;61(11):1465–1472. doi:10.1211/jpp.61.11.0005
38. Ekdahl A, Mudie D, Malewski D, Amidon G, Goodwin A. Effect of spray-dried particle morphology on mechanical and flow properties of felodipine in PVP VA amorphous solid dispersions. *J Pharm Sci.* 2019;108(11):3657–3666. doi:10.1016/j.xphs.2019.08.008
39. Kristmundsdóttir T, Gudmundsson ÓS, Ingvarsdóttir K. Release of diltiazem from Eudragit microparticles prepared by spray-drying. *Int J Pharm.* 1996;137(2):159–165. doi:10.1016/0378-5173(96)04509-7
40. Silva DM, Paleco R, Traini D, Sencadas V. Development of ciprofloxacin-loaded poly(vinyl alcohol) dry powder formulations for lung delivery. *Int J Pharm.* 2018;547(1–2):114–121. doi:10.1016/j.ijpharm.2018.05.060
41. Ogunjimi AT, Fiegel J, Brogden NK. Design and characterization of spray-dried chitosan–naltrexone microspheres for microneedle-assisted transdermal delivery. *Pharmaceutics.* 2020;12(6):496. doi:10.3390/pharmaceutics12060496
42. Cho HJ, Oh D, Kim DD. Polysaccharides-based spray-dried microspheres for maintained stability and controlled release of protein. *J Pharm Investig.* 2012;42(2):83–88. doi:10.1007/s40005-012-0013-8
43. Bodmeier R, Chen H. Preparation of biodegradable poly(±)lactide microparticles using a spray-drying technique. *J Pharm Pharmacol.* 1988;40(11):754–757. doi:10.1111/j.2042-7158.1988.tb05166.x
44. Wagenaar BW, Müller BW. Piroxicam release from spray-dried biodegradable microspheres. *Biomaterials.* 1994;15(1):49–54. doi:10.1016/0142-9612(94)90196-1
45. Wan F, Yang M. Design of PLGA-based depot delivery systems for biopharmaceuticals prepared by spray drying. *Int J Pharm.* 2016;498(1–2):82–95. doi:10.1016/j.ijpharm.2015.12.025
46. Sharma S, Parmar A, Kori S, Sandhir R. PLGA-based nanoparticles: A new paradigm in biomedical applications. *Trends Analyt Chem.* 2016;80:30–40. doi:10.1016/j.trac.2015.06.014
47. Danhier F, Ansorena E, Silva JM, Coco R, Le Breton A, Préat V. PLGA-based nanoparticles: An overview of biomedical applications. *J Control Release.* 2012;161(2):505–522. doi:10.1016/j.jconrel.2012.01.043
48. Youan BBC. Microencapsulation of superoxide dismutase into biodegradable microparticles by spray-drying. *Drug Deliv.* 2004;11(3):209–214. doi:10.1080/10717540490280363
49. Blanco MD, Sastre RL, Teijón C, Olmo R, Teijón JM. 5-Fluorouracil-loaded microspheres prepared by spray-drying poly(D,L-lactide) and poly(lactide-co-glycolide) polymers: Characterization and drug release. *J Microencapsul.* 2005;22(6):671–682. doi:10.1080/02652040500161990
50. Schafroth N, Arpagaus C, Jadhav UY, Makne S, Douroumis D. Nano and microparticle engineering of water insoluble drugs using a novel spray-drying process. *Colloids Surf B Biointerfaces.* 2012;90:8–15. doi:10.1016/j.colsurfb.2011.09.038
51. Arpagaus C. PLA/PLGA nanoparticles prepared by nano spray drying. *J Pharm Investig.* 2019;49(4):405–426. doi:10.1007/s40005-019-00441-3
52. Baras B, Benoit MA, Gillard J. Parameters influencing the antigen release from spray-dried poly(DL-lactide) microparticles. *Int J Pharm.* 2000;200(1):133–145. doi:10.1016/S0378-5173(00)00363-X
53. Johansen P, Merkle HP, Gander B. Technological considerations related to the up-scaling of protein microencapsulation by spray-drying. *Eur J Pharm Biopharm.* 2000;50(3):413–417. doi:10.1016/S0939-6411(00)00123-5
54. Aliofkhaeizaei M, ed. *Handbook of Nanoparticles*. Cham, Switzerland: Springer International Publishing; 2016. doi:10.1007/978-3-319-15338-4
55. Arpagaus C, Collenberg A, Rütli D, Assadpour E, Jafari SM. Nano spray drying for encapsulation of pharmaceuticals. *Int J Pharm.* 2018;546(1–2):194–214. doi:10.1016/j.ijpharm.2018.05.037
56. Heng D, Lee SH, Ng WK, Tan RB. The nano spray dryer B-90. *Expert Opin Drug Deliv.* 2011;8(7):965–972. doi:10.1517/17425247.2011.588206
57. Arpagaus C. A short review on nano spray drying of pharmaceuticals. *Nanomed Nanosci Res.* 2018;3(4):1–5. https://www.gavinpublishers.com/assets/articles_pdf/1542018798article_pdf1444139676.pdf Accessed June 6, 2022.
58. Schmid KC. Spray Drying of Protein Precipitates and Evaluation of the Nano Spray Dryer B-90 [doctoral dissertation]. Ludwig-Maximilian University, Munich, Germany; 2011. https://edoc.ub.uni-muenchen.de/13132/1/Schmid_Katja.pdf.
59. Schmid K, Arpagaus C, Friess W. Evaluation of the Nano Spray Dryer B-90 for pharmaceutical applications. *Pharm Dev Technol.* 2011;16(4):287–294. doi:10.3109/10837450.2010.485320
60. Lee SH, Heng D, Ng WK, Chan HK, Tan RBH. Nano spray drying: A novel method for preparing protein nanoparticles for protein therapy. *Int J Pharm.* 2011;403(1–2):192–200. doi:10.1016/j.ijpharm.2010.10.012
61. Arpagaus C. A novel laboratory-scale spray dryer to produce nanoparticles. *Dry Technol.* 2012;30(10):1113–1121. doi:10.1080/07373937.2012.686949
62. Bürki K, Jeon I, Arpagaus C, Betz G. New insights into respirable protein powder preparation using a nano spray dryer. *Int J Pharm.* 2011;408(1–2):248–256. doi:10.1016/j.ijpharm.2011.02.012
63. Li X, Anton N, Arpagaus C, Belleteix F, Vandamme TF. Nanoparticles by spray drying using innovative new technology: The Büchi nano spray dryer B-90. *J Control Release.* 2010;147(2):304–310. doi:10.1016/j.jconrel.2010.07.113
64. Kaewjan K, Srichana T. Nano spray-dried pyrazinamide–L-leucine dry powders, physical properties and feasibility used as dry powder aerosols. *Pharm Dev Technol.* 2016;21(1):68–75. doi:10.3109/10837450.2014.971373

65. Schoubben A, Blasi P, Marenzoni ML, et al. Capreomycin supergenerics for pulmonary tuberculosis treatment: Preparation, in vitro, and in vivo characterization. *Eur J Pharm Biopharm.* 2013;83(3):388–395. doi:10.1016/j.ejpb.2012.11.005
66. Dahili LA, Feczko T. Cross-linking of horseradish peroxidase enzyme to fine particles generated by nano spray dryer B-90. *Period Polytech Chem Eng.* 2015;59(3):209–214. doi:10.3311/PPch.7590
67. Feng AL, Boraey MA, Gwin MA, Finlay PR, Kuehl PJ, Vehring R. Mechanistic models facilitate efficient development of leucine containing microparticles for pulmonary drug delivery. *Int J Pharm.* 2011;409(1–2):156–163. doi:10.1016/j.ijpharm.2011.02.049
68. Nandiyanto ABD, Okuyama K. Progress in developing spray-drying methods for the production of controlled morphology particles: From the nanometer to submicrometer size ranges. *Adv Powder Technol.* 2011;22(1):1–19. doi:10.1016/j.apt.2010.09.011
69. Zellnitz S, Narygina O, Resch C, Schroettner H, Urbanetz NA. Crystallization speed of salbutamol as a function of relative humidity and temperature. *Int J Pharm.* 2015;489(1–2):170–176. doi:10.1016/j.ijpharm.2015.04.079
70. Harsha S. Pharmaceutical suspension containing both immediate/sustained-release amoxicillin-loaded gelatin nanoparticles: Preparation and in vitro characterization. *Drug Des Devel Ther.* 2013;7:1027–1033. doi:10.2147/DDDT.S39956
71. Beck-Broichsitter M, Schmehl T, Gessler T, Seeger W, Kissel T. Development of a biodegradable nanoparticle platform for sildenafil: Formulation optimization by factorial design analysis combined with application of charge-modified branched polyesters. *J Control Release.* 2012;157(3):469–477. doi:10.1016/j.jconrel.2011.09.058
72. Anzar N, Mirza MA, Anwer K, et al. Preparation, evaluation and pharmacokinetic studies of spray dried PLGA polymeric submicron particles of simvastatin for the effective treatment of breast cancer. *J Mol Liq.* 2018;249:609–616. doi:10.1016/j.molliq.2017.11.081
73. Panda A, Meena J, Katara R, Majumdar DK. Formulation and characterization of clozapine and risperidone co-entrapped spray-dried PLGA nanoparticles. *Pharm Dev Technol.* 2016;21(1):43–53. doi:10.3109/10837450.2014.965324
74. Bege N, Renette T, Endres T, Beck-Broichsitter M, Hänggi D, Kissel T. In situ forming nimodipine depot system based on microparticles for the treatment of posthemorrhagic cerebral vasospasm. *Eur J Pharm Biopharm.* 2013;84(1):99–105. doi:10.1016/j.ejpb.2012.12.016
75. Baghdan E, Pinnapireddy SR, Vögeling H, Schäfer J, Eckert AW, Bakowsky U. Nano spray drying: A novel technique to prepare well-defined surface coatings for medical implants. *J Drug Deliv Sci Technol.* 2018;48:145–151. doi:10.1016/j.jddst.2018.09.008
76. Dhillon GS, Kaur S, Brar SK. Facile fabrication and characterization of chitosan-based zinc oxide nanoparticles and evaluation of their antimicrobial and antibiofilm activity. *Int Nano Lett.* 2014;4(2):107. doi:10.1007/s40089-014-0107-6
77. Baba K, Nishida K. Calpain inhibitor nanocrystals prepared using Nano Spray Dryer B-90. *Nanoscale Res Lett.* 2012;7(1):436. doi:10.1186/1556-276X-7-436
78. Baba K, Nishida K. Steroid nanocrystals prepared using the nano spray dryer B-90. *Pharmaceutics.* 2013;5(1):107–114. doi:10.3390/pharmaceutics5010107
79. Harsha S, Aldhubiab B, Nair A, et al. Nanoparticle formulation by Büchi B-90 Nano Spray Dryer for oral mucoadhesion. *Drug Des Devel Ther.* 2015;9:273–282. doi:10.2147/DDDT.S66654
80. Beck-Broichsitter M, Strehlow B, Kissel T. Direct fractionation of spray-dried polymeric microparticles by inertial impaction. *Powder Technol.* 2015;286:311–317. doi:10.1016/j.powtec.2015.08.033
81. Amsalem O, Nassar T, Benhamron S, Lazarovici P, Benita S, Yavin E. Solid nano-in-nanoparticles for potential delivery of siRNA. *J Control Release.* 2017;257:144–155. doi:10.1016/j.jconrel.2016.05.043
82. Jafari SM, Arpagaus C, Cerqueira MA, Samborska K. Nano spray drying of food ingredients; materials, processing and applications. *Trends Food Sci Technol.* 2021;109:632–646. doi:10.1016/j.tifs.2021.01.061

